NUWC-NPT Technical Report 11,023
20 July 1995

A Bingham Flow Model to Predict the Vibrational Damping Characteristics of an Electrorheological Fluid-Filled Annulus

Stephen A. Austin
Submarine Sonar Department

Naval Undersea Warfare Center Division
Newport, Rhode Island

PREFACE

This report was prepared as a Ph.D. dissertation for the degree of Doctor of Philosophy in Mechanical Engineering from the University of Connecticut. The major advisor for this work was Professor L. S. Langston. Associate advisors were Dr. D. A. Hurdis (NUWC Detachment New London) and Professor J. C. Bennett of the University of Connecticut. The study was partially sponsored by the Independent Exploratory Development Program at NUWC Division Newport, program manager Dr. K. M. Lima (Code 102).

The technical reviewers for this report were Dr. D. A. Hurdis (Code 6291) and Dr. A. J. Hull (Code 2141) of NUWC Detachment New London.

The author gratefully acknowledges both Drs. Hurdis and Hull for their careful review of the manuscript.

Reviewed and Approved: 20 July 1995

R. J. Martin
Acting Head, Submarine Sonar Department

REPORT DOCUMENTATION PAGE

Form Approved
OMB No. 0704-0188

1. AGENCY USE ONLY (Leave Blank)	2. REPORT DATE	3. REPORT TYPE AND DATES COVERED
	20 July 1995	Ph.D. Thesis

4. TITLE AND SUBTITLE

A Bingham Flow Model to Predict the Vibrational Damping Characteristics of an Electrorheological Fluid-Filled Annulus

5. FUNDING NUMBERS

6. AUTHOR(S)

Dr. Stephen A. Austin

7. PERFORMING ORGANIZATION NAME(S) AND ADDRESS(ES)

Naval Undersea Warfare Center
Detachment New London
New London, Connecticut 06320

8. PERFORMING ORGANIZATION REPORT NUMBER

TR 11,023

9. SPONSORING/MONITORING AGENCY NAME(S) AND ADDRESS(ES)

10. SPONSORING/MONITORING AGENCY REPORT NUMBER

11. SUPPLEMENTARY NOTES

12a. DISTRIBUTION/AVAILABILITY STATEMENT

Approved for public release; distribution is unlimited.

12b. DISTRIBUTION CODE

13. ABSTRACT (Maximum 200 words)

The research discussed in this report theoretically and experimentally investigates the dissipation of vibrational energy through the relative shearing within an electrorheological (ER) fluid contained in an annulus. This work develops a model for both the damping and flow characteristics of an ER fluid due to axial excitation of the flexible structure where it is contained. Based on a creeping Bingham fluid assumption, the model calculates the radial and axial velocity components in the fluid resulting from harmonic excitation. The axial velocity is modeled as one dimensional in the axial direction and the radial velocity as two dimensional in the radial and axial directions. These velocity components are used to formulate the non-Newtonian viscous energy dissipation and calculate the total strain energy for the flexible cylinder containing the fluid. The damping ratio of the ER fluid system is predicted based on the ratio of the dissipated energy to the strain energy.

The evaluation of this Bingham fluid model relies on the development of the constitutive relationship for the ER fluid and the electric field activating the fluid. The relationship between the yield stress and the electric fields was accomplished by fitting the Bingham constitutive law to measured shear stress and shear strain rate data for corn-starch and mineral-oil ER fluid. The evaluation of the electric field strength within the fluid was analytically derived using conformal mapping techniques and Jacobian elliptic functions.

An attenuation experiment was conducted to compare model damping ratio predictions to a measured system

14. SUBJECT TERM	15. NUMBER OF PAGES
Applied Electric Field, Axial Velocity Component, Bingham Flow Model, Damping Ratio, Dissipation Energy, Electrorheological Fluid, Radial Velocity Component, Shear Strain, Shear Stress	136
	16. PRICE CODE

17. SECURITY CLASSIFICATION OF REPORT	18. SECURITY CLASSIFICATION OF THIS PAGE	19. SECURITY CLASSIFICATION OF ABSTRACT	20. LIMITATION OF ABSTRACT
UNCLASSIFIED	**UNCLASSIFIED**	**UNCLASSIFIED**	**SAR**

13. ABSTRACT (CONT'D)

response as a function of the applied electric field. The damping ratio of the ER structure was evaluated from transmissibility experiments and compared to Bingham model predictions. The comparison of the experimental results to the model showed predictions that were accurate to within 5 percent.

The capability to predict the attenuation of the longitudinal vibration in the ER fluid based on the internal velocity components provides the basis for ER fluid rheological parameter estimation. An outline for achieving this parameter estimation model is provided in the conclusions of the report.

Table of Contents

List of Nomenclature

Chapter 2: Attenuation Experiment

a_a	aft acceleration
a_f	forward acceleration
$AR(\omega)$	frequency dependent Amplitude Ratio
$c(\omega)$	dynamic viscous damping coefficient
c_c	critical damping coefficient
f_a	aft force transducer
f_f	forward force transducer
i	$\sqrt{-1}$
$Im[]$	imaginary component of argument []
$k(\omega)$	dynamic stiffness
m	mass of ER test module and point mass
r	radial coordinate direction
$Re[]$	real component of argument []
$TF\{\}$	Fast Fourier Transfer function of the ratio {}
$x(t)$	longitudinal displacement of aft position
$\dot{x}(t)$	longitudinal velocity of aft position
$\ddot{x}(t)$	longitudinal acceleration of aft position
X_0	static longitudinal displacement of aft position
$y(t)$	longitudinal displacement of forward position
$\dot{y}(t)$	longitudinal velocity of forward position
$\ddot{y}(t)$	longitudinal acceleration of forward position
Y_0	static longitudinal displacement of forward position
z	longitudinal coordinate direction
$\|\|$	magnitude of argument
$\xi(\omega)$	dynamic damping ratio

ω	circular frequency
ω_n	natural circular frequency of the system
ω_0	resonant circular frequency of 0.0 kV/mm case

Chapter 3: Electric Field Solution

a	electrode radius
d	one-half of the electrode separation
E, E'	complete elliptic integrals of the second kind
$\boldsymbol{E}(r,z)$	electric field vector
K, K'	complete elliptic integrals of the first kind
$L_{electrode}$	length of electrode
$\Phi\,(r, z)$	voltage potential scalar function
Φ_0	applied voltage potential
φ	potential function
ψ	flux function
$sn()$	Jacobian elliptic sine-amplitude function
$cn()$	Jacobian elliptic cosine-amplitude function
$dn()$	Jacobian elliptic difference-amplitude function
$\Im$	Jacobian Zeta function

Chapter 4: Electrorheological Fluid Constitutive Relationships

β	ER fluid material proportionality constant
μ	absolute viscosity of ER fluid
$\tau_0(E)$	electric field dependent yield shear stress
$\tau_0(0)$	zero state yield shear stress
E	magnitude of electric field
$\underline{\tau}$	ER fluid stress tensor
$\underline{\Delta}$	ER fluid rate of deformation tensor
$\underline{\tau} \Diamond \underline{\tau}$	double dot product of ER fluid stress tensor

$\underline{\Delta} \Diamond \underline{\Delta}$ double dot product of ER fluid rate of deformation tensor

Chapter 5: Bingham Fluid Dynamics

a radius of flexible hose

r radial coordinate direction

z axial (longitudinal) coordinate direction

L length of ER test module

h thickness of ER fluid

r_e radius of electrode

A_s cross sectional area of shell

m mass of added point mass

ρ mass density

μ absolute viscosity

E_c complex extensional elastic modulus of flexible hose

ν Poisson ratio of flexible hose

k extensional wavenumber

τ_0 electric field dependent yield shear stress

$u(z)$ axial velocity component of fluid and flexible hose

$\bar{u}(z)$ normalized axial velocity component of fluid and flexible hose

$v(r,z)$ radial velocity component of fluid

$\bar{v}(r,z)$ normalized radial velocity component of fluid

$\bar{v}_w(z)$ radial velocity component of fluid on wall of flexible hose

U_{max} maximum axial velocity of fluid

$\hat{u}(z,t)$ transient axial displacement of flexible hose

$\hat{w}(z)$ radial displacement of flexible hose

$\hat{U}_0$ amplitude of forward boundary displacement

$\hat{U}(z)$ axial displacement of flexible hose

P fluid pressure

$\underline{\tau}$	ER fluid stress tensor
τ_{ii}	normal stresses, subscript *ii* denotes the coordinate direction
$\underline{\Delta}$	ER fluid rate of deformation tensor
$\underline{\tau} \Diamond \underline{\tau}$	double dot product of ER fluid stress tensor
$\underline{\Delta} \Diamond \underline{\Delta}$	double dot product of ER fluid rate of deformation tensor
D/Dt	substantial derivative
$TF\{\}$	Fast Fourier Transfer function of the ratio { }
$\Psi(r,z)$	stream function
Re	Reynolds Number
ω	circular frequency
$[A]$	spatial coefficient matrix
$\{v\}$	radial fluid velocity vector
$\{F\}$	forcing vector
t	time

Chapter 6: Electrorheological Fluid Damping Properties

a	radius of flexible hose
E_v	local rate of dissipation of energy
$\nabla\vec{V}$	gradient of velocity vector
SE	total strain energy of flexible hose
ε_i	normal strain of shell, subscript *i* denotes the coordinate direction
γ_{rz}	shear strain of shell
E_c	complex extensional elastic modulus of flexible hose
G_c	complex shear modulus of flexible hose
ν	Poisson ratio of flexible hose
δ	thickness of flexible hose
L	length of ER test module
ξ	damping ratio

$u(z)$	axial component of velocity
$v(r,z)$	radial component of velocity
μ	absolute viscosity
τ_0	yield shear stress
r_e	radius of electrodes
τ_{ii}	normal stress, subscript *ii* denotes coordinate direction
τ_{rz}	shear stress
ω	circular frequency

List of Tables

List of Figures

A BINGHAM FLOW MODEL TO PREDICT THE VIBRATIONAL DAMPING CHARACTERISTICS OF AN ELECTRORHEOLOGICAL FLUID-FILLED ANNULUS

Chapter 1: Introduction

The electrorheological (ER) phenomenon was first identified by Winslow (1949,1989) during his research in 1940 on photoelectric switches. The early designs for these photoelectric switches were electrodes separated by a dielectric composed of starch suspended in oil. The transmission of force was observed when an electric potential was applied to the moving switch. The development of the ER phenomenon remained dormant until mid-1980. The resurgence of this technology was due mainly to applications in the field of robotics.

ER fluids are two phase systems containing micron sized particles suspended in a high dielectric carrier fluid. When the ER fluid is subjected to an electric field, the particles polarize and develop a network of three dimensional chains. This phenomenon is illustrated in Figures 1.1 through 1.3. The distribution of the particles within the ER fluid is shown in Figure 1.1 to be random in the absence of an electric field. Once a voltage potential, V, is applied to the electrodes as depicted in Figure 1.2, a complex three dimensional particle structure is formed. The cohesive strength of this developed particle structure is dependent on the magnitude of the applied potential. This strength resists the destruction of the particle structure by any applied force to the system.

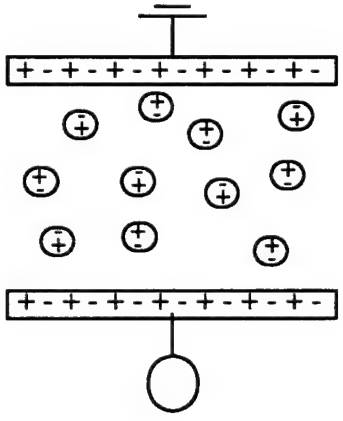

Figure 1.1. ER System Without Applied Potential.

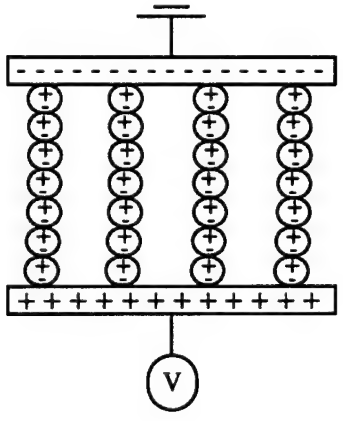

Figure 1.2. ER System Activated by Voltage Potential, V

The application of a shear stress, as shown in Figure 1.3, produces a deformation of the particle structure. If the magnitude of the applied shear stress is greater than the cohesive strength of the particle structure, then the ER fluid will yield in the form of fluid flow. The cohesive strength of this type of fluid is a rheological property termed the yield shear stress. An ER fluid will develop an electric-field dependent yield stress, when activated by an electric field. In the activated state, the ER fluid will resist an applied shear stress, providing the applied load does not exceed the developed yield stress. The time of activation for most ER fluids typically on the order of milliseconds.

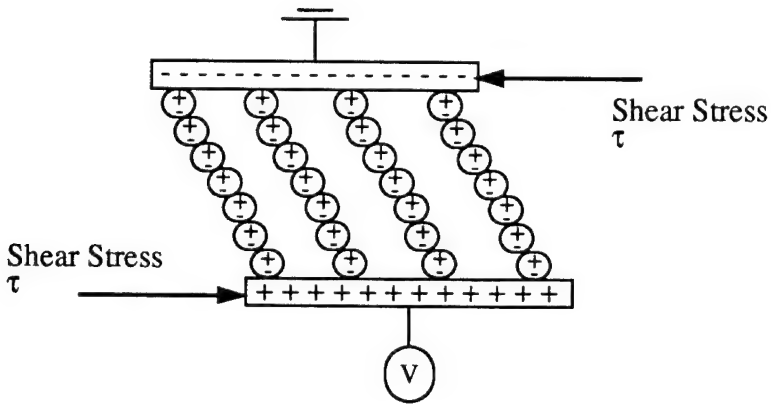

Figure 1.3. Electrically Activated ER Fluid System Resisting an Applied Shear Stress, τ

In order to exploit the ER phenomenon in an engineering application, an understanding of the constitutive properties of the fluid is required. The material behavior of an ER fluid is dependent (Klass & Martinek (1967), Jordan & Shaw (1989), Wong & Shaw (1989), Block & Kelly (1988), Brooks et al. (1986), and Tao et al. (1989)) on the applied electric field, the dielectric properties of the carrier fluid, the dielectric properties of the particles, the particle size, the concentration of particles, temperature, water content, and frequency. However, it has been shown through experimental investigations (Marshall et al. (1989), Gast & Zukoski (1989), Klingenberg (1990)) and numerical investigation (Wang et al. (1989)) that the constitutive behavior of ER fluids can be modeled accurately as a Bingham fluid. The Bingham fluid constitutive model represents the cohesive strength of the particle structure as the yield shear stress property of the fluid. The Bingham material model applied to an ER fluid depends on the applied electric field, the developed yield stress, and the plastic (Bingham) viscosity. A plot of the shear stress versus the

shear strain rate produced from a viscosity measurement experiment would produce a flow curve distinctive to a Bingham fluid. A flow curve for a Bingham fluid is schematically shown in Figure 1.4. The intercept with the y-axis defines the yield shear stress and the slope of the curve produces the absolute viscosity of the fluid.

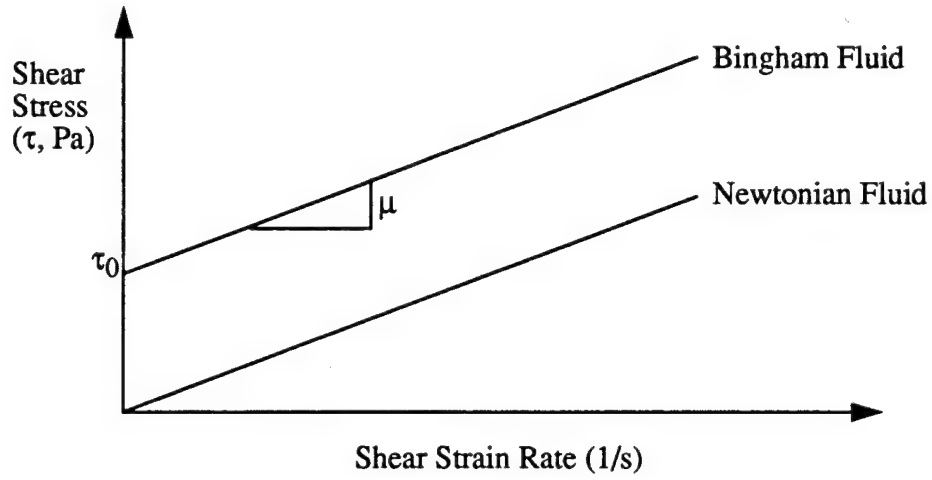

Figure 1.4. Flow Curve Comparing a Bingham Fluid to a Newtonian Fluid

The application of ER fluids has been cited by many authors, such as the plunger dashpot damper of Stanway et al. (1987), the ER fluid composite beams of Coulter et al. (1989), the plunger damper, ER disk clutch, and diaphragm engine mount of Duclos (1988), the electroviscous plunger damper of Stevens et al. (1984), and the ER box-beam of Margolis & Vahdati (1989), as an effective means for vibration isolation and control. In these vibration isolation applications, the predominant method of the vibration energy dissipation is the interaction between a plunger mechanism and the ER fluid. The fluid properties are actively altered by the magnitude of the applied electric field; thus, the response of the structure is altered and controlled.

The research discussed in this dissertation theoretically and experimentally investigates the dissipation of vibrational energy through the relative shearing within the ER fluid itself. This work develops a new relationship between the damping characteristics of an ER fluid and the flow characteristics of this fluid due to the axial excitation of the flexible structure containing the fluid. The dissipation of energy in a flexible cylinder containing an ER fluid subjected to longitudinal vibration is treated in this dissertation. The energy loss is accomplished through shear dissipation

within the ER fluid. The establishment of the yield surfaces within the ER fluid is developed by the spatial variation of the applied electric field. Since the magnitude of the yield stress is dependent on the magnitude of the applied electric field, a spatial variation in the developed yield stress will result.

The mechanics of the ER fluid response to a sinusoidal excitation is modeled herein as a creeping flow. The energy dissipation of the viscous forces in the ER fluid is then evaluated to approximate the damping characteristics of an ER device. Inherent to this fluid model of the ER fluid is the solution of the steady state electric field, the constitutive relationships of the ER fluid to the resulting electric field and the developed strain rate due to the applied boundary excitation. The predictions of this model have been compared to the experimental results and are found to be within five percent of the experiment.

The chapters used to develop the dissertation are titled, Attenuation Experiment, Electric Field Solution, ER Fluid Constitutive Relationships, non-Newtonian Fluid Dynamics, Electrorheological Fluid Damping Properties, Conclusions and Future Work, and Appendices. The Attenuation Experiment chapter discusses the transmissibility experiments conducted to measure the damping effect, as a function of electric field, of an ER fluid in a flexible hose. The Electric Field Solution chapter provides the closed form solution of the applied electric field. The Constitutive Relationships chapter relates the pertinent ER fluid properties to the applied electric field and the boundary excitation. The non-Newtonian Fluid Dynamics chapter develops the governing equations of the creeping flow of the ER fluid within the test module. The Electrorheological Fluid Damping Properties chapter, compares the fluid dynamics model predictions of damping to the measured damping characteristics of the ER device. The final chapter, Conclusions and Future Work, discusses the results of the creeping-motion Bingham fluid model as a means of predicting damping and provides suggestions for future applied research. The future research covers the development of an algorithm to specify an ER parameter envelop to direct the development of future ER fluids. The Appendices listed at the end of the dissertation include clarification to the chapters. Appendix A contains a source listing of the single degree of freedom model developed in Chapter 2. Appendix B contains a discussion on Jacobian elliptic functions, the details to the evaluation of the electric field magnitude and the source listings of the electric field solutions. Appendix C contains a source listing of the fluid model which solves the axial and radial fluid velocity components of Chapter 5. Appendix D contains the source list of the damping evaluation from Chapter 6. Appendix E contains the transfer function data from the

attenuation experiments of Chapter 2. Appendix F presents an example problem were the ER damper length is specified based on the attenuation measured in the experiments of Chapter 2.

Chapter 2: Attenuation Experiment

Introduction

The application of ER fluids as an effective means for vibration isolation and control has been cited by many authors, such as Stanway et al. (1987), Coulter et al. (1992, 1989), Duclos (1988), Stevens et al. (1984), and by Margolis & Vahdati (1989). ER fluids have been used in clutches, viscous dampers, valves, and active engine mounts. When used as a vibration isolation device, the predominant method of the vibrational energy dissipation is through the interaction between a plunger mechanism and the ER fluid.

The application of the ER fluid discussed in this dissertation relies on the exploitation of the electric field dependent yield shear stress and spatial variation of the electric field to attenuate the longitudinal vibration in the elastomer wall of a hose filled with ER fluid. Hereinafter, this hose configuration will be referred to as "the ER test module." This damping mechanism is illustrated conceptually in Figure 2.1, in which the ER test module is represented in cylindrical coordinates whose z-axis is coincident with the longitudinal center line of the hose. The electric field is created by a set of circular discs that are alternately charged with a voltage potential. This electric field device is contained within an elastomer cylinder. This is shown in Figures 2.2 and 2.3. Figure 2.2 is a photograph of the ER test module components and Figure 2.3 is a schematic illustration showing the assembled ER test module. As the cylindrical radial coordinate, r, increases, the electric field strength decreases. As the electric field decreases, the magnitude of the yield shear stress of the ER fluid decreases. Shown in Figure 2.1 are four idealized discrete regions within which the electric field strength, and therefore the yield shear stress, are constant. Vibrational energy transmitted from the hosewall into the ER fluid dissipates at the interfaces between these regions. It is the use of these interfaces within the ER fluid for energy dissipation that separates this device from those of other researchers. The mechanism dissipating the vibrational energy is the transfer of kinetic energy into thermal energy by friction forces between the layers.

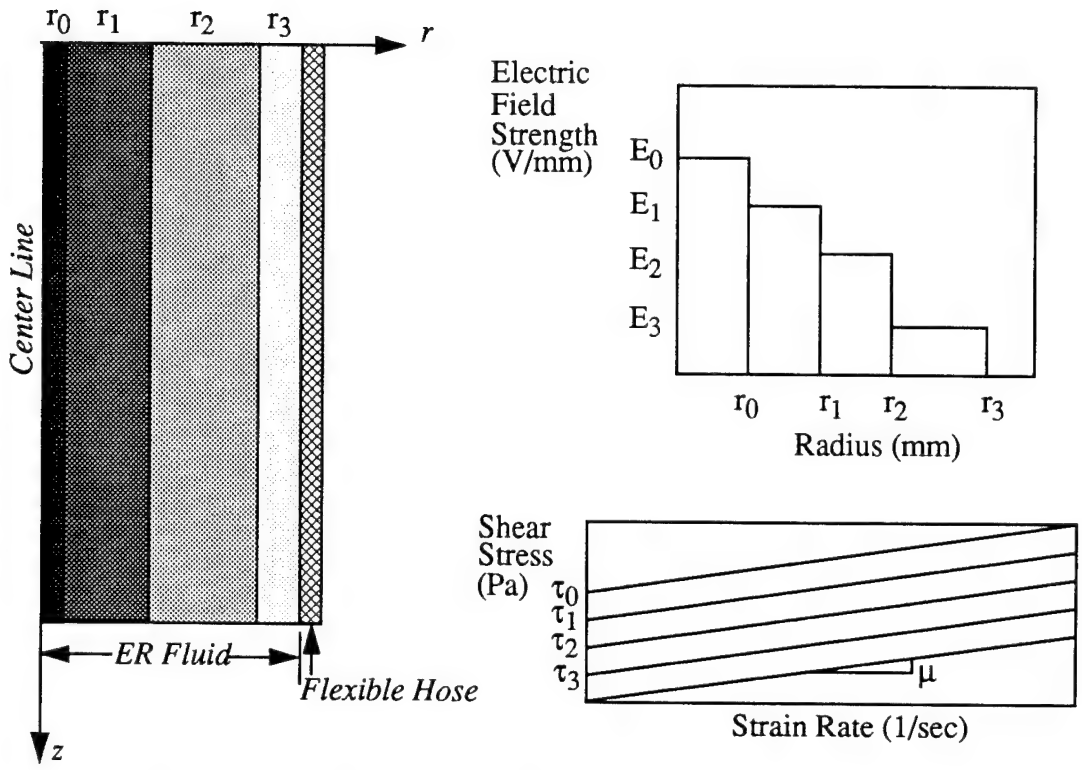

Figure 2.1. Development of Yield Surfaces Within ER Fluid

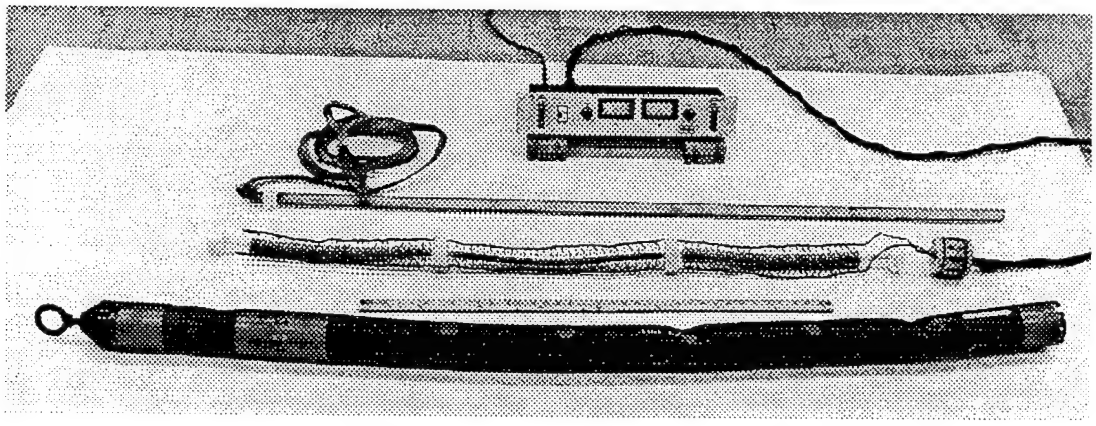

Figure 2.2. Photograph of the ER Test Module Components Showing the Flexible Hose, Electric Field Device, the High Voltage Power Supply and a Discharge Staff

Experimental Configuration

In order to quantify the damping contribution of these yield surfaces in the attenuation of longitudinal vibrations in a flexible cylinder, an ER test module was developed. The ER test module consisted of a polyester-based elastomer hose approximately 125.7 cm in length with an inner diameter of 7.5 cm. The internal components of the ER test module consisted of the ER fluid and a 110.5-cm-long electric field device centered in the hose both longitudinally and radially. This device contained 170 electrodes, each made of a single copper disk and separated with nylon washers from each other. The electric field device was centered in the hose with four nylon spacers. The electrodes and the nylon washers were placed onto a quarter inch diameter nylon rod. This rod was connected to the forward end cap of the hose. The electric potential was applied to the alternately grounded electrodes by an Acopian high voltage supply (model PO30HP2). The field was contained within a 5-mm gap between the electrodes. The diameter of the electrodes was 3.175 cm, providing a gap of 2.1625 cm between the inner wall of the flexible cylinder and the outer edge of the electrodes. It is this annulus (Figure 2.3) of electrically activated ER fluid that dissipates the vibrational energy in the flexible cylinder.

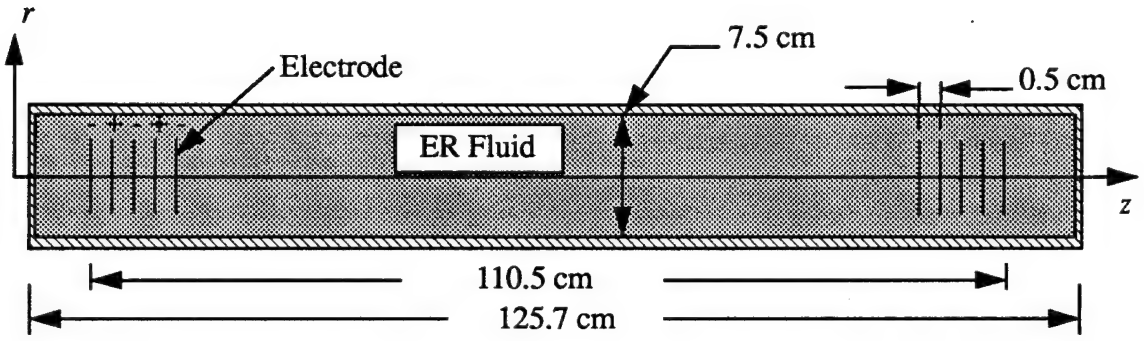

Figure 2.3. Internal View of ER Test Module

The objective of the experiment was to determine the attenuation effect, as a function of electric field and vibrational frequency, that an ER fluid has on the longitudinal vibration in a flexible structure. The ER fluid used in the experiments was a mixture of food grade corn starch and medicinal grade, paraffin based mineral oil. The water content of the corn starch was approximately two percent. This ER fluid was prepared in the following manner:

(1) The mineral oil was filtered to remove foreign particles (40 mesh filter).

(2) The starch was hand packed into a one cup measure.

(3) The starch was sifted into the mineral oil (50% by volume).

(4) The starch was blended into the mineral oil with an electric mixer (132 ml quantities, total of 8 liters).

(5) The ER fluid was de-gassed in a vacuum chamber until evidence of air entrapment ceased, typically about 20 minutes.

The experimental apparatus consisted of the ER test module attached to an electrohydraulic shaker (Zonic model 1215-10-T-ZSP86) and tensioned to a force of approximately 445 N. A point mass was added to provide a large mass dominated end impedance so that wave mechanics do not propagate into the tensioned rope. The instrumentation included a force transducer (PCB 233A) and accelerometer (PCB 348A) at each end of the ER test module as shown in Figure 2.4.

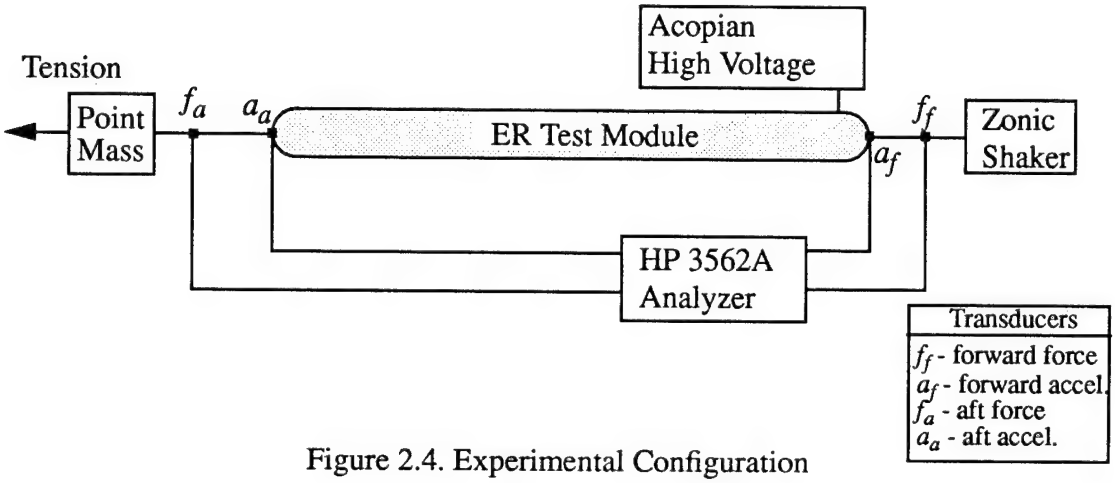

Figure 2.4. Experimental Configuration

The experiments were conducted by exciting the ER test module in the axial direction (z-axis) with a swept sine (1 - 300 Hz) input. The data (average of three samples) were recorded in the form of frequency response functions (HP 3562A Dynamic Signal Analyzer). The use of a frequency response function is preferred since the results can be applied to predict the response of the structure to other excitation functions. The recorded frequency response functions included

the ratios of the aft acceleration to the forward acceleration, the forward force to the forward acceleration and the forward force to the aft acceleration. The data used to determine the damping contribution of the ER fluid was the frequency response function of the acceleration ratio (transmissibility). The experiments were conducted at electric field strengths of 0.0, 0.4, 0.8, 1.2, and 1.6 kV/mm dc. These data sets were generated when the fluid was 1-day-old. The experiments were conducted twice at each electric field strength value. The repeatability at each value of the electric field was within ±0.2dB.

The transmissibility data acquired are shown in Figures 2.5 through 2.8. These figures represent the frequency response functions calculated from the ratio of the aft acceleration to the forward acceleration. The abscissa is frequency in the units of cycles/second (Hz). The ordinate is the magnitude of the acceleration ratio (transmissibility which is dimensionless) expressed in decibels (dB). Figures 2.5, 2.6, and 2.7 show the damping contribution of the ER fluid at 0.4, 0.8, and 1.2 kV/mm respectively. These plots show that the damping effect of the ER fluid produces a reduction in the magnitude of the resonant peak, and a slight increase in resonant frequency. The resonant frequency is shifted in Figures 2.5 through 2.7, from 11.0 Hz for the zero electric field case to 11.5 Hz at 0.4 kV/mm, 11.6 Hz at 0.8kV/mm and 11.7 Hz at 1.2kV/mm. At an electric field of 1.6 kV/mm, as shown in Figure 2.8, the magnitude of the resonant peak as well as the resonant frequency decreased due to the ER fluid effect. The resonant frequency has been reduced to 9.8 Hz. From the comparison of this data to Figures 2.5 to 2.7, there appears to be a change in the damping mechanism when the electric field was increased between 1.2kV/mm to 1.6kV/mm. This will be discussed in terms of the system model in the next section.

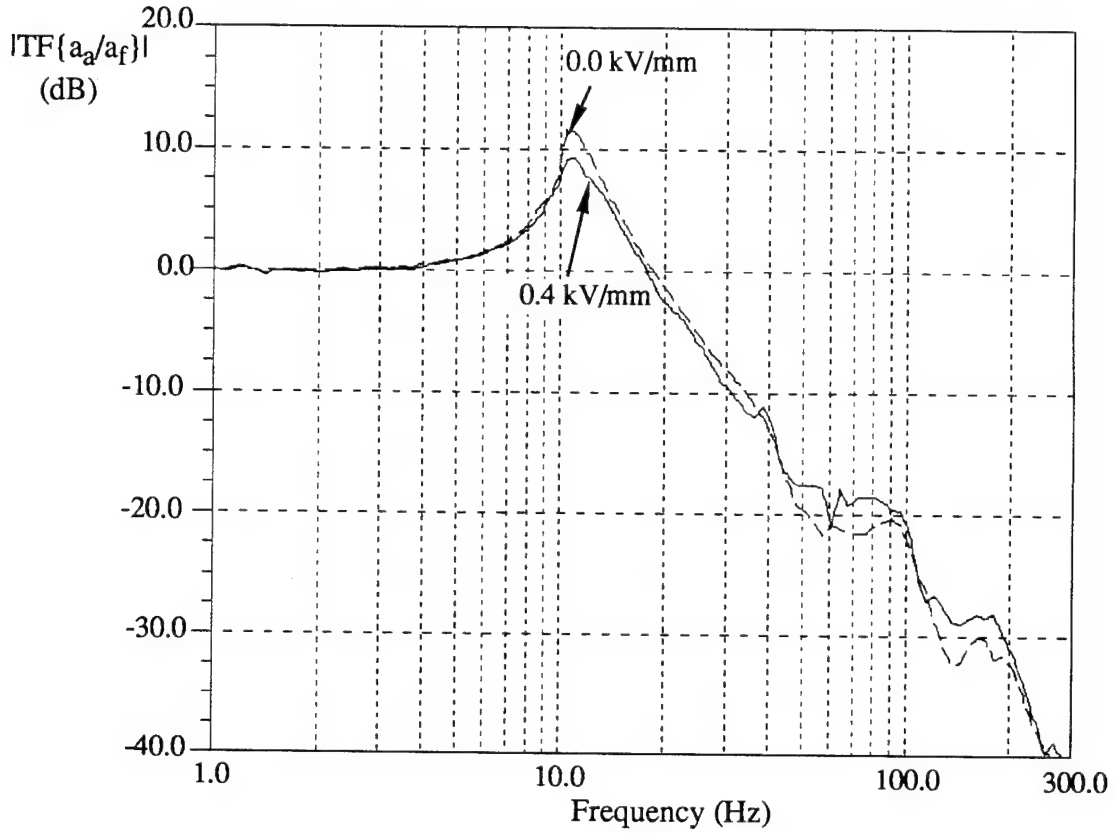

Figure 2.5. Magnitude of Transfer Function Versus Frequency for 0.0 & 0.4 kV/mm

The phase measurements show that these transmissibility experiments can be analyzed as a linear, single degree of freedom system (mass-spring-damper). This assumption is valid for the frequency range of interest (1-30 Hz) because the phase angle has only one crossing at $\pi/2$ radians (Figure 2.9).

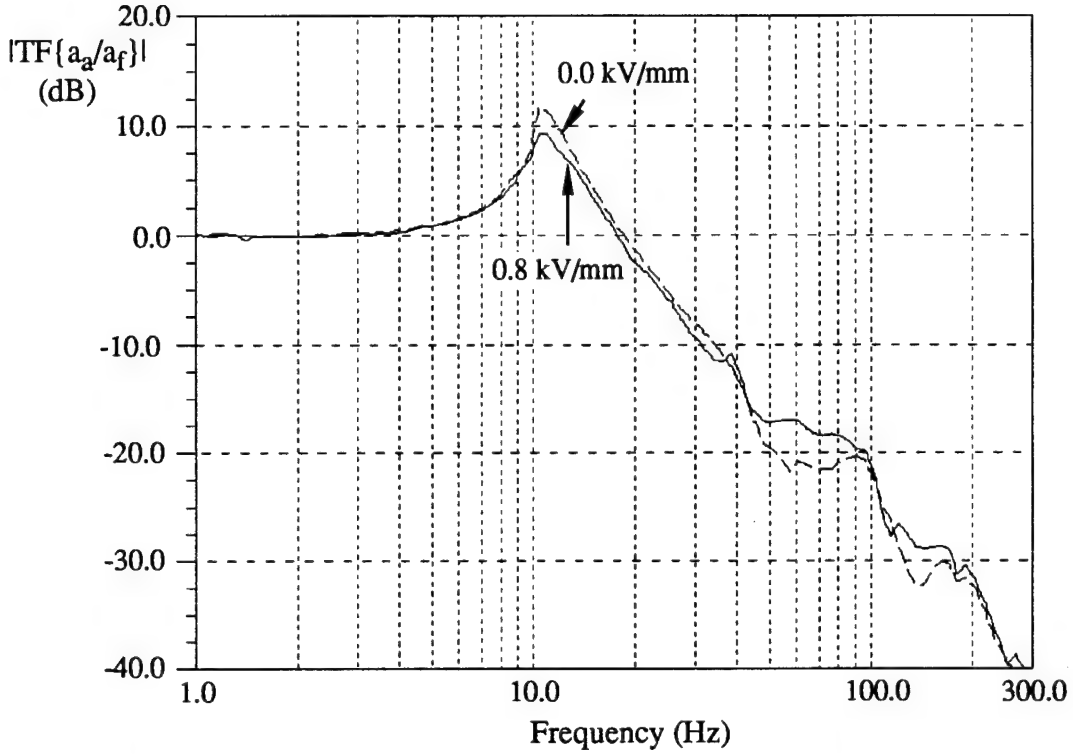

Figure 2.6. Magnitude of Transfer Function Versus Frequency for 0.0 & 0.8 kV/mm

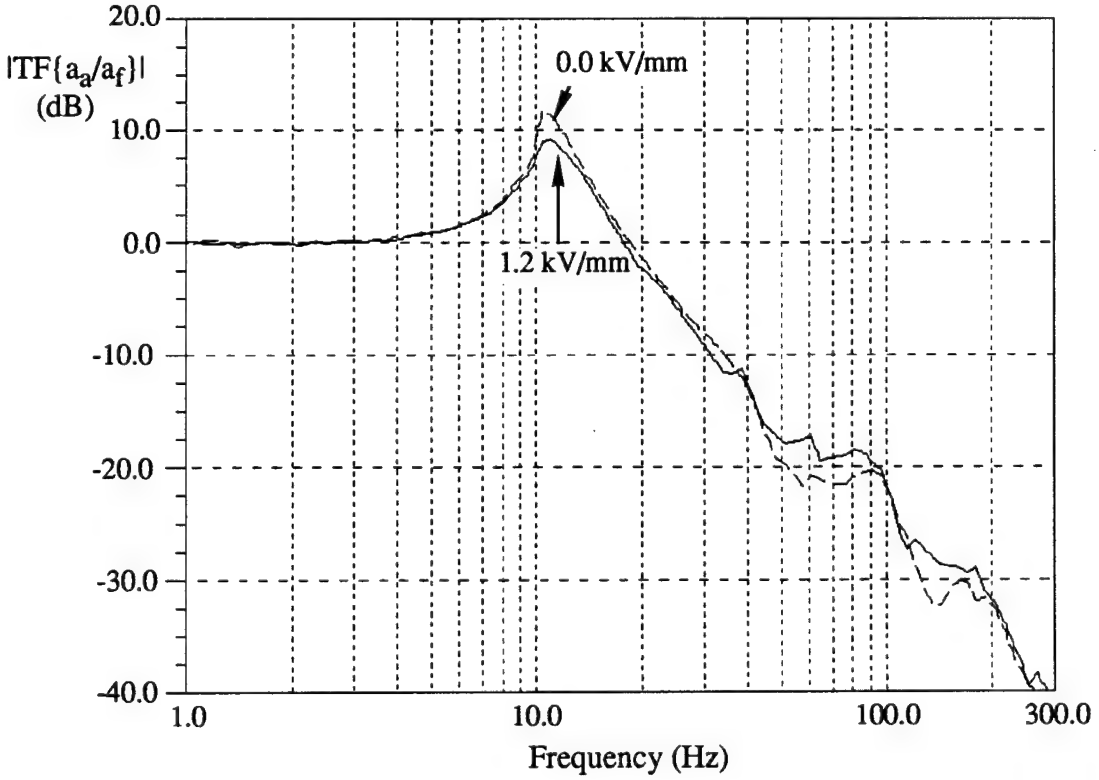

Figure 2.7. Magnitude of Transfer Function Versus Frequency for 0.0 & 1.2 kV/mm

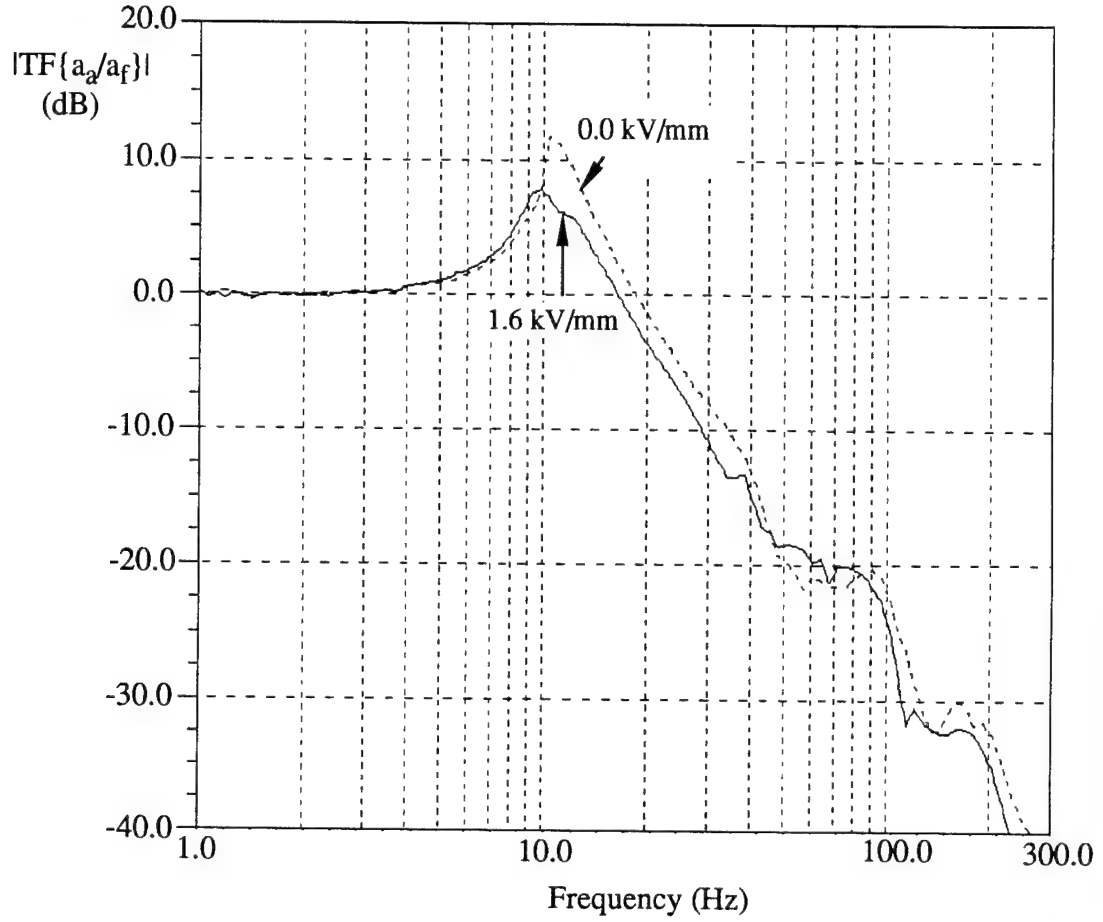

Figure 2.8. Magnitude of Transfer Function Versus Frequency for 0.0 & 1.6 kV/mm

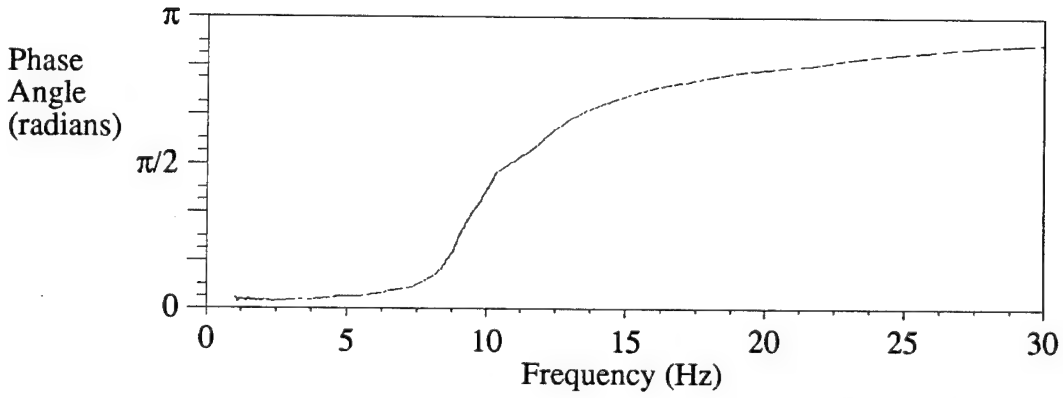

Figure 2.9. Measured Phase Angle for 1.6 kV/mm State Fluid

System Model

Since the measured phase angle data represents a single degree of freedom system, an ordinary differential equation, which describes the dynamics of a system containing a harmonically excited base, can be derived from Figure 2.10. The solution of this differential equation will result in expressions for the dynamic viscous damping and the dynamic stiffness of the system. These expressions can be used to quantify the damping effect of the ER fluid on the longitudinal vibration in the ER test module.

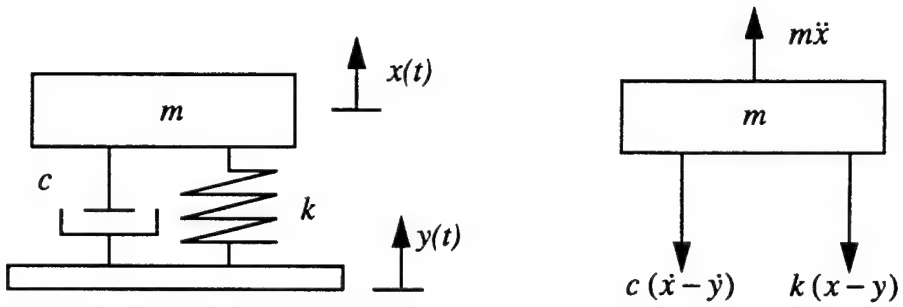

Figure 2.10. Single Degree of Freedom Model With Harmonically Excited Base

The dynamic free-body-diagram shown in Figure 2.10 contains the resulting forces generated by a harmonic excitation of the base. The summation of forces in the vertical direction (upward positive) yields the ordinary differential equation,

$$m\ddot{x} + c\dot{x} + kx = ky + c\dot{y}, \tag{2-1}$$

where m is the mass of the ER test module plus the point mass, c is the dynamic viscous damping coefficient, k is the dynamic stiffness of the ER test module, $x(t)$ is the longitudinal displacement of the aft position of the ER test module, $y(t)$ is the longitudinal displacement of the forward position of the ER test module, and the dot represents the first and second derivative of displacement with respect to time, t. If the harmonic excitation of the forward position is represented as $y(t) = Y_0 e^{i\omega t}$ and the response of the aft position is represented as $x(t) = X_0 e^{i\omega t}$, then the resulting model transfer function between the excitation and the response, from equation (2-1), is found to be

$$\frac{X_0}{Y_0} = \frac{k + ic\omega}{k - m\omega^2 + ic\omega}, \tag{2-2}$$

where X_0 is the static displacement of the aft position, Y_0 is the static displacement of the forward position, ω is the circular frequency, and i is the imaginary index ($\sqrt{-1}$).

Because the response of the aft position and the excitation of the forward position have the same steady state form of $e^{i\omega t}$, the model transfer function containing the ratio of displacements,

$$\frac{X_0}{Y_0} = \frac{\ddot{X}_0}{\ddot{Y}_0}, \tag{2-3}$$

will be the same as the ratio of accelerations. This allows the measured transfer function ($TF\{a_f/a_a\}$) consisting of the aft acceleration to the forward acceleration to be used in the definition of the dynamic viscous damping coefficient, $c(\omega)$, and the dynamic stiffness, $k(\omega)$. The development of the stiffness and viscous damping properties of the ER test module were achieved by inverting the model transfer function in equation (2-2) and multiplying by the complex conjugate of the new denominator, $(k - ic\omega)$, producing the following:

$$\frac{Y_0}{X_0} = \frac{k^2 - km\omega^2 + c^2\omega^2}{k^2 + c^2\omega^2} + \frac{cm\omega^3}{k^2 + c^2\omega^2}i = \frac{1}{TF\{\frac{a_a}{a_f}\}}, \tag{2-4}$$

where $TF\{a_a/a_f\}$ is the measured transfer function data consisting of the ratio of the aft acceleration, a_a, divided by the forward acceleration, a_f. The solution of the dynamic viscous damping coefficient and the dynamic stiffness in terms of the measured transfer function was accomplished by setting the imaginary and real components of the model transfer function equal to the respective components of the measured transfer function data,

$$\mathrm{Im}\left[TF^{-1}\{\frac{a_a}{a_f}\}\right] = \frac{cm\omega^3}{k^2 + c^2\omega^2}, \tag{2-5}$$

and

$$\mathrm{Re}\left[TF^{-1}\{\frac{a_a}{a_f}\}\right] = \frac{k^2 - km\omega^2 + c^2\omega^2}{k^2 + c^2\omega^2}, \tag{2-6}$$

where Im[] is the imaginary component and Re[] is the real component of the measured transfer function. By solving both equation (2-5) and equation (2-6) for $k^2 + c^2\omega^2$, and combining to

produce an expression for the dynamic viscous damping coefficient in terms of frequency and the dynamic stiffness,

$$c(\omega) = -\frac{k}{\omega}\left(\frac{\mathrm{Im}\left[TF^{-1}\{\frac{a_a}{a_f}\}\right]}{\mathrm{Re}\left[TF^{-1}\{\frac{a_a}{a_f}\}\right]-1}\right). \tag{2-7}$$

Substituting equation (2-7) into equation (2-5) (or equation (2-6)) produces an expression for the dynamic stiffness as a function of frequency,

$$k(\omega) = -\frac{m\omega^2\left(\mathrm{Re}\left[TF^{-1}\{\frac{a_a}{a_f}\}\right]-1\right)}{\left(\mathrm{Re}\left[TF^{-1}\{\frac{a_a}{a_f}\}\right]-1\right)^2+\left(\mathrm{Im}\left[TF^{-1}\{\frac{a_a}{a_f}\}\right]\right)^2}. \tag{2-8}$$

The dynamic damping ratio can be evaluated by dividing equation (2-7) by the critical damping coefficient, c_c. At a damping level equal to the critical damping coefficient, the system returns to the equilibrium state in a minimum amount of time and without oscillation. By definition, the critical damping coefficient can be expressed as

$$c_c = 2m\omega_n, \tag{2-9}$$

where ω_n is the natural frequency of the system. The natural frequency of the system is defined by

$$\omega_n = \sqrt{\frac{k(\omega)}{m}}. \tag{2-10}$$

The dynamic damping ratio, $\xi(\omega)$, has the following form:

$$\xi(\omega) = \frac{\omega}{2\sqrt{\frac{k(\omega)}{m}}}\frac{\mathrm{Im}\left[TF^{-1}\{\frac{a_a}{a_f}\}\right]}{\left(\mathrm{Re}\left[TF^{-1}\{\frac{a_a}{a_f}\}\right]-1\right)^2+\left(\mathrm{Im}\left[TF^{-1}\{\frac{a_a}{a_f}\}\right]\right)^2}. \tag{2-11}$$

The final qualitative measure of the frequency dependent damping characteristics of the ER test module is the amplitude ratio, $AR(\omega)$. The amplitude ratio, which is dimensionless, provides a measure of the displacement decay as a function of the damping applied to the system. For a single degree of freedom system which has a harmonically excited base, the amplitude ratio is found to be the following:

$$AR(\omega) = \sqrt{\left[\frac{1-(\omega/\omega_0)^2[1-4\xi^2]}{(1-(\omega/\omega_0)^2)^2+(2\xi(\omega/\omega_0))^2}\right]^2+\left[\frac{2\xi(\omega/\omega_0)^3}{(1-(\omega/\omega_0)^2)^2+(2\xi(\omega/\omega_0))^2}\right]^2}, \qquad (2\text{-}12)$$

where the resonant frequency, ω_0, used was for the zero volt case and the damping ratio, ξ, is dependent on frequency as described by equation (2-11).

The ***FORTRAN*** programs developed to numerically evaluate equations (2-7), (2-11), and (2-12) are found in Appendix A.

Results

Interpretation of the dynamic stiffness (equation (2-8)) and the dynamic damping ratio (equation (2-11)) results allows identification of stiffness and damping mechanisms within the ER test module with a constant electric field. The effect of the electric field is illustrated by normalizing the dynamic stiffness and the dynamic damping ratio by their respective zero state values. The plot of the normalized dynamic stiffness as a function of frequency, Figure 2.11, for various values of the electric field is represented by frequency plotted along the abscissa in units of cycles/second (Hz) and the relative decrease/increase in stiffness plotted along the ordinate. A slight increase in the dynamic stiffness of the ER test module is observed for electric field strengths between 0.4 and 1.2 kV/mm. As a result of this increase, the resonant frequency of the activated structure also slightly increased. The natural frequency corresponds to the minimum value of stiffness in Figure 2.11 at a given electric field. The increase of the resonant frequency at electric field values up to 1.2 kV/mm is similar to the results of Coulter et al. (1989).

When the electric field is increased from 1.2 kV/mm to 1.6 kV/mm, however, the dynamic stiffness of the system is reduced below that of the zero state. This reduction accounts for the decrease in the resonant frequency mentioned earlier in the discussion of Figure 2.8. Such a transition in stiffness indicates that the damping mechanism within the ER test module has shifted

from hysteretic (0.0 to 1.2 kV/mm) to viscous (1.6 kV/mm) (Nashif et al. (1985)).

An applied electric field increases the dynamic damping ratio of the ER test module. This is shown, in Figure 2.12, by the plot of the normalized dynamic damping ratio as a function of frequency for various values of the electric field, represented by frequency plotted along the abscissa in units of cycles/second (Hz) and the relative increase in damping plotted along the ordinate. The damping ratios for the intermediate range of the electric fields (0.4 - 1.2 kV/mm) are nearly identical. When the electric field is increased to 1.6 kV/mm, the damping ratio increases by a factor of 1.75 over the zero state. At frequencies greater than 17.5 Hz, the damping characteristics of the 1.2kV/mm state is approaching that of the 1.6kV/mm case. The resulting yield shear stress produced at 1.2 kV/mm is not sufficient to maintain the yield surfaces near resonance, therefore, the damping performance is typical of the lower electric field strengths. As the frequency increases past the point of resonance, the magnitude of the generated forces are less, thus, the yield surfaces produced are able to dissipate the higher frequency (> 17.5 Hz) vibrational energy in a mode similar to the 1.6kV/mm case.

The amplitude ratio can be calculated from the results of the dynamic stiffness and dynamic damping ratio. It is a convenient measure of the reduction of the vibrational energy in the system, and is plotted in Figure 2.13, where the abscissa represents the ratio of frequency to the zero state natural frequency of the ER test module and the ordinate represents the amplitude ratio (nondimensional). Figure 2.13 also clearly demonstrates how resonant frequency varies as a function of electric field strength. The reduction in the magnitude of vibrational amplitude for the 1.6-kV/mm state compared with the magnitude of the zero state represents an attenuation of 4.0 dB for the corn starch/mineral oil fluid. The amplitude ratio shows a reduction in the transmitted vibration for values of the frequency ratio less than or equal to $\sqrt{2}$ due to the viscous damping; however, at values of the frequency ratio greater than $\sqrt{2}$, the viscous damping contributes to the transmission of the vibration. This effect is characteristic of classical viscous damping devices.

The overall damping effect that the ER fluid has on the longitudinal vibration can also be expressed in the time domain. Figure 2.14 shows the rate of decay of the oscillation in the flexible cylinder. This figure compares the zero state to the 1.6-kV/mm state. The damped period of the oscillation is related to the logarithmic decrement. These results show a fourfold increase in the logarithmic decrement when the fluid is activated by the electric field. The calculated logarithmic decrement for the 1.6-kV/mm data is approximately equal to that of a 6-month-old automobile shock absorber (Steidel, (1979), p. 185).

The transition of the damping mechanism within the ER test module as the electric field is increased from 1.2 to 1.6 kV/mm can be explained by the increase in the yield shear stress of the ER fluid. The damping characteristics shown at the electric fields of 0.0, 0.4, 0.8, and 1.2 kV/mm indicate a hysteretic type mode. This is evidenced by the reduction of the transmissibility as the electric field increased with no decrease in the center frequency. The mode of damping produced at the electric field strength of 1.6kV/mm is typical of a viscous damper, since the center frequency and magnitude decreased. The transition of the damping mechanisms occurred as the electric field increased from 1.2kV/mm to 1.6kV/mm developing a fluid region which resisted the shear imposed by the boundary excitation.

The dissipation of the vibrational energy is accomplished through the resulting shear forces within the ER fluid. The establishment of yield surfaces within the ER fluid is attained by the spatial variation of the applied electric field. Since the magnitude of the yield stress is dependent on the magnitude of the applied electric field, a spatial variation in the developed yield stress will result. The mathematical understanding of the dissipation mechanisms within the ER fluid will provide an accurate model that would allow theoretical experiments to be conducted on configurations impossible to regulate through experimentation. Modeling the shear interfaces within the ER test module (see Chapter 5) will allow specification of the rheological properties that would be necessary to provide a specified amount of damping. The mathematical knowledge of these loss mechanisms in terms of the fluid dynamics of the ER test module is discussed in the following chapters.

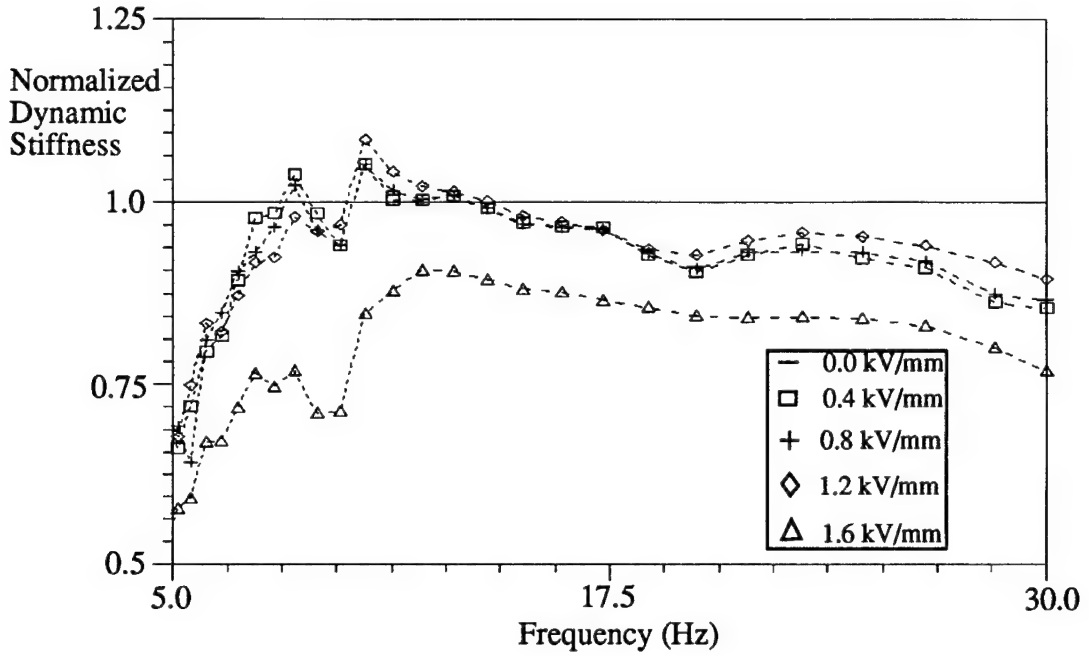

Figure 2.11. Normalized Stiffness as a Function of Frequency at Various Electric Fields

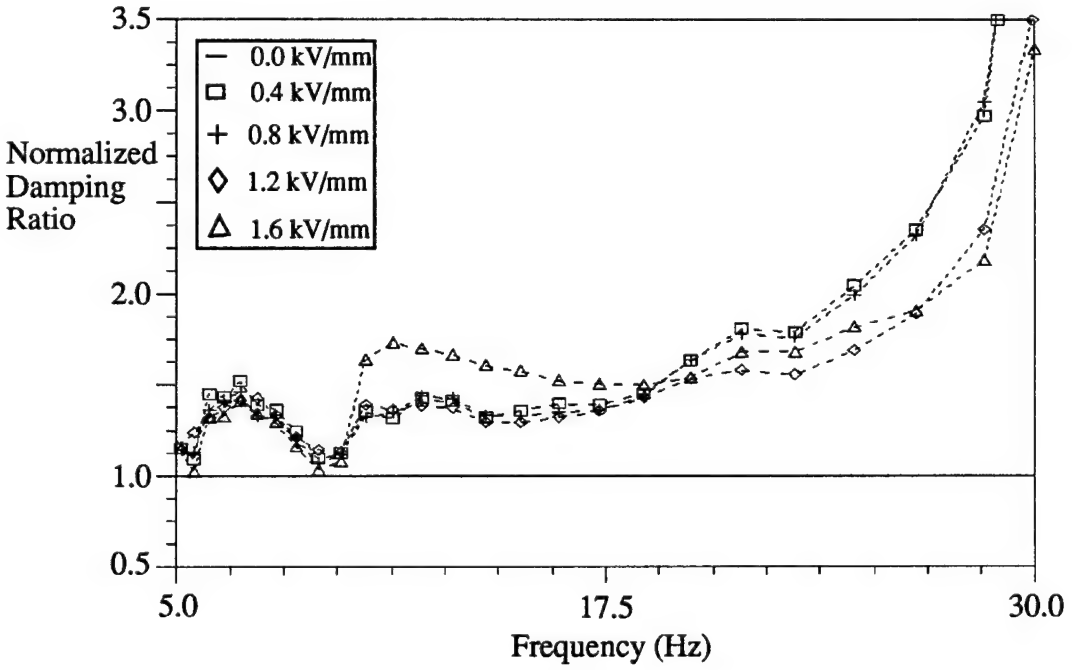

Figure 2.12. Normalized Damping as a Function Frequency at Various Electric Fields

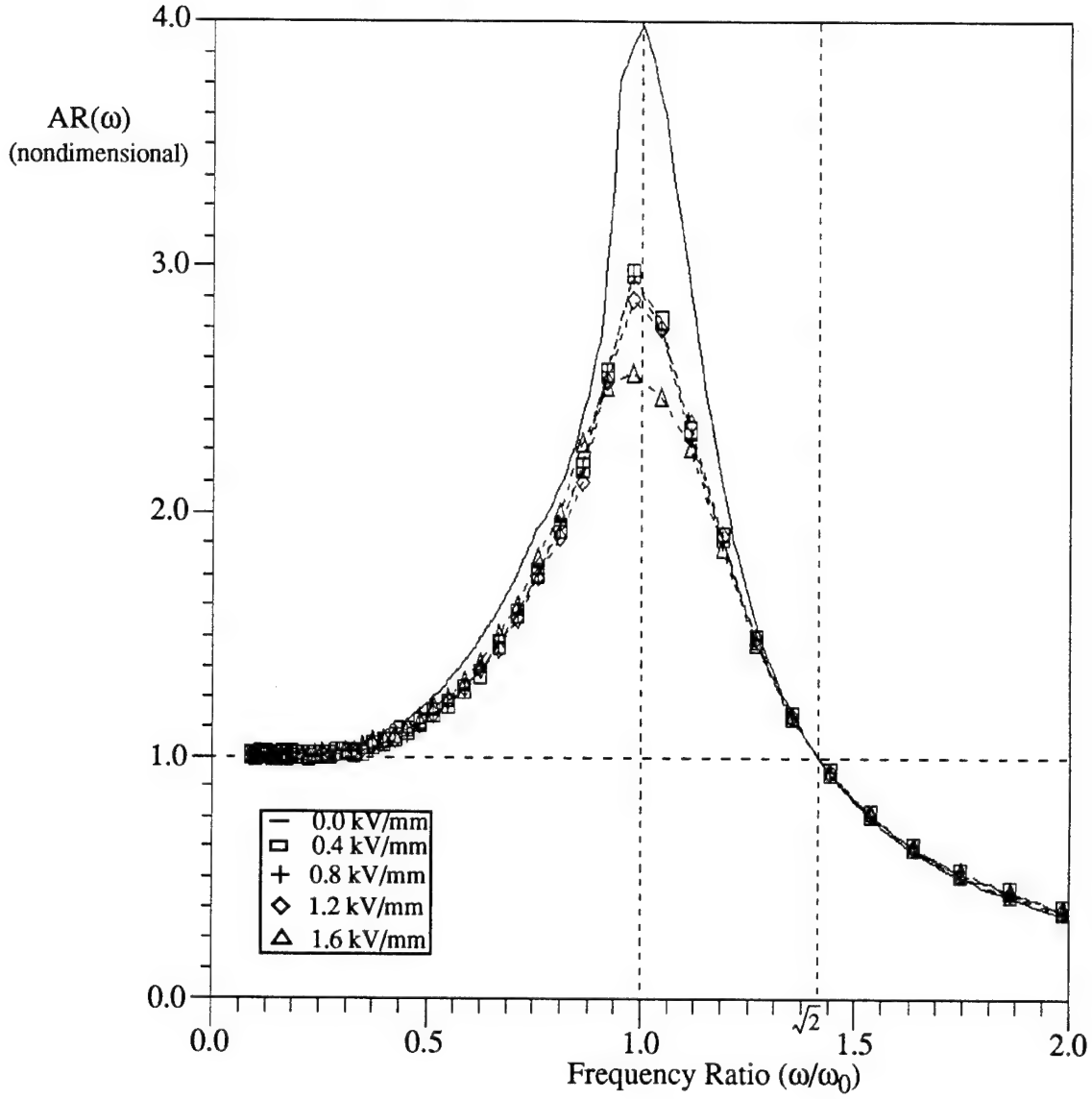

Figure 2.13. Amplitude Ratio as a Function of Frequency at Various Electric Fields

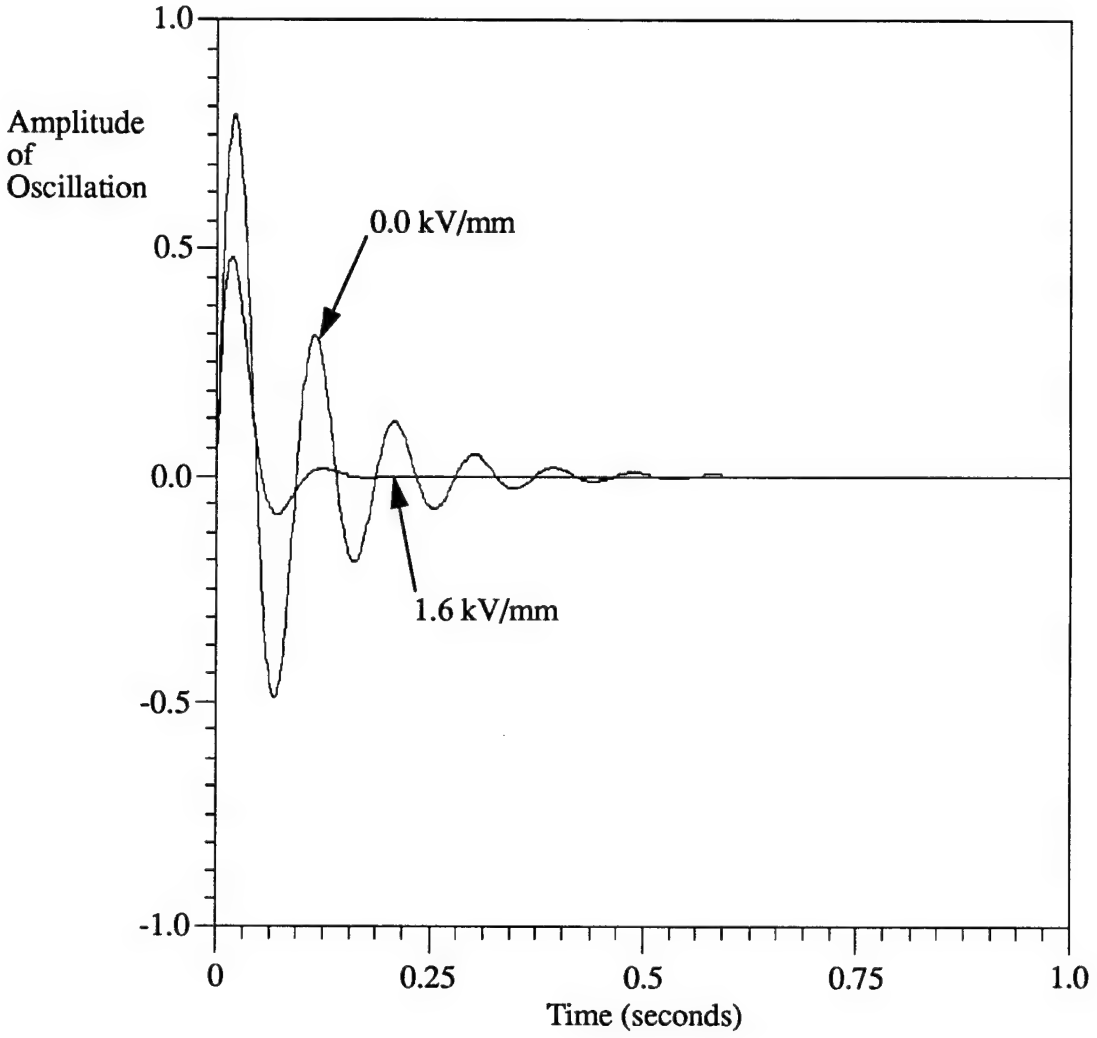

Figure 2.14. Time Decay of Oscillation for ER System at 0.0 kV/mm and 1.6 kV/mm

Summary

The application of an ER fluid to attenuate the longitudinal vibrations in a flexible cylinder is modeled with a second order transfer function and validated with an experiment. Based on the system model and the data from the transmissibility experiments, the electric field dependence of the ER fluid damping mechanisms was illustrated. The application of an electric field produced an increase in the resonant frequency as well as a reduction in the amplitude of the oscillation. The analysis of these experiments using the system model illustrated a transition in the damping mechanism of the ER fluid. This transition produced a reduction in both magnitude and resonant frequency when the electric field was increased to 1.6 kV/mm. This transition to the 1.6 kV/mm electric field developed a fluid region which was able to resist the shear imposed by the boundary excitation. The fluid state at 1.6 kV/mm produced a significant increase in the damping ratio and the logarithmic decrement compared to the other electric field values. The data sets for the zero state and the 1.6 kV/mm are found in Appendix E.

Chapter 3: Electric Field Solution

Introduction

The experimental results in Chapter 2 showed that the damping characteristics of the ER fluid changed dramatically when the applied electric field transitioned from 1.2 kV/mm to 1.6kV/mm. In order to model the fluid damping mechanisms of the system, the electric field producing the rheological changes in the system must be analyzed. The solution to the applied electric field was accomplished using closed form conformal transformation techniques. This method was used instead of numerical simulation in order to reduce the computational time required. The resulting solution utilizes Jacobian elliptical functions and integrals which were evaluated numerically.

Electric Field Problem Statement

An electrostatic field was used to activate the electrorheological fluid inside the test module. The governing equations used to describe the electrostatic field, containing no space charges, are as follows (Schwab (1988)):

$$\nabla^2 \Phi (r, z) = 0 \tag{3-1}$$

$$\boldsymbol{E}(r, z) = -\nabla\Phi(r, z) \tag{3-2}$$

where Φ is the voltage potential scalar function, $\boldsymbol{E}$ is the resulting electric field vector, ∇^2 is the Laplacian operator in cylindrical coordinates, and ∇ is the gradient operator in cylindrical coordinates. The solution of Laplace's equation provides a voltage potential function (Φ) and the resulting electric field $(\boldsymbol{E})$ can be found from the negative gradient of this voltage potential function. In this application, the electric field between the electrodes and the fringe field around the electrodes is of interest. The fringe field will influence the properties of the electrorheological fluid as the electric field decays from the center of the electrorheological test module to the inner wall of the module. Based on the magnitude of the electric field within the electrorheological test module, the rheological properties of the fluid, as a function of the radial and longitudinal directions, are calculated. The rheological properties of importance are the pre-yield shear stress, τ_o, and the post-yield viscosity, μ. The relationship between the rheological properties of the fluid and the applied electric field will be discussed in the next chapter.

The electrostatic problem is defined as an array of electrodes parallel to each other and perpendicular to the longitudinal axis of the test module (Figure 3.1).

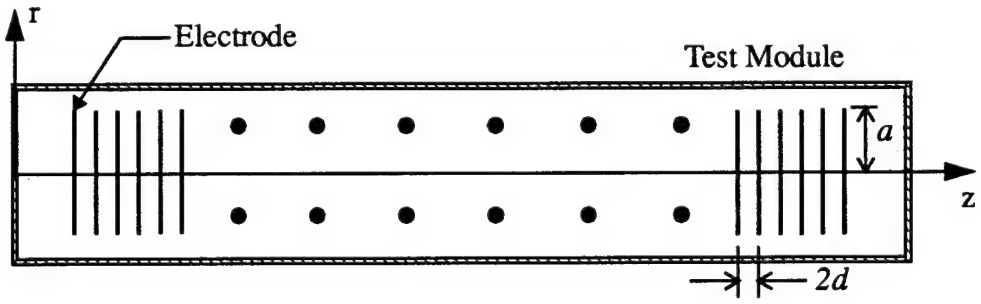

Figure 3.1. Electric Field Device

The electrodes are circular disks of radius *a* separated by a distance of 2*d*. The gap between the electrodes is measured between the inner faces of neighboring disks. The thickness of the electrodes has been neglected. The configuration of the electric device in the electrorheological

module consists of 170 electrodes each having a diameter ($2a$) of 31.75 millimeters (mm) and a spacing ($2d$) of 5 mm. The voltage potential, Φ_0, on the electrodes is assumed uniform across the face of the disk. This model simulates the electric field device from Chapter 2.

Closed form solutions of electrostatic problems have been accomplished in Cartesian coordinates by Mitchell (1894) for a two plate condenser problem, Love (1924) for a two plate electrode problem, Binns & Lawernson (1963) for the fringe field between two parallel plate electrodes, and Lawden (1989) for the parallel plate capacitor problem, as well as others. Solution technique utilized in the literature for the parallel plate electrodes has been by conformal transformation (complex potential functions) of Laplace's partial differential equation. The analytical solution to the parallel circular disk problem is presented in Moon & Spencer (1953), and involves the use of conformal transformations based on elliptic functions.

Conformal Transformation

The conformal transformation, based on elliptic functions, proposed by Moon & Spencer (1951, 1953), was used to determine the electrostatic field and the decrease in the magnitude of the electric field strength as the radial distance increases.

If a conformal transformation exists for a regular function, the equipotential and flux curves can be plotted to produce a field map. A function is classified as a regular function provided that all of the derivatives exist, are continuous and satisfy the Cauchy-Riemann equations. The regular function considered in this transformation consists of a complex variable $y = r + iz$ as a function of another complex variable $w = u + iv$. This requires the conformal transformation to have the form

$$y(r, z) = r + iz \Rightarrow w(u, v) = \varphi(u, v) + i\psi(u, v), \tag{3-3}$$

where φ represents the potential function, ψ represents the flux function, and u,v are the independent variables of the transformed w space. The flux crossing a line between two points or the potential difference between two points is not altered by the transformation. Thus, conservation of flux and potential is maintained through the transformation. For the given problem, the transformation provided in Moon and Spencer (1988) gives the field solution in the form of equation (3-3) as

$$y(r,z) = r - iz \Rightarrow \frac{2Kd}{\pi}\Im(w + iK') + id, \tag{3-4}$$

where d is one-half the electrode separation, $\Im$ is the Jacobian Zeta function, K and K' are the complete elliptic integrals of the first kind. In terms of the physical problem, the complete elliptic integral of the first kind, K, represents the voltage potential applied to the electrodes. The expressions defining the Jacobian Zeta function, the Jacobian elliptic functions and the elliptic integrals can be found in Appendix B. These doubly periodic, meromorphic functions are plotted in Figure 3.2. Expressed in the form of equations (3-3) and (3-4), w is the complex variable containing a real component u and an imaginary component v. When substituting $w = u + iv$ into equation (3-4), the potential and flux functions from the transformation equation [Equation J6C, page 85, of Moon & Spencer (1988)] were obtained as

$$\varphi(u,v) = \frac{2Kd}{\pi}\left(\Im(u) + \frac{m\,sn(u)\,cn(u)\,dn(u)\,sn(v')^2)}{1 - dn(u)^2 sn(v')^2}\right) \tag{3-5}$$

$$\psi(u,v) = \frac{2Kd}{\pi}\left(\Im(v') + \frac{\pi v}{2KK'} - \frac{dn(u)^2 sn(v')\,cn(v')\,dn(v')}{1 - dn(u)^2 sn(v')^2}\right) \tag{3-6}$$

where φ represents the potential function, ψ represents the flux function, $v' = v + K'$, *sn()*, *cn()*, and *dn()* are the Jacobian elliptic functions evaluated at the argument u with modulus m and the argument v' with modulus m'. At the modulus value of 0.5, the modulus is equal to the complementary modulus ($m = m'$) and the elliptic integrals K, K', E and E' are also equal to their respective complementary value. This analysis was completed with a modulus value of 0.5, although m can range from zero to one. The choice of a modulus value of 0.5 was made to simplify the evaluation of the elliptic integrals and Jacobian functions.

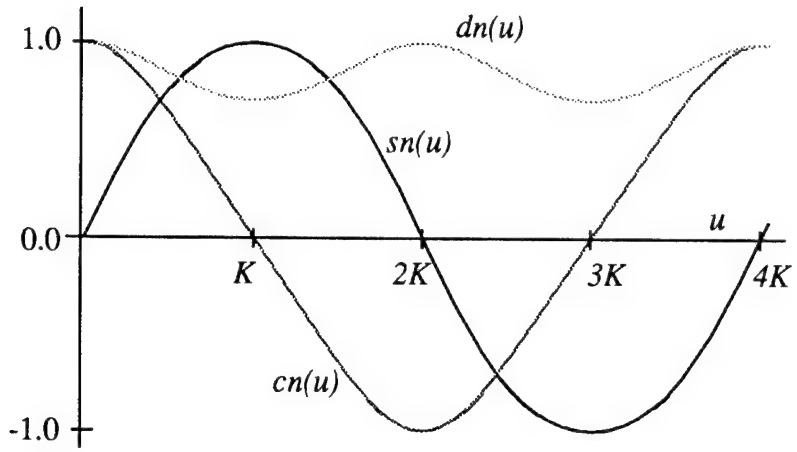

Figure 3.2. Jacobian Elliptic Functions

Electric Field Calculation

The solution transformation is of the form $y = f(w)$, which allows the direct calculation of the electric field. The field calculation is made by setting u and v to values between zero and K. The algorithms used to evaluate the Jacobian elliptic functions were power series approximations found in Abramowitz & Stegun (1970). The Jacobian Zeta function was evaluated using (Abramowitz & Stegun (1970))

$$\Im(u) = \int_0^u dn(t)^2 dt - u\frac{E}{K}. \tag{3-7}$$

The elliptic integrals were numerically calculated using a twelve point Gaussian integration scheme. The evaluation of the Jacobian elliptic functions, the Jacobian Zeta function and the elliptic integrals were made by the *FORTRAN* programs listed in Appendix B. The accuracy of these routines is of the order of six places, and was evaluated by comparison to tabulated values in Milne-Thomson (1932).

The geometric value of the electrode radius is defined by the following expression

$$L_{electrode} = \frac{2Kd}{\pi}\Im_{max}. \tag{3-8}$$

This relationship is dependent on the values of the complete elliptic integral of the first kind and the maximum value of the Jacobian Zeta function at the given modulus of one-half. The electrode dimension was calculated from equation (3-8) as 0.4334 mm. Since the problem is linear and homogeneous, the solution can be scaled in the radial direction to approximate the given geometry of the specific problem. The resulting scale factor for the radial direction was found from the ratio of the actual electrode radius (15.875 mm) to the transformation defined electrode radius (0.4334 mm) to be $sf = 36.63$.

The transformation, as given by equation (3-5) and equation (3-6), models the electric field between two isolated electrodes. The resulting electric field map for two isolated electrodes is illustrated in Figure 3.3. The solution of the electric field for an array of electrodes (Figure 3.1) will be accomplished by using this solution and the existing symmetry planes. The symmetry of the electric field produced by the electrode array allows certain regions of the field to be rotated about the vertical electrode axis to build the electric field of the 170 electrode array. The symmetry planes, shown in Figure 3.3, consist of a vertical plane where the potential function is zero ($\varphi = 0$) and a second vertical plane where the flux function is zero ($\psi = 0$). By mirror imaging the electric field in the region between the symmetry planes, the complete electric field for the full electrode array can be developed. In addition to the symmetry, the potential curves are concentric symmetric ellipses centered about the electrode locations. This condition is not valid for the two end electrodes. The electric field map for the end electrodes is also represented by the isolated electrode pair solution. The region of the field utilized from the isolated pair solution for the two end electrodes in the full array is shown in Figure 3.3 where the dots depict the potential and flux lines of the electric field. The potential lines have a characteristic shape of an ellipse, while the flux lines are perpendicular to the potential lines. The electric field contour lines have the same mapping as the flux lines.

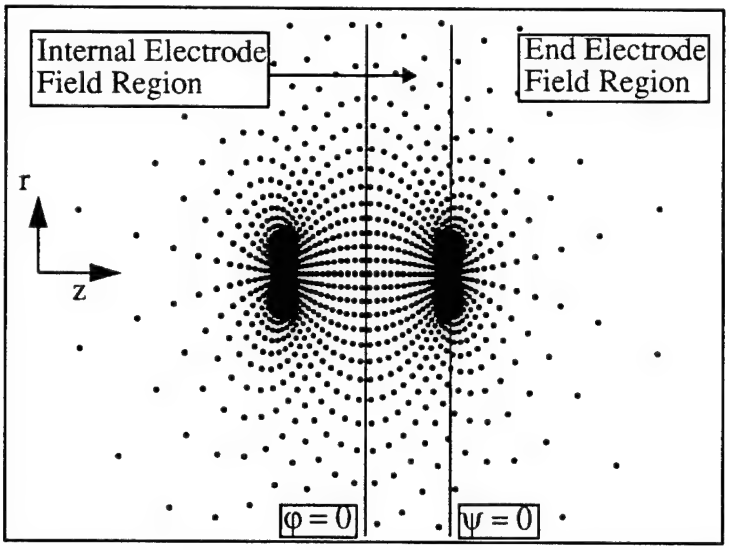

Figure 3.3. Electric Field Solution for Isolated Electrode Pair

Due to the large size of the electric field device, an electric field plot for the complete 170 electrode array would be too dense to graphically resolve the detail of the field. The above solution technique for resolving the electric field generated by an array of parallel electrodes can be illustrated by considering the electrode array shown in Figure 3.4. The electric field of the three electrode array will be developed based on the solution of the isolated pair (Figure 3.3). The boundary conditions for the three electrode example consist of a voltage potential Φ_o, positive in value, on electrodes A and C. The voltage potential applied to electrode B has a value of - Φ_o.

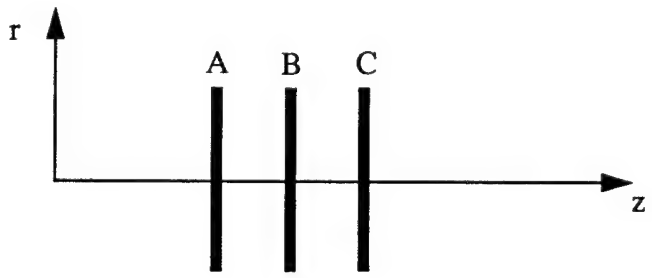

Figure 3.4. Three Electrode Example

The electric field surrounding the center electrode, B, is influenced by the electrodes on either side (A and C); therefore, the electric field would not be of the form illustrated in Figure 3.3. The

potential curves will be concentric, symmetrical ellipses centered about the vertical axis of electrode B; the potential curves in Figure 3.3 are asymmetric with respect to the vertical axis of the electrodes. This symmetry is due to the influence of the surrounding electrodes (A and B). The internal electrode region of the transformation solution (Figure 3.3) was used to resolve the electric field between the three electrodes. By reflecting this portion of the solution about the electrode axis, the solution to the electric field of the middle electrode, B, was obtained. The outer field solution for the two end electrodes (A and C) was accomplished by using the end electrode region of the electric field map (Figure 3.3). The electric field solution for any number of intermediate electrode cells can be obtained by duplicating the results of the middle electrode, B. The resulting electric field produced by the three electrode array is shown in Figure 3.5. This electric field is consistent with that presented in Maxwell (1892, Figure XI.), for an array of parallel, rectangular plate electrodes. The potential curves are symmetric about the middle electrode and the potential curves about the two end electrodes exhibit an asymmetry with respect to the vertical axis. The electric field plots shown in Figure 3.3 and Figure 3.5 were generated by encoding the conformal transformation solution in *FORTRAN*. This program, called *EFIELD*, is included in Appendix B.

The final solution for the electric field of the full electrode array would consist of three hundred and thirty-six repetitions of the internal electric field solution bounded by the end electric field solution. The three hundred and thirty-six repetitions of the internal electric field solution is due to the domain of the internal solution. The internal solution domain is from an electrode to the midpoint distance between the electrode pair (Figure 3-3). Therefore, for each electrode pair the internal solution must be repeated twice to complete the distance between them. The rheological properties of the electrorheological fluid depend on the magnitude of the electric field strength as a function of the longitudinal direction (z-axis) and the radial direction (r-axis). Once the voltage potential function is known, the electric field strength can be calculated from equation (3-2). The decay of the electric field strength as a function of the radial direction and the characteristics of the electric field strength as a function of the longitudinal direction is determined by the closed form conformal transformation solution discussed in this section. The formulation of the magnitude of the electric field strength is developed in the following section. The result that was applied to the constitutive relationship of the electrorheological fluid was a spatial description of the electric field strength of the one hundred seventy electrode array.

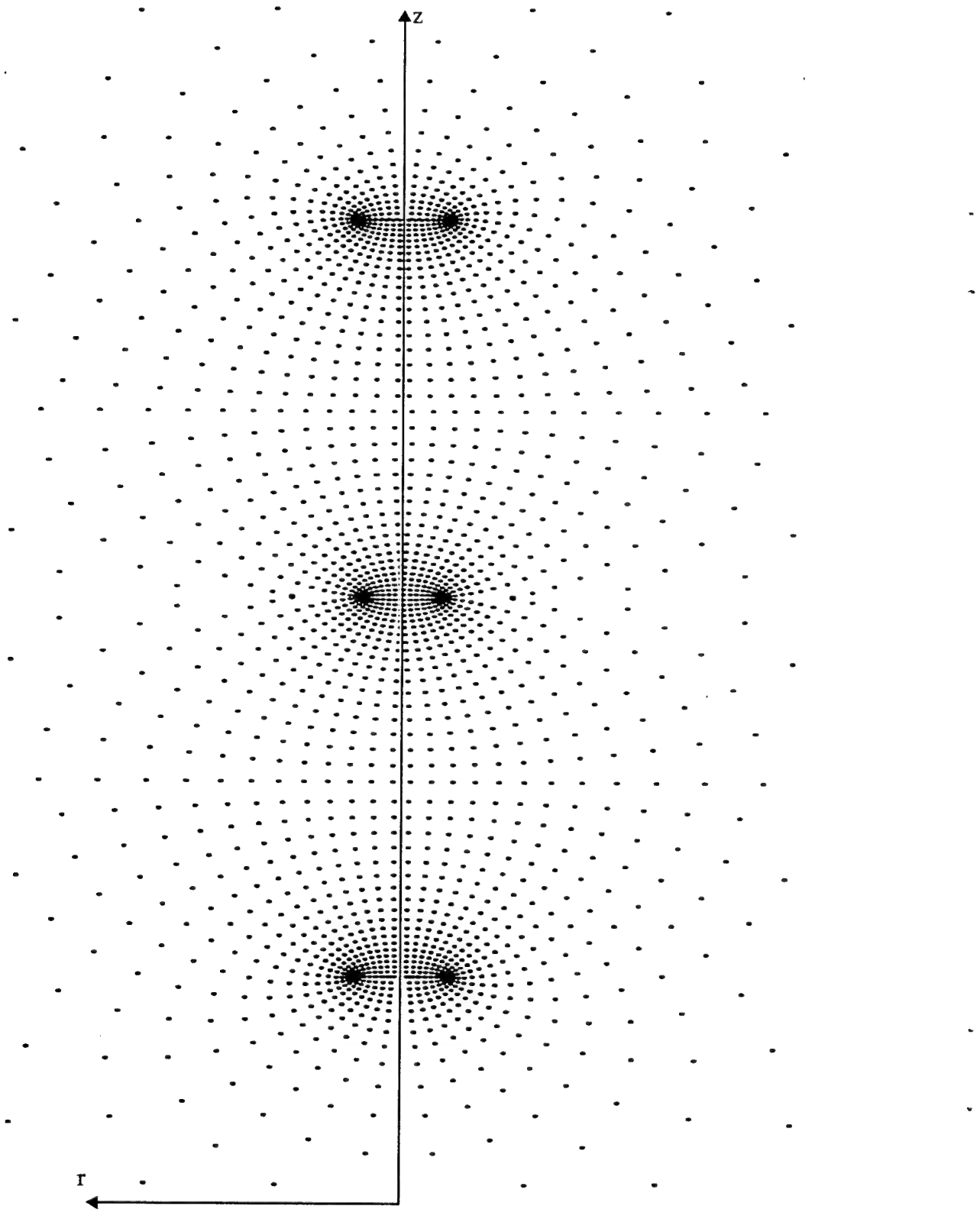

Figure 3.5. Electric Field Map Resulting from the Three Electrode Example.

Electric Field Strength Calculation

The magnitude of the electric field evaluated by the conformal transformation discussed in section 3.3 was developed from equation (3-2) and the Cauchy-Riemann relationships (equation (3-9)) for potential functions. The Cauchy-Riemann conditions require the flux and potential functions to have the following relationships:

$$\frac{\partial \varphi}{\partial r} = \frac{\partial \psi}{\partial z}$$
$$\frac{\partial \varphi}{\partial z} = -\frac{\partial \psi}{\partial r} \tag{3-9}$$

It has been shown (Binns & Lawrenson, (1963)) that the derivative of the conformal transformation, applying the Cauchy-Riemann conditions, yields the electric field strength as a function of the radial and longitudinal directions. The magnitude of this expression can be evaluated at discrete spatial locations in the electric field to calculate the electric field strength. The magnitude of the electric field strength can be expressed as

$$|\boldsymbol{E}| = \left|\frac{dw}{dy}\right|, \tag{3-10}$$

for an electrostatic field containing no space charges. The form of differentiation in equation (3-10) matches the reciprocal of the transformation given in equation (3-4). The differentiation of equation (3-4) produces the following expression (details in Appendix B):

$$\frac{dy}{dw} = -2K\frac{d}{\pi}\left[\left[\frac{cn(w)}{sn(w)}\right]^2 + \frac{E}{K}\right]. \tag{3-11}$$

By substituting the independent variables for the complex potential function w, the real and imaginary parts of the expression can be separated so that the magnitude of the electric field strength can be evaluated from expression (3-11). The substitution of $w = u + iv$ reveals the real and imaginary components of equation (3-11) to be

$$\frac{dy}{dw} = -2K\frac{d}{\pi}\left[\left[\frac{\Theta\Delta - \Xi^2}{\Omega} + \frac{E}{K}\right] - i\left[\frac{\Xi\Theta + \Xi\Delta}{\Omega}\right]\right], \tag{3-12}$$

where

$$\begin{aligned}\Theta &= (cn(v)\,sn(u)\,dn(v))^2 - (sn(v)\,cn(u)\,dn(u)\,(cn(v))^2)^2 \\ \Delta &= (cn(v))^4\,(cn(u))^2 + (sn(u)\,sn(v)\,dn(u)\,dn(v)\,cn(v))^2 \\ \Xi &= 2\,(cn(v))^3 cn(u)\,sn(u)\,sn(v)\,dn(u)\,dn(v) \\ \Omega &= (\Theta)^2 + (\Xi)^2\end{aligned} \tag{3-13}$$

From equations (3-12) and (3-13), the strength of the electric field at a discrete point (u,v) within the field can be calculated by equation (3-14).

$$|\boldsymbol{E}| = \left|\frac{dw}{dz}\right| = \left[\left[-2K\frac{d}{\pi}\right]^2\left[\left[\frac{\Theta\Delta - \Xi^2}{\Omega} + \frac{E}{K}\right]^2 + \left[\frac{\Theta\Xi + \Delta\Xi}{\Omega}\right]^2\right]\right]^{-0.5} \tag{3-14}$$

The evaluation of the electric field strength as a function of radial and longitudinal direction, for the one hundred seventy electrode array was accomplished using equation (3-14). The electric field strength was calculated as the radial dimension was increased from the radius of the electrode to 600 mm at a longitudinal position fixed between two electrodes. The maximum magnitude of the electric field was found at the midpoint between the electrode separation. The magnitude of the electric field decreased as the longitudinal location approached that of the electrode. At the vertical plane of the electrodes, the magnitude of the electric field becomes zero. The decay of the electric field is shown in Figure 3.6 for a potential of ±1854 volts applied to the electrodes. Figure 3.6 depicts the electric field between an electrode pair. The solution for the electric field strengths used in the Attenuation Experiment (Chapter 2) will be scaled from this solution. The conformal transformation solution sets the potential applied to the electrodes equal to the elliptic integral of the first kind, K (K = 1.854 at m = 0.5). Equation (3-14) was numerically evaluated using the *FORTRAN* program *EMAG* found in Appendix B.

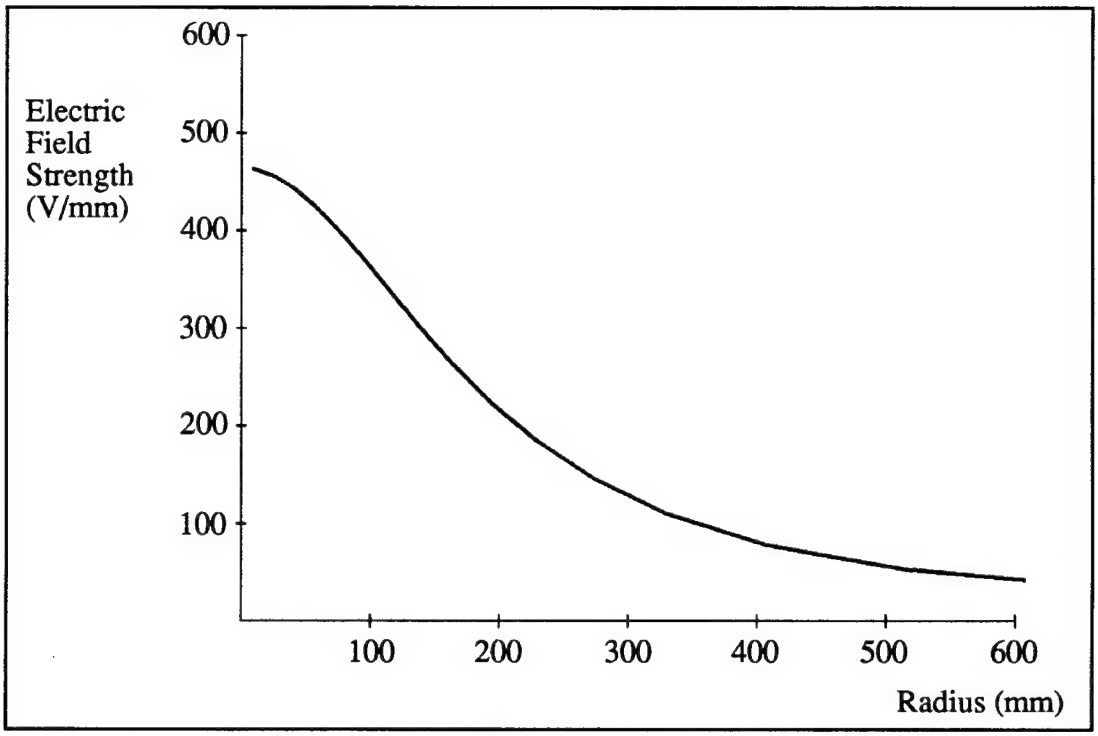

Figure 3.6. Decay of Electric Field Strength Between Electrode Pair

The magnitude of the electric field at any location within the field can be calculated from equation (3-5), equation (3-6) and equation (3-14) to evaluate the pertinent rheological properties of the electrorheological fluid within the test module. Since the electric field is a steady state, direct current application, the magnitude of the field cannot change. This allows a table of the magnitude of the electric field, at specific locations in the field, to be constructed. The local values of the electric field can be utilized to determine the appropriate rheological parameters governing the fluid flow at that specific location. The steady nature of the electric field allows the field magnitudes to be calculated only once for each applied voltage considered.

Summary

The application of the ER phenomenon requires an understanding of the electric field necessary to activate the fluid. The closed form solution to the electric field between an array of circular electrodes is developed to resolve the spatial decay of the field in terms of Jacobian elliptic functions. A conformal transformation solution technique is used to develop a potential function and a flux function. The magnitude of the electric field is evaluated from these elliptic

function based expressions. The expression derived in this chapter for the magnitude of the electric field, as a function of radial and axial locations, is used to determine the rheological parameters of the corn starch and mineral oil ER fluid used in the attenuation experiments.

Chapter 4: ER Fluid Constitutive Relationships

Introduction

In order to exploit the ER phenomenon in an engineering application, an understanding of the constitutive properties of the working fluid is required. The material behavior of an ER fluid has been found to depend on the applied electric field, the dielectric properties of the carrier fluid, the dielectric properties of the particles, the particle size, the concentration of particles, temperature, water content, and frequency. Klass & Martinek (1967) discuss the dependence of the yield shear stress on the square of the electric field magnitude. They also discuss the effect of ER particle volumetric concentration, and the dielectric properties of the particles on the apparent viscosity. Jordan & Shaw (1989) provide a direct link between the particle structure development and the rheological changes of the ER fluid as a function of the electric field. Wong & Shaw (1989) discuss the role of water content in the ER fluid as the mechanism dictating the particle structure. This is investigated in terms of the electric field strength, moisture content, and dynamic oscillatory shear. Block & Kelly (1988) discuss the relationship of Bingham behavior to particle concentration. They find that the optimum yield shear stress is achieved at volumetric concentrations between 0.1 and 0.4. They also report that the particle size is not a critical parameter. Brooks et al. (1986) discuss the effect on the yield shear stress of the electric field strength, volume fraction, and water content of the particles. Bonnecaze & Brady (1992) determine the Bingham yield shear stress from a microstructural model. Tao et al. (1989) formulates the Helmholtz free energy expression of an ER fluid system. This free energy expression is used to determine a critical electric field at which a phase transition occurs in the fluid. It has been shown through experimental methods that the effect of volumetric concentration and temperature (Marshall et al. (1989)), the effect of the electric field strength on the particle structure (Gast & Zukoski (1989)), and the Bingham parameter dependence on the electric field, particle size, and concentration (Klingenberg (1990)) alter the Bingham parameters. Additionally, numerical methods illustrate the use of the quadratic electric field strength relationship to the yield shear stress of the fluid (Wang (1989)). The conclusion of these researchers is that the

constitutive behavior of ER fluids can be modeled accurately as a Bingham fluid. The Bingham material model applied to an ER fluid depends on the applied electric field, the developed yield shear stress, and the plastic viscosity.

Before the damping mechanisms along the ER fluid yield surfaces can be modeled for the present investigation, the Bingham fluid properties have to be defined for the corn starch and mineral oil ER fluid described in Chapter 2. The measured properties of that fluid consisted of the electric field dependent yield shear stress and the fluid viscosity.

Classification of non-Newtonian Fluids

The behavior of ER fluids has been classified as a non-Newtonian fluid, because the Bingham fluid model has the capability to resist an applied shear stress. The general behavior of non-Newtonian fluids can be categorized into three groups: time dependent fluids, visco-elastic fluids, and time independent fluids. The time dependent fluids are characterized by the dependence of the shear strain rate on the magnitude and duration of the applied shear stress. In addition, the time history of the shear stress application may also influence the shear strain rate. There are two types of time dependent fluids, Thixotropic and Rheopectic. The thixotropic fluid features a reduced shear stress with time at a constant rate of shear strain. The internal component structure of the thixotropic fluid breaks down progressively with time. The rheopectic fluid exhibits the opposite characteristics in that the shear stress increases with time at a constant rate of shear strain. In this case, the internal component structure of the rheopectic fluid builds with a low rate of shear strain. In both types of fluids, the processes are reversible and illustrate a hysteric profile. These characteristics are shown conceptually in Figure 4.1. Examples of thixotropic fluids are margarine and printing ink, and examples of rheopectic fluids are clay suspensions and gypsum suspensions.

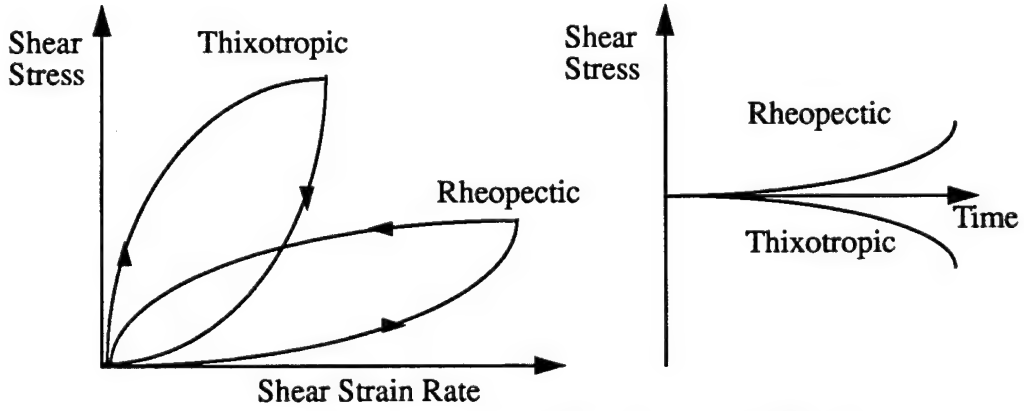

Figure 4.1. Flow Curves for Time Dependent Fluids

The second classification of a non-Newtonian fluid is the visco-elastic fluids. The visco-elastic fluids show partial recovery when the deforming shear stress is removed. These materials exhibit the properties of fluids and solids such that the material may be viscous and retain a certain elastic shape. The effects of elastic recovery are only influential when the flow occurs through irregular shapes, as in flow through orifices and valves. The common examples of the visco-elastic fluids are pine pitch, napalm jelly and certain polymer melts such as nylon. The constitutive relationships governing visco-elastic materials are typically expressed as mechanical analogies such as the Voigt body and the Maxwell body (Wilkinson, (1960)). These relationships model the rheological parameters as springs and dash-pot dampers. The spring represents the Hookean elasticity properties while the dash-pot represent the Newtonian viscosity of the material.

The final classification of non-Newtonian fluids is the time independent fluid. Time independent fluids have the characteristic that at any location in the fluid, the rate of shear strain is only dependent on the shear stress at that location. The time independent fluids can be further subdivided into pseudoplastic fluids, dilatant fluids, and Bingham plastic fluids. Figure 4.2 represents the characteristics of the flow curves typical of these fluid classifications.

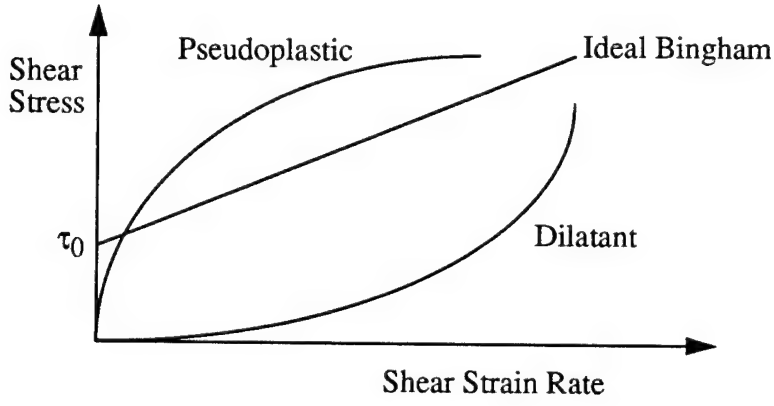

Figure 4.2. Time Independent Non-Newtonian Fluid Flow Curves

The pseudoplastic fluids are also referred to as shear thinning fluids. The characteristic of the pseudoplastic fluid is the viscosity decreases as the strain rate increases. The fluids that exhibit this behavior are typically suspensions consisting of asymmetric particles. The reduction in viscosity of pseudoplastic fluids as strain rate increases is due to the alignment of the particles in

the fluid. Examples of shear thinning fluids include greases, soap, and paper pulp.

The second category of time independent fluids are dilatant or shear thickening fluids. These fluids are characterized by an increase in viscosity as the rate of shear strain increases. Dilatant fluids usually have a high solid content. The increase in the fluid viscosity is due to the liquid acting as a lubricant for the particle motion at low rates of shear strain. As the shear strain rate increases, the initial dense packing of the particles disperse causing the particle volume to increase, thus, decreasing the available volume to the lubricating liquid. A result of the reduction in the lubrication of the particle motion is an increase in the required shear stress. Examples of shear thickening fluids are quicksand and wet beach sand.

The final category of the time independent fluids are the Bingham plastic fluids. The representative feature of these fluids is the ability to resist a static shear stress. This static shear stress, or yield shear stress, is shown in Figure 4.2 as τ_0. The behavior of fluids possessing a yield shear stress is explained by the presence of a three dimensional, internal structure. The cohesive forces containing the internal structure have the ability to resist an applied shear stress. This yield shear stress phenomenon can be illustrated by Figures 4.3 and 4.4. Figure 4.3 shows a portion of the electrode assembly used in Chapter 2 without an electric field applied. When the electrodes are lowered into the ER fluid and raised out of the ER fluid bath, the fluid does not remain in between the electrodes. Figure 4.4 shows the electrode assembly with an applied electric field (3kV/mm) containing ER fluid after the electrodes are lowered and raised from the ER fluid bath. The resistance to the gravity force by the ER fluid is due to the yield shear stress developed by the applied electric field. At shear stress values below the yield value, the fluid behaves as a solid. When the applied shear stress exceeds the yield value, the internal structure collapses, allowing the fluid to flow with a viscosity similar to that of a Newtonian fluid. The recovery of the internal structure when the applied shear stress is reduced to a value less than the yield stress is instantaneous. For the ER fluid used in the attenuation experiments (Chapter 2), the recovery time was on the order of a millisecond.

The flow curve for a Bingham plastic fluid can have a pseudoplastic, dilatant, or an ideal structure (Figure 4.5). The current literature has shown the ideal Bingham plastic model to be sufficient in describing the stress-strain rate relationship of ER fluids. The additional requirement for an ER fluid is the electric field dependence of the yield shear stress. This requirement, as well as the Bingham plastic properties, will be developed in Section 4.3.

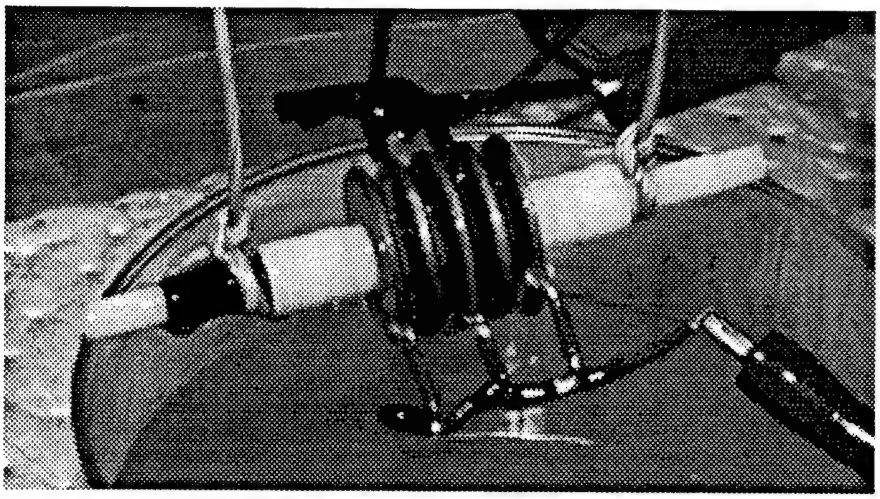

Figure 4.3. Electrodes Without Voltage Potential and ER Fluid

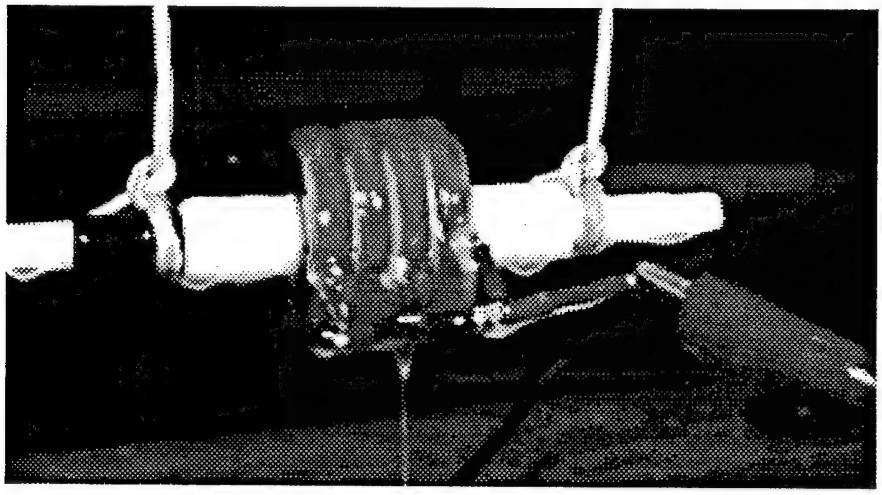

Figure 4.4. Electrodes With Voltage Potential and Contained ER Fluid

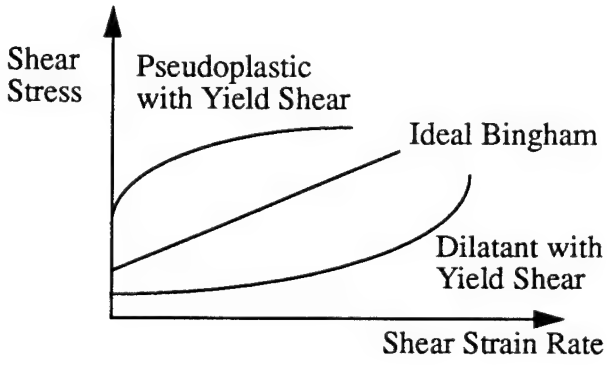

Figure 4.5. Flow Curves for Typical Yield Shear Stress Fluids

Bingham Properties of Corn Starch and Mineral Oil ER Fluid

The representation of an engineering fluid, such as the corn starch and mineral oil ER fluid used in the Attenuation Experiments (Chapter 2), by the ideal Bingham constitutive relationship requires the behavior of the fluid to be approximated. The constitutive relationship used to predict the behavior of the ER fluid utilizes the expression as found for a Bingham fluid in Bird et al. (1960):

$$\underline{\tau} = -\left\{\mu + \frac{\tau_0}{\left|\sqrt{\frac{1}{2}\underline{\Delta} \Diamond \underline{\Delta}}\right|}\right\}\underline{\Delta} \qquad \frac{1}{2}(\underline{\tau} \Diamond \underline{\tau}) > \tau_0^2$$
$$\underline{\Delta} = 0 \qquad \frac{1}{2}(\underline{\tau} \Diamond \underline{\tau}) \leq \tau_0^2 \tag{4-1}$$

where $\underline{\tau}$ represents the stress tensor in the fluid, $\underline{\Delta}$ represents the rate of deformation tensor in the fluid, τ_0 represents the yield shear stress, μ represents the viscosity of the fluid, $\underline{\tau} \Diamond \underline{\tau}$ is the double dot product of the stress tensor, which represents the momentum flux, and $\underline{\Delta} \Diamond \underline{\Delta}$ is the double dot product of the rate of deformation tensor. The application of equation (4-1) and the definition of the double dot products will be discussed in greater detail in Chapter 5. The remaining parameters to define for the ER fluid are the viscosity and the yield shear stress. The ER fluid properties were measured by Maciejewski & Tryon (1992) of the Materials Laboratory at the Naval Undersea Warfare Center for the corn starch and mineral oil ER fluid used in the Attenuation Experiments (Chapter 2). The density of this ER fluid was measured as 995 kg/m^3. The measurement of the electric field dependence of the yield shear stress and the post-yield characteristics of the fluid was accomplished utilizing the dynamic ER test apparatus (Maciejewski Patent No. 5,177,997) attached to an Instron analyzer. The measurement apparatus involved a concentric cylinder configuration where the inner cylinder was oscillated in the longitudinal direction. The sample of ER fluid is contained within the annulus between the inner and outer cylinders. The oscillating inner cylinder is attached to the dc high voltage power supply; whereas, the outer cylinder is electrically grounded. The data collected included the shear stress on the inner cylinder as a function of the speed of the inner plunger at various voltage potential values.

The collected data for the corn starch and mineral oil ER fluid was then incorporated into the Bingham relationship of equation (4-1). The resulting flow curve representing the Bingham

parameters for the ER fluid used is shown in Figure 4.6. This figure is a plot of the shear stress, in pascals, on the ordinate versus the shear strain rate on the abscissa in units of 1/seconds. It can be seen that the ER fluid is non-Newtonian at the zero state. The yield shear stress is shown to be a strong function of the electric field; whereas, the viscosity is not a strong function of the electric field. The zero state viscosity is approximately 931 Pa-sec and the energized viscosities are approximately 1340 Pa-sec. This variation between the energized and zero state viscosities have been shown by Brooks (1989) for a thirty-five percent volume fraction commercial fluid.

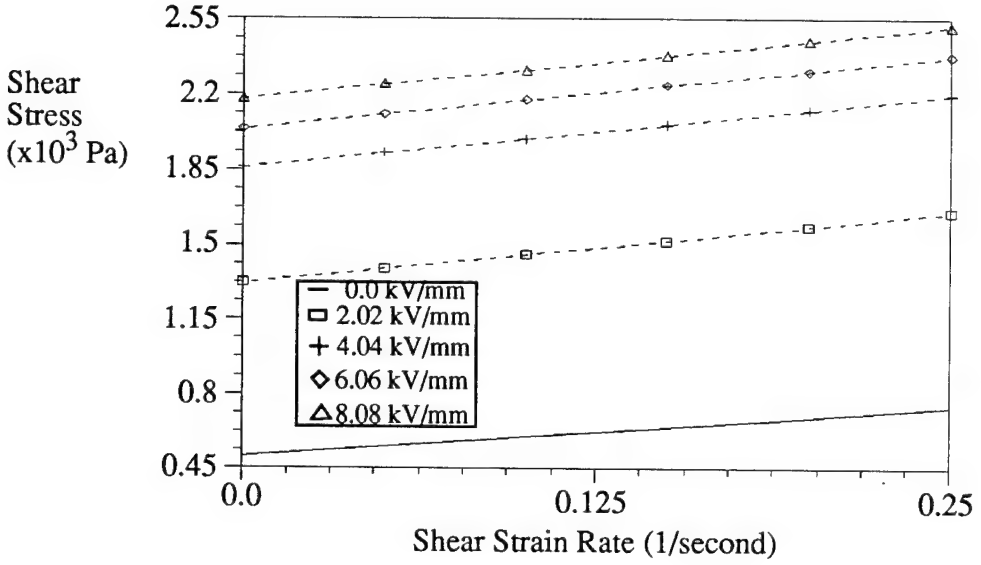

Figure 4.6. Flow Curve of Corn Starch and Mineral Oil ER Fluid

The dependence of the yield shear stress on the applied electric field has been shown by Brooks (1989) to be a parabolic relationship. This relationship has the form of

$$\tau_0(E) = \beta E^2 + \tau_0(0), \qquad (4\text{-}2)$$

where $\tau_0(E)$ is the electric field dependent yield shear stress in units of pascals, E is the magnitude of the applied electric field in units of kV/mm, β is the proportionality constant based on the ER fluid composition, and $\tau_0(0)$ is the zero state yield shear stress of the fluid. Since the electric fields used in the Attenuation Experiments (Chapter 2) ranged from zero to 1.6kV/mm,

the fit of the measured data to equation (4-2) included only the zero to 2.02kV/mm data sets. The result of this fit is illustrated in Figure 4.7.

The evaluation of the yield shear stress in the ER fluid will depend on the electric field as defined by equation (4-2). The electric field has been shown, in Chapter 3, to vary spatially; therefore, the yield shear stress will also be dependent on the spatial location within the fluid. The remaining Bingham parameter required for the corn starch and mineral oil ER fluid is the fluid viscosity. This can be evaluated from the flow curve in Figure 4.6. The Bingham parameters for the corn starch and mineral oil used in the Attenuation Experiments (Chapter 2) are listed in Table 4.1.

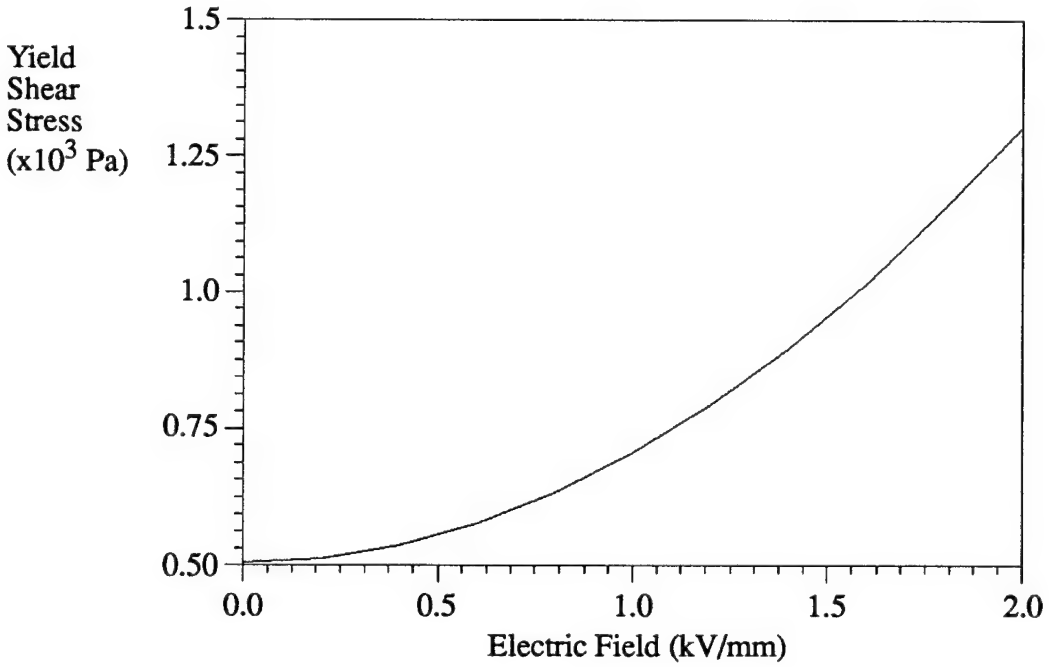

Figure 4.7. Electric Field Dependence of Yield Shear Stress for Corn Starch and Mineral Oil ER Fluid

Bingham Parameters for the Corn Starch and Mineral Oil ER Fluid
Absolute viscosity, (zero state) μ: 931.0 Pa-sec (energized) μ : 1340.0 Pa-sec Mass Density, ρ: 995 kg/m^3
Zero state yield shear stress, $\tau_0(0)$: 505 Pa
Material proportionality constant, β: 200.0 (N/m^2)/(kV/mm)^2

Table 4.1. Bingham Parameters for Corn Starch and Mineral Oil ER Fluid

The application of equations (4-1), and (4-2), together with the evaluated Bingham parameters in Table 4.1, provide the constitutive relationship for the ER fluid used in the Attenuation Experiments. The use of the Bingham model to relate the shear stress to the ER fluid velocity gradients will be utilized in the next chapter, Chapter 5, to model the non-Newtonian fluid dynamics within the ER test module.

Summary

The behavior of the ER fluid is determined to be non-Newtonian since the fluid exhibits a yield shear stress phenomenon. The chapter discusses the three categories of non-Newtonian fluids and finds that ER fluids can be approximated as time independent. The ideal Bingham plastic constitutive relationship is used to predict the behavior of the ER fluid. This relationship describes the dependence of the fluid stress tensor on the rate of deformation tensor with two rheological parameters. The rheological parameters described in the ideal Bingham constitutive relationship are the absolute viscosity and the static yield shear stress.

Since the static yield shear stress of an ER fluid is dependent on the electric field, a relationship between the applied electric field and the static yield shear stress is developed for the corn starch and mineral oil fluid used. The flow curve for the corn starch and mineral oil ER fluid is provided based on experimentation and the developed relationship between the electric field and the yield shear stress.

The ideal Bingham parameters for the corn starch and mineral oil ER fluid are presented

which include the absolute viscosity, density, zero state yield shear stress, and a material proportionality constant. This material proportionality constant is used to evaluate the static yield shear stress of the ER fluid at any applied electric field.

Chapter 5: Bingham Fluid Dynamics

Introduction

The damping capacity of the ER test module is characterized by the amount of energy dissipated in the flexible cylinder. Energy dissipation in the test module depends mainly on the generation of a shear flow field within the ER fluid by the interaction of the fluid with the structure of the module. This chapter treats the modeling of that flow field. The solution of Bingham fluid applications has been discussed in the following references. Lipscome & Denn (1984) investigated the flow of Bingham fluids through complex geometries such as the pressure driven flow of a Bingham fluid between diverging plates. The formulation of their analysis was for one-dimensional, fully developed flows. Edwards et al. (1972) and Duggins (1972) present solutions to the unsteady flow of Bingham fluids in pipes. These solutions are one-dimensional in nature. Atkin et al. (1991) presents solutions to one-dimensional, fully developed flows including Poiseuille and Couette applications. Walton & Bittleston (1991) discuss the flow of a Bingham fluid in an eccentric annulus. The axisymmetric motion of the ER fluid in the ER test module is three dimensional, quasi-static in nature. The equations governing this type of motion are developed in the following sections using the Cauchy formulation for the equations of motion as the starting point.

Bingham Equations of Fluid Motion

The geometry of the ER test module, shown in Figure 5.1, is approximated in an axisymmetric, cylindrical coordinate system. Circumferential velocity components, if any, will be assumed constant. Hence the continuity equation (5-1) and the Cauchy equations in the radial, axial, and circumferential directions ((5-2), (5-3), and (5-4)), in the absence of body forces, have the following form:

$$\frac{\partial \rho}{\partial t} + \frac{1}{r}\frac{\partial}{\partial r}(\rho r v) + \frac{\partial}{\partial z}(\rho u) = 0 \qquad (5\text{-}1)$$

$$\rho\frac{Dv}{Dt} = -\frac{\partial P}{\partial r} - \left[\frac{1}{r}\frac{\partial}{\partial r}(r\tau_{rr}) - \frac{\tau_{\theta\theta}}{r} + \frac{\partial}{\partial z}(\tau_{rz})\right] \tag{5-2}$$

$$\rho\frac{Du}{Dt} = -\frac{\partial P}{\partial z} - \left[\frac{1}{r}\frac{\partial}{\partial r}(r\tau_{rz}) + \frac{\partial}{\partial z}(\tau_{zz})\right] \tag{5-3}$$

$$\frac{\partial P}{\partial \theta} = 0 \tag{5-4}$$

where v is the radial component of velocity (m/s), u is the axial component of velocity (m/s), ρ is the mass density of the fluid (kg/m^3), P is the pressure (N/m^2), τ_{rr} is the normal stress in the radial direction (N/m^2), τ_{zz} is the normal stress in the axial direction (N/m^2), $\tau_{\theta\theta}$ is the normal stress in the circumferential direction (N/m^2), r is the radial coordinate (m), z is the axial coordinate (m), D/Dt is the substantial derivative, and t is time in seconds. The continuity equation can be simplified further by applying the restriction of incompressibility. Therefore, equation (5-1) becomes:

$$\frac{1}{r}\frac{\partial}{\partial r}(rv) + \frac{\partial u}{\partial z} = 0. \tag{5-5}$$

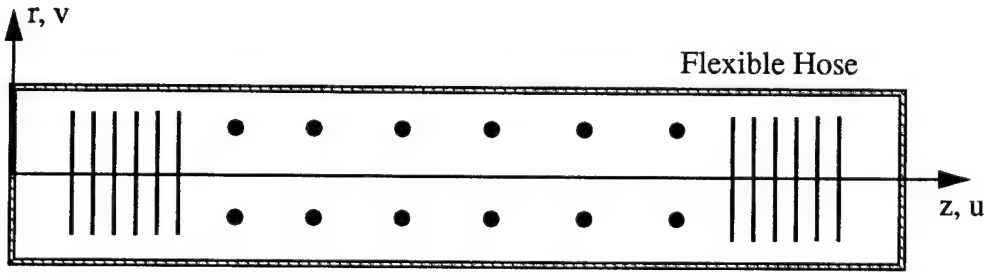

Figure 5.1. ER Test Module Geometry

In order to relate the applied boundary conditions imposed onto the ER fluid by the flexible cylinder, the momentum equations will be expressed in terms of the velocity components. The relationship between the stress tensor, $\underline{\tau}$, and the rate of deformation tensor, $\underline{\Delta}$, for a Bingham plastic fluid (Bird et al. (1960)) is found to be:

$$\underline{\tau} = -\left(\mu + \frac{\tau_0}{\left|\sqrt{\frac{1}{2}\underline{\Delta} \Diamond \underline{\Delta}}\right|}\right)\underline{\Delta} \qquad \frac{1}{2}(\underline{\tau} \Diamond \underline{\tau}) > \tau_0^2 \tag{5-6}$$

where τ_0 is the yield stress of the ER fluid at the particular electric field value (N/m^2), μ is the viscosity of the ER fluid (Pa-sec), $\underline{\tau} \Diamond \underline{\tau}$ is the double-dot product of the stress tensor to itself, and $\underline{\Delta} \Diamond \underline{\Delta}$ is the double-dot product of the rate of deformation tensor to itself. The double-dot product of the symmetric stress tensor and the double-dot product of the rate of deformation tensor are defined in equation (5-7) as follows:

$$\underline{\Delta} \Diamond \underline{\Delta} = 2\left(2\left[\left(\frac{\partial v}{\partial r}\right)^2 + \left(\frac{v}{r}\right)^2 + \left(\frac{\partial u}{\partial z}\right)^2\right] + \left[\frac{\partial v}{\partial z} + \frac{\partial u}{\partial r}\right]^2\right)$$

$$\underline{\tau} \Diamond \underline{\tau} = \tau_{rr}^2 + \tau_{\theta\theta}^2 + \tau_{zz}^2 + 2\tau_{rz}^2 \tag{5-7}$$

When the momentum flux ($\frac{1}{2}(\underline{\tau} \Diamond \underline{\tau})$) is less than the yield stress of the fluid squared, the rate of deformation tensor is equal to zero. The characteristic feature of flows satisfying the requirement that the rate of deformation tensor becomes zero, is the existence of a plug flow region. A plug flow region has a spatial velocity profile which is flat in the non-yielded region of the fluid in a pipe flow application. The plug flow region is supported by the through flow of the fluid, which carries the undeformed or unyielded fluid downstream. Since the ER fluid is confined in the ER test module, the existence of a plug flow region is not possible. The absence of through flow properties in the ER test module will produce no fluid motion when the ER fluid is not yielded. The application of the Bingham fluid constitutive relationship, equation (5-6), to the components of the stress tensor and the substitution of these individual stress components into the Cauchy equation in the radial direction (equation (5-2)) and the Cauchy equation in the axial direction,

equation (5-3), produces the equations of motion in terms of the velocity components. The momentum equation in the radial direction, after substituting the expressions for the stress components and the continuity equation, becomes:

$$\rho\frac{Dv}{Dt} = -\frac{\partial P}{\partial r} + (\mu + \frac{\tau_0}{\Upsilon})\left[\frac{1}{r}\frac{\partial v}{\partial r} + \frac{\partial^2 v}{\partial r^2} + \frac{\partial^2 v}{\partial z^2} - \frac{v}{r^2}\right] - \frac{\tau_0}{\Upsilon^2}\left[2\frac{\partial v}{\partial r}\frac{\partial \Upsilon}{\partial r} + \frac{\partial \Upsilon}{\partial z}(\frac{\partial v}{\partial z} + \frac{\partial u}{\partial r})\right]. \qquad (5\text{-}8)$$

In a similar analysis, the Bingham stress components are substituted into the momentum equation in the axial direction to produce:

$$\rho\frac{Du}{Dt} = -\frac{\partial P}{\partial z} + (\mu + \frac{\tau_0}{\Upsilon})\left[\frac{1}{r}\frac{\partial u}{\partial r} + \frac{\partial^2 u}{\partial r^2} + \frac{\partial^2 u}{\partial z^2}\right] - \frac{\tau_0}{\Upsilon^2}\left[2\frac{\partial u}{\partial z}\frac{\partial \Upsilon}{\partial z} + \frac{\partial \Upsilon}{\partial r}(\frac{\partial v}{\partial z} + \frac{\partial u}{\partial r})\right]. \qquad (5\text{-}9)$$

The variable Υ is defined as,

$$\Upsilon = \left|\frac{1}{2}\sqrt{\underline{\Delta} \Diamond \underline{\Delta}}\right|. \qquad (5\text{-}10)$$

The set of equations including equation (5-5), equation (5-8), equation (5-9), and (5-10), describe the motion of an incompressible, axisymmetric, Bingham plastic fluid. In the limit when the yield shear stress goes to zero, these equations revert to the Newtonian Navier-Stokes formulation. The unknowns in the resulting equations are the pressure field and the velocity components in the radial and axial directions. The pressure variable can be removed from the momentum equations by taking the partial derivative of the momentum equation in the radial direction (equation (5-8)) with respect to the axial direction and subtracting the partial derivative of the axial momentum equation (equation (5-9)) with respect to the radial direction. The overall order of differentiation is increased in the resulting equation, however, the number of unknowns is

reduced by one. The resulting momentum equation becomes

$$
\begin{aligned}
&-\frac{\partial}{\partial z}\left[\rho\frac{Dv}{Dt}\right]+\frac{\partial}{\partial z}\left[(\mu+\frac{\tau_0}{\Upsilon})\left(\frac{1}{r}\frac{\partial v}{\partial r}+\frac{\partial^2 v}{\partial r^2}+\frac{\partial^2 v}{\partial z^2}-\frac{v}{r^2}\right)\right] \\
&\quad -\frac{\partial}{\partial z}\left[\frac{\tau_0}{\Upsilon^2}(2\frac{\partial v}{\partial r}\frac{\partial \Upsilon}{\partial r}+\frac{\partial \Upsilon}{\partial z}(\frac{\partial v}{\partial z}+\frac{\partial u}{\partial r}))\right]= \\
&-\frac{\partial}{\partial r}\left[\rho\frac{Du}{Dt}\right]+\frac{\partial}{\partial r}\left[(\mu+\frac{\tau_0}{\Upsilon})\left(\frac{1}{r}\frac{\partial u}{\partial r}+\frac{\partial^2 u}{\partial r^2}+\frac{\partial^2 u}{\partial z^2}\right)\right] \\
&\quad -\frac{\partial}{\partial r}\left[\frac{\tau_0}{\Upsilon^2}(2\frac{\partial u}{\partial z}\frac{\partial \Upsilon}{\partial z}+\frac{\partial \Upsilon}{\partial r}(\frac{\partial v}{\partial z}+\frac{\partial u}{\partial r}))\right]
\end{aligned}
\tag{5-11}
$$

The developed non-Newtonian momentum equation is simplified further by using the assumptions of creeping motion and the effects of geometry (other than axisymmetry) of the ER test module. These simplifications are developed in the next section.

Creeping Motion of an ER Fluid

The existence of creeping motion is governed by the Reynolds number characterizing the flow application. For the creeping motion approximation to be valid, the Reynolds number must be considered very small (Schlichting (1979), White (1974)). Therefore, at a Reynolds number much less than unity, the viscous effects are much greater than the inertia effects. The applicability of the creeping motion assumption to the ER fluid is tested by computing a reduced Reynolds number of the form described in Schlichting (1979). This reduced Reynolds number characterizes two dimensional problems in which the height of the fluid is very small compared to the length. In the ER test module, the height of the ER fluid between the electrodes and the flexible cylinder is 0.021625 m. The length of ER fluid in the test module is 1.257 m. Based on the reduced Reynolds number of Schlichting (1979), the maximum value for the Reynolds number is calculated as follows:

$$
Re = \frac{\rho L U_{max}}{\mu}\left(\frac{h}{L}\right)^2 \approx 0.002 \ll 1.0 \tag{5-12}
$$

where ρ is the ER fluid mass density (994.76 kg/m^3), L is the length (1.257 m), U_{max} is the maximum velocity the ER fluid experiences (4.0 m/s), h is the thickness of the ER fluid (0.026125 m), and μ is the viscosity of the zero state ER fluid (931 Pa-sec). It can be seen from the result of equation (5-12), that the Reynolds number is within the valid range for the creeping motion approximation to be applied to the ER fluid in the test module.

The creeping motion simplification applied to equation (5-11) is obtained by neglecting the squares of the velocity components and the product of the velocity gradients. This produces a reduced expression for the combined momentum equation in the form:

$$\frac{\partial}{\partial z}\left[-\rho\frac{\partial v}{\partial t}\right] + \left(\mu + \frac{\tau_0}{\Upsilon}\right)\left(\frac{1}{r}\frac{\partial^2 v}{\partial r \partial z} + \frac{\partial^3 v}{\partial r^2 \partial z} + \frac{\partial^3 v}{\partial z^3} - \frac{1}{r^2}\frac{\partial v}{\partial z}\right) = \frac{\partial}{\partial r}\left[-\rho\frac{\partial u}{\partial t}\right] + \left(\mu + \frac{\tau_0}{\Upsilon}\right)\frac{\partial}{\partial r}\left[\frac{1}{r}\frac{\partial u}{\partial r} + \frac{\partial^2 u}{\partial r^2} + \frac{\partial^2 u}{\partial z^2}\right] \tag{5-13}$$

The assumption of creeping motion applied to the flow of the ER fluid also approximates the motion as quasi-static. In a real fluid, the inertia of the fluid continues the motion for a period of time after the excitation has stopped. When fluid motion is approximated as a creeping motion, the fluid description does not have a mechanism for supporting this residual motion. The dependence on time for a viscous creeping flow enters the problem through the boundary conditions. At any instance of time, the variation of the velocity components depend on position only. Therefore, the combined momentum expression shown in equation (5-13) will become:

$$\frac{1}{r}\frac{\partial^2 v}{\partial r \partial z} + \frac{\partial^3 v}{\partial r^2 \partial z} + \frac{\partial^3 v}{\partial z^3} - \frac{1}{r^2}\frac{\partial v}{\partial z} = \frac{\partial}{\partial r}\left[\frac{1}{r}\frac{\partial u}{\partial r} + \frac{\partial^2 u}{\partial r^2} + \frac{\partial^2 u}{\partial z^2}\right]. \tag{5-14}$$

The resulting momentum expression (equation (5-14)) provides a creep flow description of the velocity components in terms of only the spatial coordinates of the problem. The velocity components in the flow field are not dependent on the rheological properties of the fluid. The absolute viscosity, mass density, and yield shear stress of the ER fluid will influence the dissipation of the viscous energy but will not influence the boundary conditions in terms of the

fluid velocity. This is a characteristic of the creeping motion class of problems. A solution to equation (5-14) can be developed using a stream function that satisfies the continuity equation (5-5); however, the stream function transforms the boundary value problem from a Dirichlet problem to a Neumann problem formulation. This occurs from the assignment of the stream function, $\Psi(r,z)$, as according to equation (5-15).

$$v = -\frac{1}{r}\frac{\partial \Psi}{\partial z}$$
$$u = \frac{1}{r}\frac{\partial \Psi}{\partial r} \tag{5-15}$$

The substitution of equation (5-15) into equation (5-14) results in the biharmonic equation (5-16) in cylindrical coordinates for axisymmetric geometry which is the traditional formulation of creep flow problems.

$$\nabla^4 \Psi(r, z) = 0. \tag{5-16}$$

This is the normal formulation of creep flow problems (Langlois (1964)). However, because the order of differentiation is reduced in equation (5-14) (compared to equation (5-16)), and the computational treatment for Dirichlet boundary conditions is more straightforward than for the Neumann problem, the solution for the velocity field within the ER test module was accomplished using equation (5-14) directly rather than equation (5-16).

The momentum expression represented by equation (5-14) is simplified by applying one last approximation. This relies on the wide range of the spatial coordinates of the problem. The thickness of the annular section in which the ER fluid is contained is two orders of magnitude smaller than the length. The axial velocity component will be predominantly influenced in the direction of motion by the flexible cylinder. Since the excitation of the ER test module is one-dimensional, the axial component of velocity of the ER fluid will depend on only the axial direction, $u=u(z)$. Applying this approximation to equation (5-14) produces the governing equation for the radial velocity component which is dependent on the radial and axial directions. The axial component of velocity vanishes from the right side of equation (5-14) when the derivative with respect to the radial direction is applied.

$$\frac{1}{r}\frac{\partial^2 v}{\partial r \partial z} + \frac{\partial^3 v}{\partial r^2 \partial z} + \frac{\partial^3 v}{\partial z^3} - \frac{1}{r^2}\frac{\partial v}{\partial z} = 0 \tag{5-17}$$

The governing equations developed to describe the confined, creeping motion of the incompressible ER fluid within the axisymmetric ER test module consist of equation (5-5) and equation (5-17). The axial motion of the flexible cylinder and the boundary conditions influencing the ER test module are developed in the following section.

ER Test Module Boundary Conditions

The axial velocity in the ER test module is expressed from the thin shell equations governing the axial motion of a harmonically excited cylinder containing a fluid. The basic equation of motion for the structure is found in Jones (1975) and Junger & Feit (1986) to be:

$$\rho_m \frac{\partial^2 \hat{u}}{\partial t^2} = E_c \frac{\partial^2 \hat{u}}{\partial z^2} + \frac{\nu E_c}{a}\frac{\partial \hat{w}}{\partial z} \tag{5-18}$$

where $\hat{u}(z, t)$ is the axial displacement of the flexible cylinder (m), $\hat{w}(z, t)$ is the radial displacement of the flexible cylinder (m), E_c is the complex axial elastic modulus of the flexible cylinder (N/m^2), ν is the Poisson ratio of the flexible cylinder (unitless), a is the radius of the flexible cylinder (m), z is the axial spatial location (m), t is time (s), and ρ_m is the mass density of the flexible cylinder (kg/m^3). As discussed in Chapter 2, during the experiment the ER test module was excited by a longitudinal shaker. This boundary condition was modeled as a harmonic excitation in the axial direction by equation (5-19)

$$\hat{u}_0(0, t) = \hat{U}_0 e^{i\omega t} \tag{5-19}$$

where $\hat{U}_0$, is the amplitude of the displacement at the forward boundary (m), i is the square root of -1, and ω is the frequency (rad/s). The second boundary condition needed to solve for the axial displacement in equation (5-18) was obtained by a force balance at the aft end of the ER test module (Figure 2.4) ($z = L$). This condition is derived by applying Newton's second law to the end of the ER test module.

$$A_s E_c \frac{\partial}{\partial z}\hat{u}(L, t) = -m\frac{\partial^2}{\partial t^2}\hat{u}(L, t) \tag{5-20}$$

The longitudinal force at the end of the shell is balanced by the inertia of the added point mass. The undefined variables in equation (5-20) are the cross-sectional area, A_s (m^2), and the mass of the added point mass, m (kg). This investigation is unique from other researchers because the problem formulation does not assume an infinite flexible hose and includes a mass loading boundary condition.

An approximate solution to equation (5-18), using boundary conditions (5-19) and (5-20), can be developed for the axial displacement of the ER test module. This solution is based on the one-dimensional nature of the axial excitation and the assumption that the time and spatial modes of the problem decouple. Since a harmonic forcing function is used, the non-conforming, approximate solution for the flexible cylinder displacements can be written as

$$\hat{u}(z,t) = \hat{U}(z)\, e^{i\omega t}, \tag{5-21}$$

where $\hat{U}(z)$ is the axial displacement of the flexible cylinder. The dynamic coupling of the radial displacement into equation (5-18), for axial excitation, has been shown by Hull (1994) to be negligible. Therefore, given the form of the steady state solution in equation (5-21), the longitudinal displacement equation (5-18) becomes:

$$\frac{d^2\hat{U}}{dz^2} + k^2\hat{U} = 0 \tag{5-22}$$

with

$$k = \omega/\sqrt{E_c/\rho} \tag{5-23}$$

where k is the extensional wavenumber (rad/m). The general solution to equation (5-22) becomes,

$$\frac{\hat{U}(z)}{\hat{U}_0} = Me^{ikz} + Ne^{-ikz}. \tag{5-24}$$

The solution to the constants M and N, in equation (5-24), are obtained by using the boundary conditions expressed in equation (5-19) and equation (5-20). The resulting expressions for the

constants in equation (5-24) are

$$M = \frac{[\beta + 1]\, e^{-ikL}}{[\beta - 1]\, e^{ikL} + [\beta + 1]\, e^{-ikL}} \tag{5-25}$$

and

$$N = \frac{[\beta - 1]\, e^{ikL}}{[\beta - 1]\, e^{ikL} + [\beta + 1]\, e^{-ikL}} \tag{5-26}$$

with

$$\beta = \frac{iA_s E_c k}{m\omega^2}. \tag{5-27}$$

The axial displacement of the flexible cylinder is approximated by equations (5-24) through (5-27). The excitation of the ER test module was measured in the attenuation experiments as transfer functions consisting of ratios between the aft acceleration and the forward acceleration. A more convenient form for the axial displacement of the ER test model would be to normalize equation (5-24) by the forward displacement, $\hat{u}_0$. Since the equations of motion for the ER fluid are represented in the velocity components, the normalized version of the displacement equation (equation (5-21)) should be differentiated with respect to time to obtain

$$\bar{u}(z) = \frac{\partial}{\partial t}\left(\frac{\hat{u}}{\hat{u}_0}\right) = \frac{i\omega\hat{U}(z)}{i\omega\hat{U}_0}\frac{e^{i\omega t}}{e^{i\omega t}} = \frac{\hat{U}(z)}{\hat{U}_0} \tag{5-28}$$

where $\bar{u}(z)$ is the normalized axial velocity component of the fluid and the shell.

The axial velocity of the forward and aft ends of the ER test module were determined from the experimentally measured transfer functions. The transfer functions recorded were in the form of accelerations; however, through an analysis similar to that employed to produce equation (5-28) from equation (5-21), the forward and aft velocities were obtained from the experimental transfer functions. It can be seen from equation (5-29) that the experimentally measured transfer function consisting of accelerations is equivalent to the ratio of the aft velocity to the forward velocity. This occurs since the excitation of the structure is a harmonic function.

$$TF\{\frac{a_a}{a_f}\} = TF\left\{\frac{\frac{\partial}{\partial t}(u_a e^{i\omega t})}{\frac{\partial}{\partial t}(u_f e^{i\omega t})}\right\} = TF\{\frac{u_a}{u_f}\} \tag{5-29}$$

The resulting boundary conditions of the ER test module, in terms of the velocity components are shown in Figure 5.2.

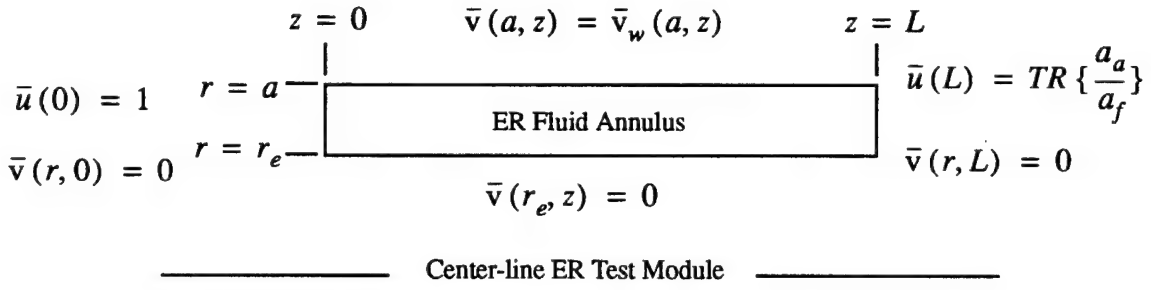

Figure 5.2. Boundary Conditions on the ER Test Module

The velocity at the wall ($r = a$) in the radial direction is defined by balancing the stresses in the circumferential and longitudinal directions between the shell and the ER fluid. The expression relating the longitudinal stress of the thin, axisymmetric shell to the axial and circumferential displacements is (Jones 1975):

$$\tau_{zz_{shell}}(z,t) = E_c\frac{\partial \hat{u}}{\partial z} + \nu E_c\frac{\hat{w}}{a} \tag{5-30}$$

where $\hat{u}(z,t)$ is the axial displacement of the shell (m), and $\hat{w}(z,t)$ is the radial displacement of the shell (m). For the quasi-static, harmonic motion considered in this problem, the displacements in equation (5-30) can be represented as velocities by integrating the respective velocity component over time. Therefore, the longitudinal stress equation for the shell in terms of the axial and radial velocities is

$$\tau_{zz_{shell}}(z,t) = \frac{E_c\partial u}{i\omega\partial z} + \nu E_c\frac{v_w}{ai\omega}. \tag{5-31}$$

The longitudinal stress representing the Bingham fluid at the wall of the shell is obtained by

$$\tau_{zz_{fluid}}(z,t) = \left[\mu + \frac{\tau_0}{\Upsilon}\right]\left[2\frac{\partial u}{\partial z}\right]. \tag{5-32}$$

In order to maintain continuity at the interface of the shell and the fluid, the stress in the shell must equal the stress in the fluid. This equality of the longitudinal stresses produces

$$\left[\mu + \frac{\tau_0}{\Upsilon}\right] = \left[\frac{E_c}{i\omega}\frac{\partial u}{\partial z} + \nu E_c \frac{v_w}{ai\omega}\right]\left[2\frac{\partial u}{\partial z}\right]^{-1}. \tag{5-33}$$

The analysis can be repeated in the circumferential direction to obtain an expression for the radial velocity component at the wall of the shell. The relationship between the hoop stress and the circumferential displacement for an axisymmetric thin shell (Jones (1975)) is

$$\tau_{\theta\theta_{shell}}(z,t) = E_c\frac{\hat{w}}{a} + \nu E_c\frac{\partial \hat{u}}{\partial z}. \tag{5-34}$$

The hoop stress in terms of the velocity components is

$$\tau_{\theta\theta_{shell}}(z,t) = \frac{E_c v_w}{ai\omega} + \frac{\nu E_c}{i\omega}\frac{\partial u}{\partial z}. \tag{5-35}$$

The hoop stress in the Bingham fluid is expressed as

$$\tau_{\theta\theta_{fluid}}(z,t) = \left[\mu + \frac{\tau_0}{\Upsilon}\right]\left[\frac{2v_w}{a}\right]. \tag{5-36}$$

At the interface of the shell and the fluid, the hoop stress must be the same to preserve continuity across the interface. When equation (5-35) is equated to equation (5-36), a result similar to equation (5-33) is derived

$$\left[\mu + \frac{\tau_0}{\Upsilon}\right] = \left[\frac{a}{2v_w}\right]\left[\frac{E_c v_w}{ai\omega} + \frac{\nu E_c}{i\omega}\frac{\partial u}{\partial z}\right]. \tag{5-37}$$

The final development of the non-dimensional radial velocity at the wall in terms of the non-dimensional axial velocity is accomplished by equating equation (5-33) to equation (5-37) to produce

$$\overline{v_w} = a\left[\frac{\partial \bar{u}}{\partial z}\right], \tag{5-38}$$

where the over-bar denotes normalized velocity.

The application of the boundary conditions illustrated in Figure 5.2 to the equations of fluid motion derived in section 5.3 will provide the description of the radial velocity field inside the ER test module. Based on the full velocity field and the stresses in the ER fluid constrained by the test module, the amount of viscous dissipation within the ER fluid can be calculated. The solution of the radial velocity field is accomplished using finite difference techniques which are developed in the following section.

Numerical Solution of Radial Velocity Field

The evaluation of the radial velocity component is done by using central, forward, and backward difference schemes to approximate the differential equations (5-5) and (5-17) developed in Section 5.3. The selection of the type of difference equation used depends on where in the calculation domain the evaluation is being made. This is illustrated in Figure 5.3. The approximation of the third partial derivative of v with respect to z in equation (5-17) at the axial location $j = 2$ must be accomplished using a forward difference scheme. If this term is approximated using a central difference equation, a velocity value outside the computational domain is required. In a similar manner, the approximation of this term at the $j = n - 1$ axial location requires a backward difference formulation.

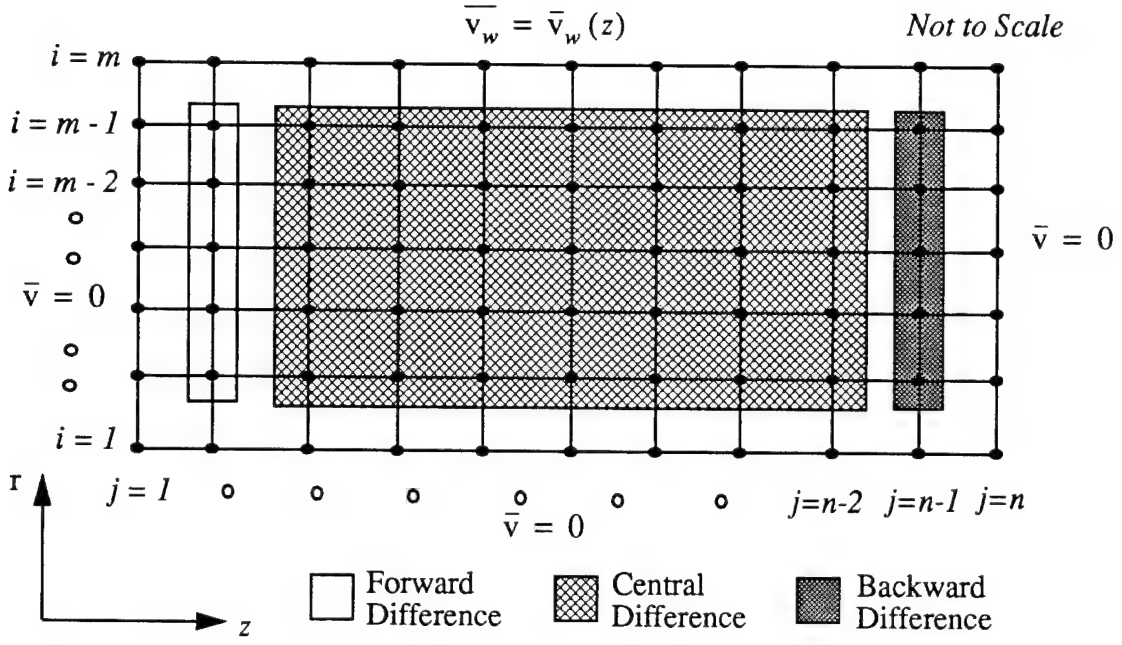

Figure 5.3. Finite Difference Mesh Layout for ER Fluid Annular Region for Approximating the Third Derivative Term of Equation (5-39)

The difference formulations used to represent the derivatives in equation (5-17) are second order accurate and can be found in numerous references (Anderson et al. (1984), Ames (1977)). The combination of equations (5-5) and (5-17) is used to produce

$$\frac{\partial^3 \bar{v}}{\partial r^2 \partial z} + \frac{\partial^3 \bar{v}}{\partial z^3} - \frac{2}{r^2}\frac{\partial \bar{v}}{\partial z} = \frac{1}{r}\frac{d^2 \bar{u}}{dz^2} \qquad (5\text{-}39)$$

where the axial velocity is dependent on only the axial location. The discretization of equation (5-39) will depend on a central difference formulation for all terms except the third derivative with respect to the axial location, which is approximated as shown in Figure 5.3. The solution of the radial velocity component becomes a system of algebraic equations representing equation (5-39) and the boundary equations of Section 5.4 (at z=0; $\bar{u}(0) = 1$, $\bar{v}(r,0) = 0$; at z=L; $\bar{u}(L)$=$TF\{a_a/a_f\}$, $\bar{v}(r,L)$=0; at r=a; $\bar{v}(a,z)$=$\bar{v}_w(z)$; at r=r_e; $\bar{v}(r_e,z)$=0). These equations are combined into the following banded matrix form:

$$[A]\{v\} = \{F\}, \tag{5-40}$$

where $[A]$ is the coefficient matrix representing spatial terms from the difference equations, $\{v\}$ is the unknown radial velocity vector, and $\{F\}$ is the forcing vector. The discretization of equation (5-39) produces a hexadiagonal matrix in the central difference region of the computational domain. The solution to the radial velocities is obtained by inverting the coefficient matrix and multiplying to produce

$$\{v\} = [A]^{-1}\{F\}. \tag{5-41}$$

The number of grid points used in the axial and radial directions was determined by increasing the grid density until the difference between solutions was negligible. The computational size used to evaluate the radial velocity components was forty grid points in the axial direction ($n = 40$) and ten grid points in the radial direction ($m=10$).
This resulted in a [400 x 400] coefficient matrix, a {400 x 1} radial velocity vector and a {400 x 1} forcing vector in the form of equation (5-41).

The FORTRAN program, RVEL, was written to assemble the coefficient matrix, invert the coefficient matrix, multiply the inverted coefficient matrix by the complex forcing vector to obtain the complex radial components of velocity in the ER fluid. A program listing is given in Appendix C. The calculated velocity distributions are shown in the Figures 5.4 to 5.11 for the zero and 1.6 kV/mm cases.

The axial velocity as a function of frequency is illustrated in Figure 5.4, for the 0.0 kV/mm case, and Figure 5.5, for the 1.6 kV/mm case. The ordinate is the normalized axial velocity and the abscissa represents the normalized axial position along the ER test module (Figure 2.4). From Chapter 2 we recall that the resonant frequency was 11.0 Hz for the 0.0 kV/mm case and 9.8 Hz for the 1.6 kV/mm case.

The variation of the normalized fluid axial velocity, $\bar{u}(z)$, for frequencies below the resonant frequency can be seen in Figure 5.4 to be significantly different from that for frequencies above resonance. Curves for frequencies above resonance exhibit a characteristic decrease in wave speed due to damping, while curves for frequencies below resonance do not have that shape. For the hypothetical case of a structure without damping, the axial velocity curve would intersect the

abscissa. The intersection with the abscissa would represent a null in the response of the structure.

All four curves in Figure 5.5 are for frequencies at or above the 9.8 Hz resonant frequency. All, therefore, exhibit the characteristic decrease in the normalized fluid axial velocity from damping.

The radial velocity as a function of frequency and spatial coordinates is shown in Figures 5.6 through 5.11. The Figures 5.6 and 5.7 illustrate the dependence of the radial velocity on the axial direction for selected frequencies at a normalized radius of 0.223 in the ER fluid. The axial dependence is negligible for the radial velocity within the ER fluid. This substantiates the assumption that the dynamic coupling of the radial displacement in equation (5-18) is negligible. The comparison of Figures 5.6 and 5.7 shows that the radial velocity is reduced approximately seventy-five percent when the electric field of 1.6 kV/mm is applied. The frequency dependence of the electrically energized fluid is not as strong as that of the zero state fluid. This can be attributed to effects on the system's boundary conditions resulting from the changes in fluid rheological properties caused by the electric field. Figures 5.8 and 5.9 are plots of the radial velocity at the wall of the flexible cylinder. These figures exhibit characteristics similar to those shown in Figures 5.6 and 5.7.

The radial velocity as a function of frequency and the normalized radial position is shown in Figures 5.10 and 5.11. In both figures, the non-dimensional radial velocity is plotted on the ordinate and the non-dimensional radial position is shown on the abscissa at a normalized axial position of 0.05 from the forward end of the ER test module. The zero volt results are shown in Figure 5.10 and the 1.6 kV/mm electric field results are shown in Figure 5.11. The comparison of Figures 5.10 and 5.11 shows that the radial velocity at the wall is reduced approximately sixty-eight percent when the electric field of 1.6 kV/mm is applied. The frequency dependence of the electrically energized fluid is shown again to be not as strong as the zero state fluid.

Summary

The governing equations of motion for the ER fluid contained in the ER test module are developed using the Cauchy Equations as the starting point. The Cauchy equations are formulated for an axisymmetric application without body forces. The constitutive relationship for an ideal Bingham fluid is substituted into these momentum equations to produce a set of nonlinear, non-Newtonian momentum equations. The resulting set of equations are simplified by assuming a creeping fluid motion. Inherent in the creeping motion assumption is that the fluid motion is

quasi-static in nature. The momentum equation in the radial direction and the momentum equation in the axial direction are combined through the second derivative of the pressure with respect to the radial and axial directions. This reduced equation is simplified further by an assumption based on the wide range of the spatial coordinates and the manner of excitation of the structure. This assumption is that the axial velocity will depend on only the axial direction. The radial component of velocity is a function of the radial and axial coordinate directions.

The analytical solution to the axial velocity is developed from the response of a thin shell containing a fluid subjected to an axial, harmonic excitation. Based on this solution, the balance of the stresses between the shell and the fluid, and the measured end response of the structure, the radial velocity component is solved using finite difference representation of the resulting equation. The finite difference approximation to the remaining equation produces a system of algebraic equations. These equations are solved using simple matrix operations.

The effect of the electric field on the velocity components dynamics are illustrated and the dependence of the velocity on frequency is shown to be stronger for the zero state fluid than the energized cases. The solution of the axial component and the radial component is used to compute the dissipation of energy by the viscous forces in the following chapter.

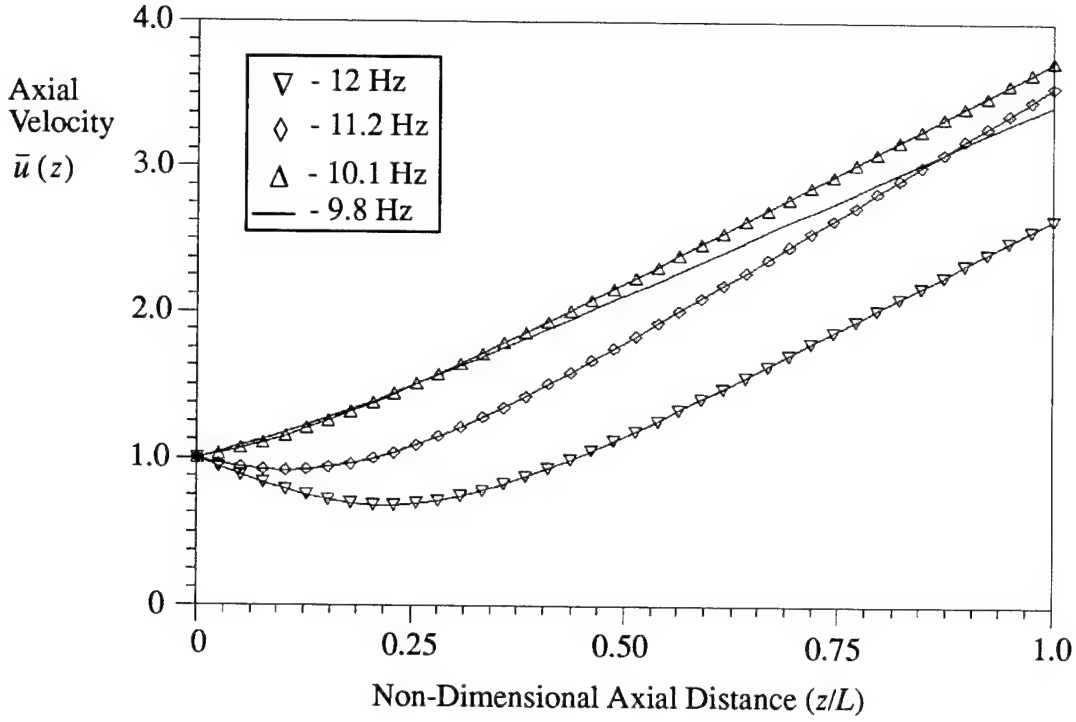

Figure 5.4. Non-Dimensional Axial Velocity Variation With Respect to Axial Position at Various Frequencies for 0.0 kV/mm Electric Field Application.

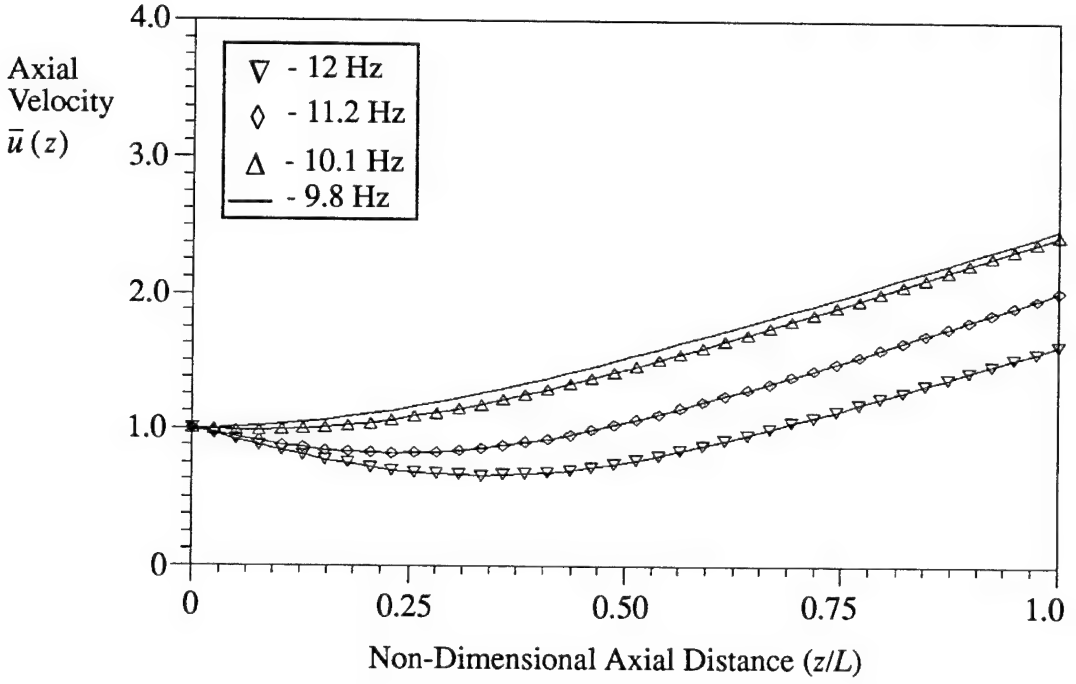

Figure 5.5. Non-Dimensional Axial Velocity Variation With Respect to Axial Position at Various Frequencies for 1.6 kV/mm Electric Field Application.

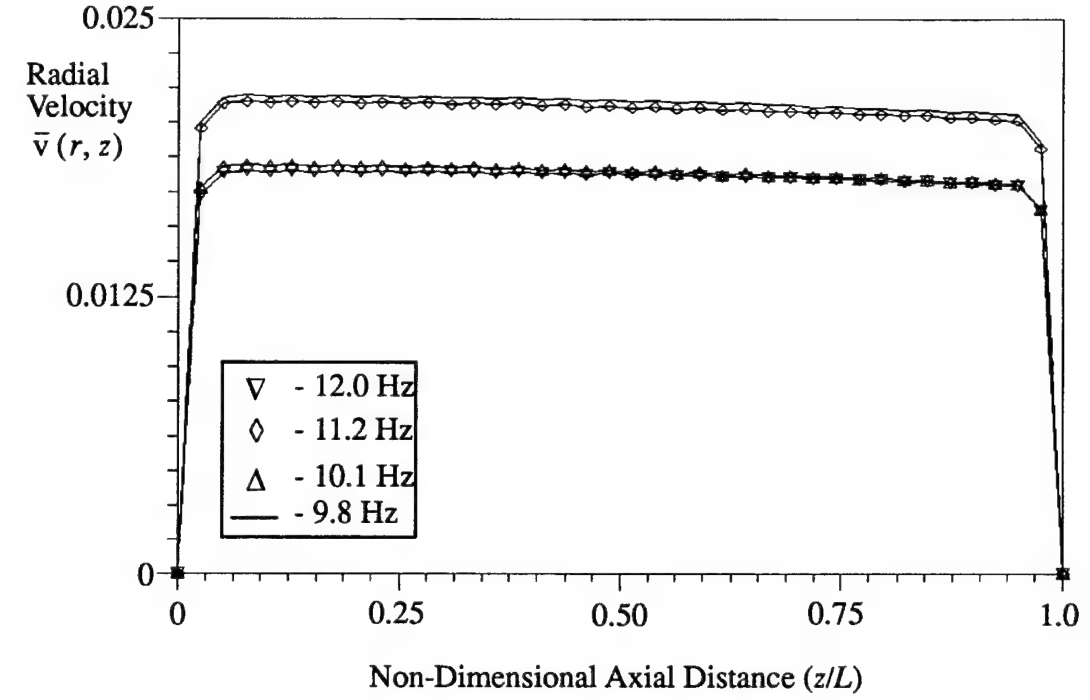

Figure 5.6. Non-Dimensional Radial Velocity Variation With Respect to Axial Position at Non-Dimensional Radius 0.223 for 0.0 kV/mm Electric Field Application.

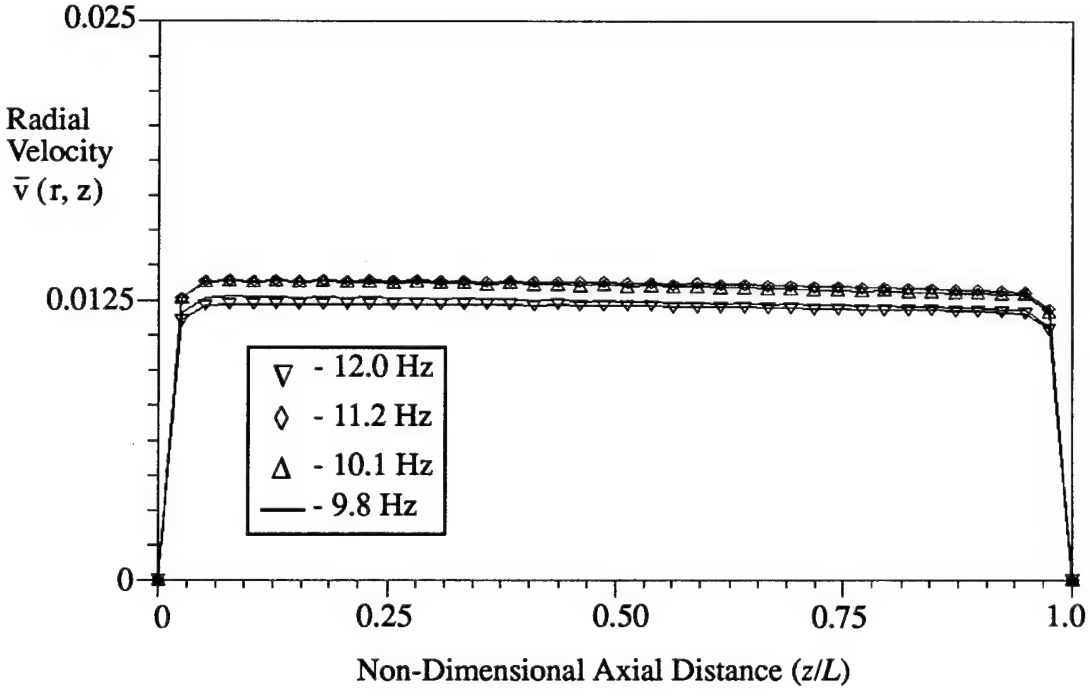

Figure 5.7. Non-Dimensional Radial Velocity Variation With Respect to Axial Position at Non-Dimensional Radius 0.223 for 1.6 kV/mm Electric Field Application.

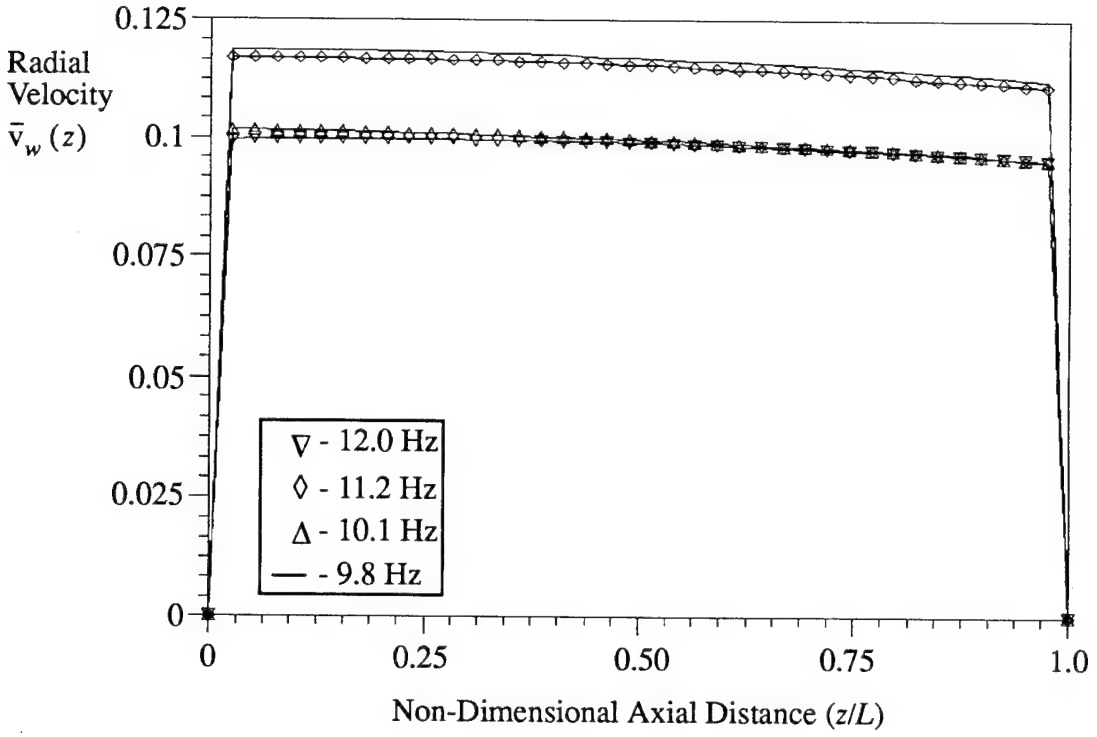

Figure 5.8. Non-Dimensional Radial Velocity Variation With Respect to Axial Position at the Wall for 0.0 kV/mm Electric Field Application.

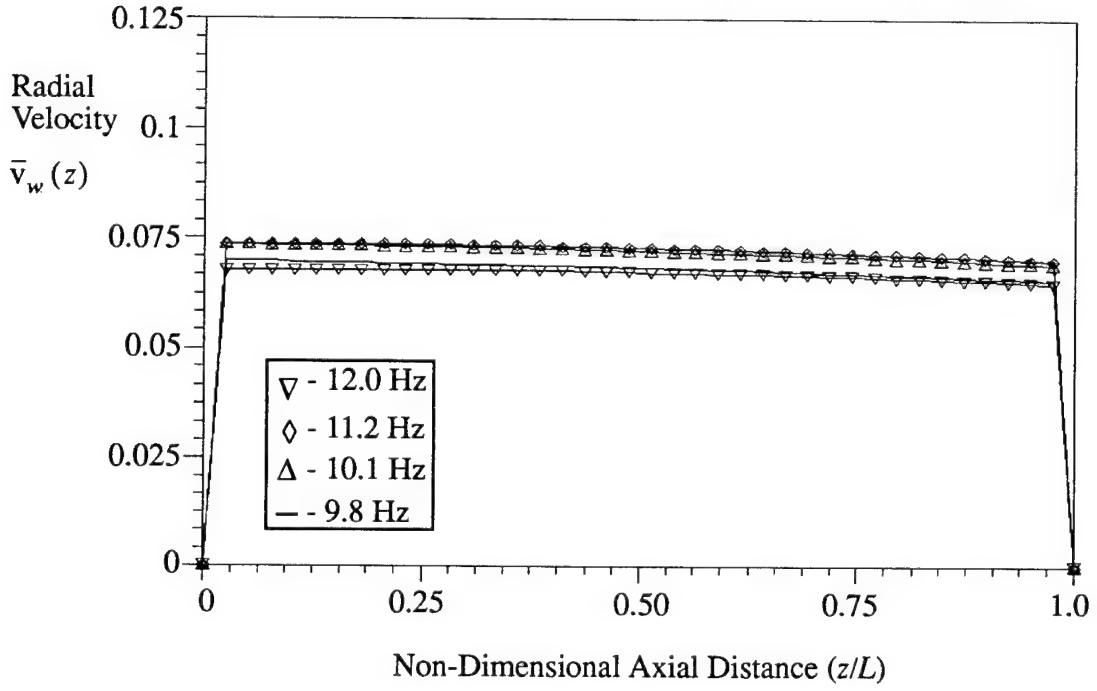

Figure 5.9. Non-Dimensional Radial Velocity Variation With Respect to Axial Position at the Wall for 1.6 kV/mm Electric Field Application.

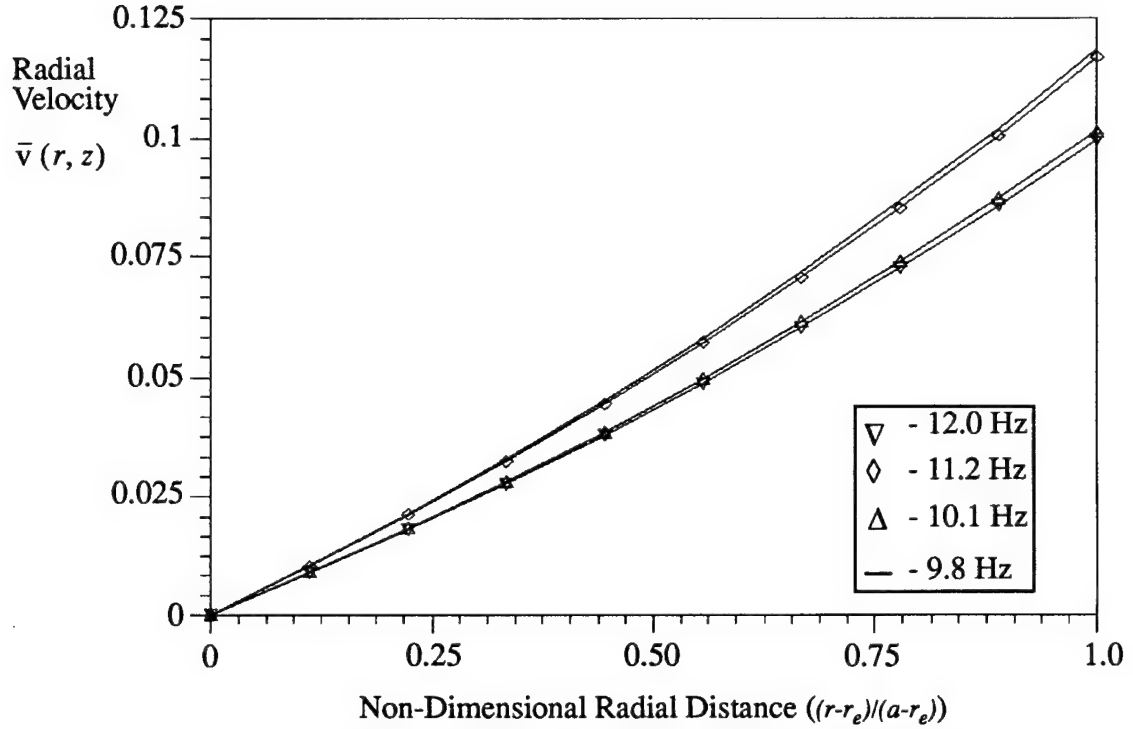

Figure 5.10. Non-Dimensional Radial Velocity Variation With Respect to Radial Position at 0.05 Non-Dimensional Axial Location for 0.0 kV/mm Electric Field Application.

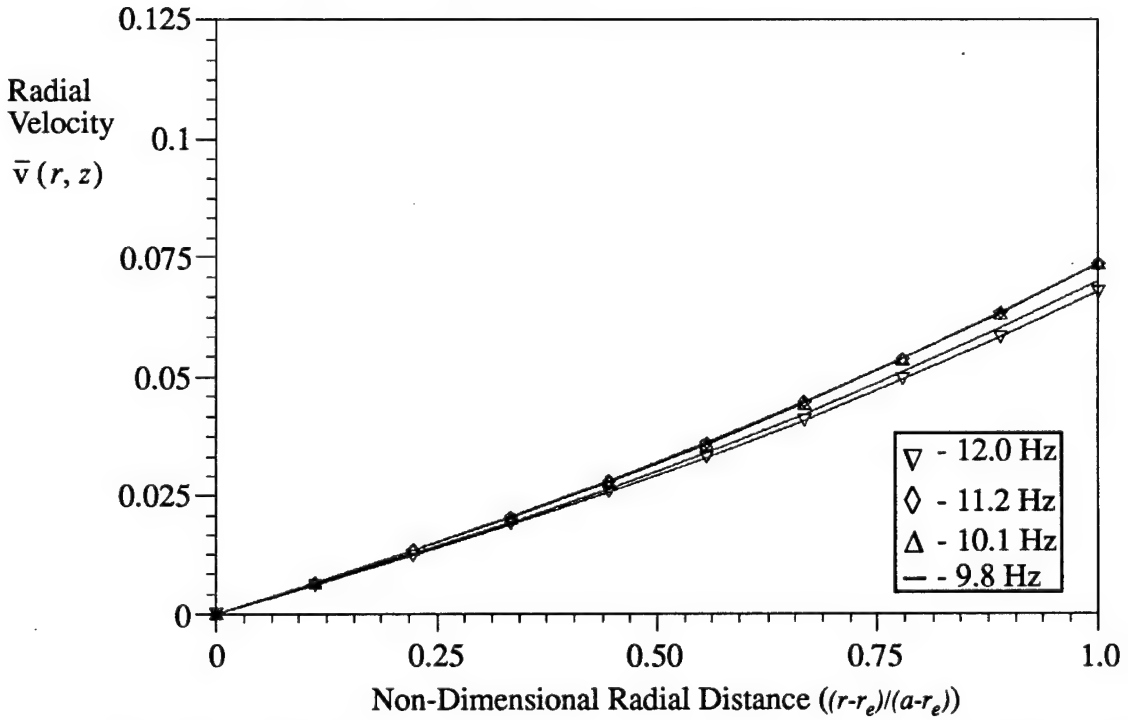

Figure 5.11. Non-Dimensional Radial Velocity Variation With Respect to Radial Position at 0.05 Non-Dimensional Axial Location for 1.6 kV/mm Electric Field Application.

Chapter 6: Electrorheological Fluid Damping Properties

Introduction

The motion of the ER fluid inside the ER test module has been shown to be governed by a Bingham, creep flow approximation. A function approximating the dissipation of the viscous energy was developed based on this fluid description and shown to revert to the Newtonian fluid description in the limit of the Bingham yield stress becoming zero. The expression for the damping property of the ER fluid is developed in the following sections. The damping capacity of the ER fluid is then compared to the results of the measurements discussed in Chapter 2.

Bingham Dissipation Function

The damping characteristics of the ER fluid inside the ER test module are quantified through the evaluation of the energy dissipation of the viscous forces. The dissipation function for a viscous fluid is found (Bird (1957)) to be

$$E_v = -\int_{Volume} [\underline{\tau} \Diamond \nabla \vec{V}]\, dVolume \tag{6-1}$$

where E_v is the local rate of dissipation of energy integrated over the volume of the fluid (Pa/sec), and $\nabla \vec{V}$ is the gradient of the velocity vector. The double-dot product between the symmetric stress tensor, $\underline{\tau}$, and the dyadic product of the velocity vector, $\nabla \vec{V}$, is evaluated in cylindrical coordinates as

$$[\underline{\tau} \Diamond \nabla \vec{V}] = -[\mu \Upsilon^2 + \tau_0 \Upsilon]\,. \tag{6-2}$$

In the limit as the yield stress, τ_0, goes to zero, the Newtonian expression for the dissipation function is obtained. The integration of equation (6-2) over the volume of the annular ER fluid region quantifies the amount of energy dissipated (i.e. converted kinetic energy to heat) in the ER fluid. This evaluation is compared to the total strain energy in the flexible cylinder in order to estimate the damping property of the ER fluid in terms of the electric field and frequency.

Damping Capacity of the ER Fluid

The damping capacity of the ER fluid can be defined as the ratio of the energy dissipated to the total strain energy in the structure. The dissipation of the viscous energy was evaluated by equation (6-1) in Section 6.2. The damping ratio calculation based on the amount of dissipated energy to the total strain energy is expressed as (Nashif et al. (1985))

$$\xi = \frac{\int_{volume} (E_v)\, dVolume}{4\pi \int_{volume} (SE)\, dVolume} \tag{6-3}$$

where E_v is the dissipated viscous energy defined by equation (6-1), and SE is the total strain energy in the structure. The damping ratio evaluated in equation (6-3) is equivalent to the expression developed in Chapter 2, equation (2-11).

Strain Energy in the Flexible Cylinder

The calculation of the strain energy in the flexible cylinder approximated as a thin shell has the form from Jones (1975)

$$SE = \frac{1}{2} \int_{Volume} (\tau_{\theta\theta}\varepsilon_{\theta\theta} + \tau_{zz}\varepsilon_{zz} + \tau_{rz}\gamma_{rz})\, dVolume \tag{6-4}$$

where $\varepsilon_{\theta\theta}$ is the circumferential strain, ε_{zz} is the longitudinal strain and γ_{rz} is the shear strain in the flexible shell. The determination of the strains in terms of the shell velocities are accomplished in a manner similar to Chapter 5. The resulting strains expressed in terms of the shell velocity components are

$$\varepsilon_{\theta\theta} = \frac{\mathrm{v}}{ai\omega} \tag{6-5}$$

$$\varepsilon_{zz} = \frac{1}{i\omega}\frac{du}{dz} \tag{6-6}$$

and

$$\gamma_{rz} = \frac{1}{i\omega}\frac{\partial v}{\partial z}. \tag{6-7}$$

The equation for the shear stress in terms of the velocity components of the flexible cylinder is expressed as

$$\tau_{rz} = \frac{G_c}{2i\omega}\frac{\partial v}{\partial z} \tag{6-8}$$

where G_c is the complex shear modulus of the flexible shell material. The circumferential and longitudinal stresses are evaluated from equations (5-36) and (5-31) respectively. The substitution of the stress and strain components into the strain energy equation produces

$$SE/Volume = \frac{1}{4\pi}\left[\frac{E_c}{i^2\omega}\left[\frac{v^2}{a^2} + 2\frac{vv}{a}\frac{du}{dz} + \left(\frac{du}{dz}\right)^2\right] + \frac{G_c}{i^2\omega}\left[\left(\frac{\partial v}{\partial z}\right)^2\right]\right], \tag{6-9}$$

for the flexible shell on a per volume basis.

Total Strain Energy and Total Viscous Dissipation Calculation

The damping ratio expressed, on a per volume basis, is

$$\xi/Volume = \frac{\omega\left[\mu\Upsilon^2 + \tau_0\Upsilon\right]}{E_c\left[\frac{v^2}{a^2} + 2\frac{vv}{a}\frac{du}{dz} + \left(\frac{du}{dz}\right)^2\right] + G_c\left[\left(\frac{\partial v}{\partial z}\right)^2\right]}. \tag{6-10}$$

Equation (6-10) shows that the damping ratio per volume has a direct functional dependence on the circular frequency, ω. This dependence is characteristic of the viscous damping phenomenon. The dissipation of the viscous energy in the ER fluid and the total strain energy in the elastomer shell must be evaluated for the entire structure as opposed to a per volume basis. The volumetric integral for the thin elastomer shell strain energy becomes

$$SE = 2\pi \int_0^{L} \int_0^{\delta} \left[\frac{1}{4\pi} \left[\frac{E_c}{i^2\omega} \left[\frac{v^2}{a^2} + 2\frac{vv}{a}\frac{du}{dz} + \left(\frac{du}{dz}\right)^2 \right] + \frac{G_c}{i^2\omega} \left[\left(\frac{\partial v}{\partial z}\right)^2 \right] \right] \right] r dr dz, \tag{6-11}$$

where δ is the thickness of the flexible shell in meters. The radial velocity component at the wall of the shell can be expressed in terms of the axial velocity by equation (5-38). Therefore, the strain energy of the flexible shell can be analytically evaluated in the form

$$SE = \frac{1}{2i^2\omega} \left[E_c \delta^2 (1+\nu) \left[\frac{kM^2}{2i} [1 - e^{2ikL}] + \frac{kN^2}{2i} [e^{-2ikL} - 1] + 2k^2 MNL \right] \right] + \frac{1}{2i^2\omega} \left[\frac{G_c \delta^2 a^2}{2} \left[\frac{k^3 M^2}{2i} [e^{2ikL} - 1] + \frac{k^3 N^2}{2i} [1 - e^{-2ikL}] + 2k^4 MNL \right] \right], \tag{6-12}$$

where the constants M and N are given from Chapter 5.

The integration of the viscous dissipation cannot be accomplished analytically. The evaluation of the dissipated energy in the ER fluid is obtained from the numerical integration of

$$\int_{Volume} E_v dVolume = 2\pi \int_0^{L} \int_{r_c}^{a} [\mu \Upsilon^2 + \tau_0 \Upsilon] r dr dz. \tag{6-13}$$

The modified Trapezoidal Rule was used to evaluate the total energy dissipated in the ER fluid. This integration technique should be accurate, since a fine grid resolution was used in the axial and radial directions.

The calculation of the damping coefficient, as described in equation (6-3), was made by evaluating equation (6-13) and dividing by equation (6-12). The comparison of the damping ratio for the various electric fields between the attenuation experiments and the fluid model is discussed in the next section.

Damping Ratio Comparison at Resonance

The application of damping to alter the dynamics of a structure is most effective near the resonant frequency of that structure. The dynamic components of the structure influence the response in a specific manner. The predominate influence of mass on the response of a structure occurs at frequencies above the system natural frequency. The predominate influence of stiffness on the response of a structure occurs at frequencies below the system natural frequency. The application of viscous damping will decrease the resonant frequency and lower the magnitude of the response. This is shown schematically in Figure 6.1. Figure 6.1 illustrates the regions of a typical system response and where the dynamic parameters impact the response. The magnitude of the transfer function measuring the structural response is plotted on the ordinate and the abscissa represents frequency. The values f_1 and f_2 are the half power point frequencies. These are the frequency values when the magnitude is equal to the magnitude at resonance divided by the square root of two. The damping ratios evaluated at the half power point frequencies will be used to compare the predicted results of the fluid model.

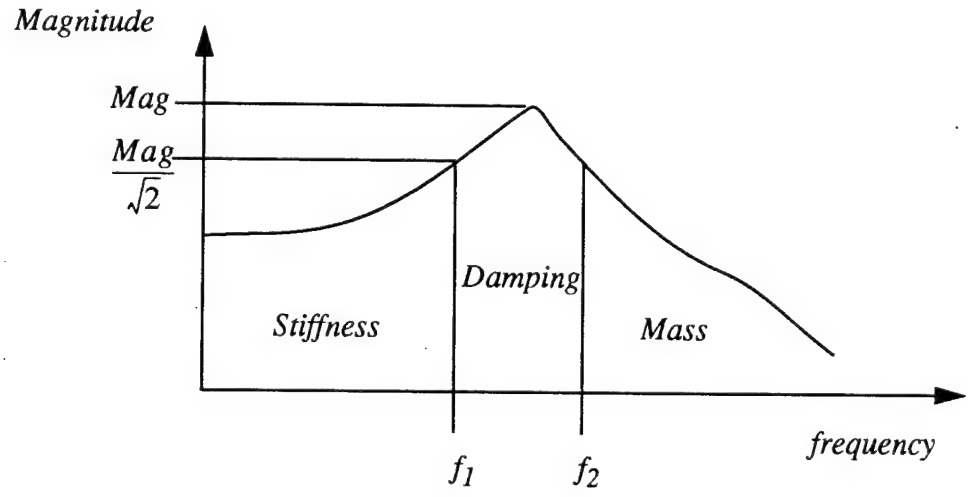

Figure 6.1. Influence of Dynamic Properties on the Response of a Structure

The single degree of freedom model developed in Chapter 2 provides a means to investigate the effects the electric field has on the dynamic stiffness of the structure, and to represent the damping capacity of the structure. However, it is best to evaluate the damping capacity of the ER

test module at resonance, since in practical application ER damping would be employed to influence resonant behavior. The results of this comparison are shown in Table 6.1. The difference at resonance between the fluid model predictions and the experimental measurements is at a maximum of five percent.

Electric Field (kV/mm)	**DATA** Half Power Point	**MODEL** Fluid Dynamic	%Δ
0.0	0.123	0.120	2.4
0.4	0.157	0.164	4.5
0.8	0.158	0.166	5.0
1.2	0.166	0.168	1.2
1.6	0.210	0.206	1.9

Table 6.1. Comparison of Predicted Damping Ratio to Measured

Outside the damping region of influence (refer to Figure 6.1), the predictions from the fluid model compared to the single degree of freedom model developed in Chapter 2 will diverge. This divergence is expected since the fluid model is purely a dissipation model, whereas, the single degree of freedom model includes the dynamic stiffness effects on the ER test module. However, the single degree of freedom model could not be used as a design tool for determining values of ER fluid rheological properties required to obtain damping at resonance.

The influence of the radial velocity component on the damping ratio predicted by the fluid model is significant. A test case was run for the 1.6 kV/mm data set in which the damping ratio was evaluated setting the radial velocities equal to zero. The resulting damping ratio calculated was seventy-six percent in error compared to the experiments from Chapter 2. This stresses the two dimensional nature of the fluid motion in the ER test module.

The final chapter will discuss how this viscous fluid model can be used to determine the rheological parameters of an ER fluid based on performance requirements. A program listing, DAMP, of the damping evaluation is given in Appendix D.

Summary

The damping characteristics of the ER fluid are derived based on the calculation of the energy dissipation due to the viscous forces. The dissipation of energy by the viscous forces is evaluated for an ideal Bingham fluid. The damping capacity of the ER fluid is found to be the ratio of the dissipated energy to the total strain energy in the flexible cylinder.

The damping ratio calculated by the ideal Bingham fluid model is compared to the damping ratio measured in the attenuation experiments of Chapter 2. The damping ratios evaluated from the half power point frequencies are used to compare to the predicted results of the fluid model. The comparison of the fluid model to the experiments of Chapter 2 produced differences of up to five percent.

Chapter 7: Conclusions and Future Work

Conclusions

The dissipation of longitudinal vibrational energy was experimentally measured and theoretically predicted for an ER fluid annulus contained by a flexible cylinder. The attenuation experiments (Chapter 2) illustrated the electric field dependence of the dynamic damping coefficient and the dynamic stiffness of the ER test module. The results of these attenuation experiments are that the resonant frequencies have been shifted as a function of applied electric field, the amplitude of the oscillation has been decreased, and the dynamic damping ratio has been increased by a factor of 1.75 due to an applied electric field of 1.6 kV/mm. The new mechanism of damping exploited in these experiments is the action of the shearing forces within the ER fluid. Previous researchers have relied on the interaction of a dash-pot type plunger mechanism for the damping applications of ER fluids.

In Chapter 3, the electric field strength is evaluated from Jacobian elliptic functions. This closed form solution to the electric field is used in Chapter 4 to derive the rheological parameters of the ER fluid. The Bingham rheological parameters were evaluated for the corn starch and mineral oil ER fluid used in the experiments described in Chapter 2. The relationship between the yield shear stress and the applied electric field is included in this discussion of the Bingham rheological parameters.

Once the ER fluid rheological properties were evaluated, a creeping, Bingham fluid model was developed in Chapter 5. This model predicts the radial and the axial velocity components in

the fluid resulting from the harmonic excitation. The axial velocity component was modeled as one-dimensional in the axial direction. The radial velocity component was modeled as two-dimensional in the radial and axial directions. These velocity profiles were used to formulate the Bingham viscous energy dissipation and the total strain energy for the flexible cylinder containing the fluid. The two-dimensional solution of the radial velocity component and the calculation of the energy dissipation by the viscous forces are new to this work. Additionally, the flexible hose boundary to the viscid internal ER fluid is a new contribution to the analysis of ER fluid applications.

The evaluation of the damping ratio based on the dissipated energy of the viscous forces and the total strain energy of the ER test module has not been found in the current literature. This evaluation of the damping ratio was made in Chapter 6. The Bingham fluid model predictions were within five percent of the measured damping ratios from Chapter 2.

The theoretical and experimental investigation of the dissipation of longitudinal vibrational energy in an ER fluid filled annulus by the action of shearing forces within the fluid has been presented in the dissertation. The deviation between the theoretical model prediction and the experimental measurements are within five percent. This successful mathematical formulation describing the damping contribution of an ER fluid will provide a manner of determining the necessary values of ER fluid parameters for various applications. An outline discussing the use of the developed Bingham fluid model for the application of the ER phenomenon is developed in the following section on Future Work.

Future Work

This numerical simulation of the developed theoretical model provides the ability to predict the required rheological properties of future ER fluids and system configurations. The prediction of the rheological properties could be accomplished as illustrated in the flow chart in Figure 7.1, which maps the logical progression of the numerical solution algorithm. The Bingham fluid motion program, developed in this dissertation, could be configured to solve the vibrational energy dissipation problem in reverse order. An attenuation would be specified as input to this reconfigured program and its output would be required values of ER fluid parameters. From the definition of the damping ratio, equation (6-1), the required amount of dissipated energy could be estimated to obtain the specified attenuation. Based on the amount of the dissipated energy, the magnitude of the viscous forces will define the two rheological parameters as defined by the

Bingham constitutive relationship, namely, the yield stress and the absolute viscosity.

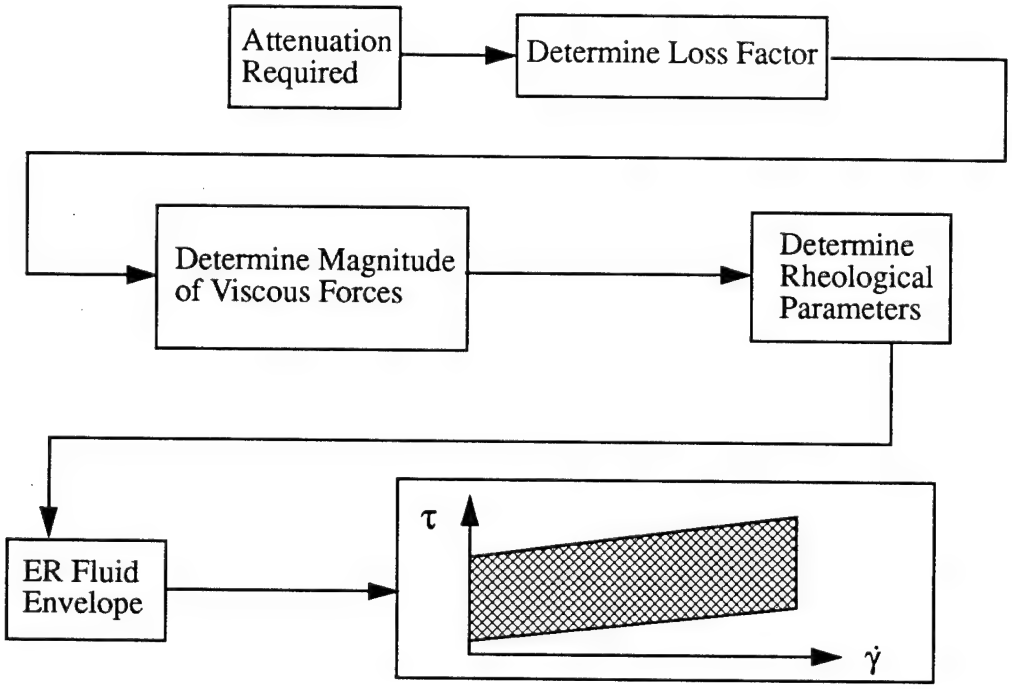

Figure 7.1. Proposed ER Rheological Parameter Estimation Algorithm

This technique will provide an electric field dependent parameter envelop. This parameter envelop, such as shown in Figure 4.6, will define the operational limitations of the required ER fluid. The parameter specification can be displayed as the ideal flow curve ($\tau - \dot{\gamma}$) for the candidate ER fluid which satisfies the boundary conditions.

The parameter estimation model, based on the Bingham fluid model developed in this dissertation, will provide ER fluid manufacturers with a tool for designing a fluid to achieve a specific damping performance.

Bibliography

Abramowitz, M., Stegun, I.E., eds, (1970) *Handbook of mathematical functions with formulas, graphs, and mathematical tables*, Dover Publications, New York, New York.

Ames, W.F., (1977) *Numerical Methods for Partial Differential Equations*, Second Edition, Academic Press, Inc., New York, NY.

Anderson, D.A., Tannehill, J.C., and Pletcher, R.H., (1984) *Computational Fluid Mechanics and Heat Transfer*, McGraw-hill Book Company, New York, NY.

Atkin, R.J., Shi, X., Bullough, W.A., (1991) Solutions of the constitutive equations for the flow of an electrorheological fluid in radial configurations, *J. Rheology* **35**, 1441-1461.

Binns, K.J., Lawrenson, P.J., (1963) *Analysis and Computation of Electric and Magnetic Field Problems*, Pergamon Press Limited, Oxford, England.

Bird, R.B., Stewart, W.E., Lightfoot, E.N., (1960) *Transport Phenomena*, John Wiley & Sons, New York, NY.

Bird, R.B., (1957) The equations of change and the macroscopic mass, momentum, and energy balances, *Chemical Engineering Science* **6**, 123-131.

Block, H., Kelly, J., (1988) Electro-rheology, *J. Phys D: Appl. Phys.* **21**, 1661-1677.

Bonnecaze, R.T., Brady, J.F., (1992) Yield stresses in electrorheological fluids, *J. Rheology* **36**, 73-114.

Brooks, D.A., Goodwin, J., Hjelm, C., Marshall, L., Zukoski, C., (1986) Visco-elastic studies on an electro-rheological fluid, *Colloids and Surfaces* **18**, 293-312.

Brooks, D.A., (1989) Devices using electro-rheological fluids, *Proceedings of the Second International Conference on ER Fluids*, Edited by J.D. Carlson, A.F. Sprecher, H. Conrad, Technomic Publishing Co., Inc., Lancaster, PA, 371-401.

Coulter, J.P., Duclos, T.G., Acker, D.N., (1989) The usage of electrorheological materials in visoelastic layer damping applications, *Proceedings of DAMPING'89*, CAA1-CAA17.

Coulter, J.P., Weiss, K.D., Carlson, J.D., (1992) Electrorheological materials and their usage in intelligent material systems and structures, part II: applications, *Recent Advances in Adaptive and Sensory Materials and Their Applications*, Edited by C.A. Rogers and R.C. Rogers, Technomic Publishing Co., Inc., Lancaster, PA, 507-523.

Duclos, T.G., (1988) Designs of devices using electrorheological fluids, *Society of Automotive Engineers Technical Paper 881134*, Warrendale, PA.

Duggins, R.K., (1972) The commencement of flow of a Bingham plastic fluid, *Chem. Eng. Sci.* **27**, 1991-1996.

Edwards, M.F., Nellist, D.A., Wilkinson, W.L., (1972) Unsteady laminar flows of non-Newtonian fluids in pipes, *Chem. Eng. Sci.* **27**, 295-306.

Gast. A.P., Zukoski, C.F., (1989) Electrorheological fluids as colloidal suspensions, *Adv. Colloid Interface Sci.* **30**, 153.

Gradshteyn, I.S., Ryzhik, I.M., (1980) *Table of integrals, series, and products*, Academic Press, Inc., New York, NY.

Greenhill A.G., (1959) *The Application of Elliptic Functions*, Dover Publications, New York, NY.

Hull, A.J., (1994) A non-conforming approximate solution to a specially orthotropic axisymmetric thin shell subjected to a harmonic displacement boundary condition, *J. of Sound and Vibration* **177**, 611-621.

Jones, R.M., (1975) *Mechanics of composite materials*, Scripta Book Company, Washington, D.C.

Jordan, T.C., Shaw, M.T., (1989) Structure in electrorheological fluids, *Proceedings of the Second International Conference on ER Fluids*, Edited by J.D. Carlson, A.F. Sprecher, H. Conrad, Technomic Publishing Co., Inc., Lancaster, PA, 231-251.

Junger, M.C., Feit, D., (1986) *Sound, structures, and their interaction*, Second Edition, MIT Press, Cambridge, MA.

Klass, D.L., Martinek, T.W., (1967) Electroviscous fluids I. Rheological properties, *J. Appl. Phys.* **38**, 67-74.

Klass, D.L., Martinek, T.W., (1967) Electroviscous fluids II. Electrical properties, *J. Appl. Phys.* **38**, 75-80.

Klingenberg, D.J., Zukoski, C.F., (1990) Studies on the steady shear behavior of electrorheological suspensions, *Langmuir* **6**, 15.

Langlois, W.E., (1964) *Slow viscous flow*, The Macmillan Company, New York, NY.

Lawden, D.F., (1989) *Elliptic functions and applications*, Springer-Verlag, New York, NY.

Lipscomb, G.G, Denn, M.M., (1984) Flow of Bingham fluids in complex geometries, *J. Non-Newtonian Fluid Mechanics* **14**, 337-346.

Love, A.E.H., (1924) Some electrostatic distributions in two dimensions, *London Math Soc. Proc.* **22**, 337.

Maciejewski, W., Tryon, R., (1992) Rheology of corn starch and mineral oil ER fluid, NUWC Memorandum.

Margolis, D.L, Vahdati, N., (1989) The control of damping in distributed systems using ER fluids, *Proceedings of the Second International Conference on ER Fluids*, Edited by J.D. Carlson, A.F. Sprecher, H. Conrad, Technomic Publishing Co., Inc., Lancaster, PA, 326-348.

Marshall, L., Goodwin, J.W., Zukoski, C.F., (1989) Effects of electric fields on the rheology of nonaqueous concentrated suspensions, *J. Chem. Soc. Faraday I* **85**, 2785-2795.

Maxwell, C., (1892) *Electricity and magnetism*, Oxford University Press, Volume I.

Milne-Thomson, L.M., (1932) The zeta function of Jacobi, *Proc. Royal Soc. Edinburgh* **52**, 236-250.

Milne-Thomson, L.M., (1950), *Jacobian elliptic function tables*, Dover Publications, Inc., New York, NY.

Mitchell, J.H., (1894) A map of the complex z-function: a condenser problem, *Mess. of Math.* **23**, 72-78.

Moon, P, Spencer, D.E., (1953) Some coordinate systems associated with elliptic functions, *J. Franklin Inst.* **255**, 531-543.

Moon, P., Spencer, D.E., (1951) Cylindrical and rotational coordinate systems, *J. Franklin Inst.* **252**, 327-344.

Moon, P., Spencer, D.E., (1988) *Field theory handbook*, Second Edition, Springer-Verlag, New York, NY.

Moretti, G., (1964) *Functions of a complex variable*, Prentice-Hall, Inc., Englewood, NJ.

Nashif, A.D., Jones, D.I.G., Henderson, J.P., (1985) *Vibration damping*, John Wiley & Sons, New York, NY.

Schlichting, H., (1979) *Boundary-layer theory*, Seventh Edition, McGraw-Hill Book Company, New York, NY.

Schwab, A.J., (1988) *Field theory concepts*, Springer-Verlag, New York, NY.

Stanway, R., Sproston, J.L., Stevens, N.G., (1987) Non-linear modelling of an electro-rheological vibration damper, *J. of Electrostatics* **20**, 167-184.

Steidel, R.E., Jr., (1979) *An Introduction to Mechanical Vibrations, Second Edition*, John Wiley and Sons, New York, NY.

Stevens, N.G., Sproston, J.L., Stanway, R., (1984) Experimental evaluation of a simple electroviscous damper, *J. of Electrostatics* **15**, 275-283.

Tao, R., Woestman, J.T., Jaggi, N.K., (1989) Electric field induced solidification, *Appl. Phys. Lett.* **55**, 1844-1846.

Walton, I.C., Bittleson, S.H., (1991) The axial flow of a bingham plastic in a narrow eccentric annulus, *J. Fluid Mech.* **222**, 39-60.

Wang, K.C., McLay, R., Carey, G.F., (1989) ER fluid modeling, *Proceedings of the Second International Conference on ER Fluids*, Edited by J.D. Carlson, A.F. Sprecher, H. Conrad, Technomic Publishing Co., Inc., Lancaster, PA, 41-52.

White, F.M., (1974) *Viscous fluid flow*, McGraw-Hill Book Company, New York, NY.

Wilkinson, W.L., (1960), *Non-Newtonian fluids*, Pergamon Press, New York, NY.

Winslow, W.M., (1989) The Winslow effect, Keynote Address, *Proceedings of the Second International Conference on ER Fluids*, Edited by J.D. Carlson, A.F. Sprecher, H. Conrad, Technomic Publishing Co., Inc., Lancaster, PA.

Winslow, W.M., (1949) Inducted vibration of suspensions, *J. Appl. Phys.* **20**, 1137-1140.

Wong, W., Shaw, M.T., (1989) Role of water in electrorheological fluids, *Proceedings of the Second International Conference on ER Fluids*, Edited by J.D. Carlson, A.F. Sprecher, H. Conrad, Technomic Publishing Co., Inc., Lancaster, PA, 191-195.

Appendix A

The single degree of freedom model developed in Chapter 2 was coded in ***FORTRAN*** to evaluate the electric field and frequency dependent dynamic stiffness and dynamic damping. This program also evaluates the amplitude ratio and the decay in oscillation of the amplitude. This model reads the experimentally measured transfer function and operates on the equations developed. The resulting graphics were produced using standard PLOT10 routines. The computer utilized was a Sun Microsystems SparcStation 1+.

```
C MCK-given the M value determine a frequency dependent C and K (N*m*s*kg)
C
 PROGRAM NEWMOD0
C
 REAL*4 FREQ(1000),REDA(1000),IMDA(1000)
 REAL*4 EMAG(1000),EPHA(1000),MMAG(1000),MPHA(1000)
 REAL*4 C(1000),K(1000),M,DMPRAT(1000)
 REAL*4 XWN(2),YWN(2),RDI,IDI,NUM,DOM
 REAL*4 FMAX,MAX,NAT
C
 COMPLEX*8 CTEMP1,CTEMP2,CTEMP3,RCTEMP
C
 INTEGER INUM,I
C
 OPEN(11,FILE='zstiff.dat',STATUS='OLD')
 OPEN(12,FILE='zdam.dat',STATUS='OLD')
C******* MASS GIVEN IN UNITS OF KILOGRAMS (kg) ********
C
 M = 30.0
 NAT = 11.0*2.0*3.141593
 XWN(1) = 11.0
 XWN(2) = 11.0
 YWN(1) = 0.0
 YWN(2) = 5.E6
C
C--Read the data
C
 INUM = 1
100 CONTINUE
 OPEN (10,FILE='zvolt.dat',STATUS='OLD')
 READ (10,*,END=110) FREQ(INUM),REDA(INUM),IMDA(INUM)
 CTEMP3 = CMPLX(REDA(INUM), IMDA(INUM))
 RCTEMP = (-1.,0.0)*CTEMP3
 REDA(INUM) = REAL(RCTEMP)
 IMDA(INUM) = IMAG(RCTEMP)
 INUM = INUM + 1
 GOTO 100
110 CONTINUE
 CLOSE (10)
```

```
 INUM = INUM - 1
C
C--Get the magnitude and phase data
C
 MAX = 0.0
C
 DO 200 I = 1, INUM, 1
 EMAG(I) = SQRT ( (REDA(I)**2) + (IMDA(I)**2) )
 IF (EMAG(I).GT.MAX) THEN
 MAX = EMAG(I)
 FMAX = FREQ(I)
 END IF
 EPHA(I) = ATAN2 ( IMDA(I), REDA(I) )
 EPHA(I) = ( 180.0 / 3.141592 ) * EPHA(I)
200 CONTINUE
 WRITE(10,*)FMAX,MAX
C
C--Create the model by matching it to a spring, mass, damper system
C
 DO 500 I = 1, INUM, 1
C
 W = FREQ(I) * 2.0 * 3.141592
 CTEMP3 = CMPLX(REDA(I),IMDA(I))
 RCTEMP = (1.0,0.0)/CTEMP3
 RDI = REAL(RCTEMP)
 IDI = IMAG(RCTEMP)
 DOM = (RDI-1.)**2 + IDI**2
 NUM = (RDI - 1.)
 K(I) = -1.0*( M * (W**2)*NUM ) / DOM
 C(I) = -1.*K(I)*IDI/(W*NUM)
C
DMPRAT(I) = C(I) / (2.0*M*NAT)
      WRITE(11,*)FREQ(I),K(I)
      WRITE(12,*)FREQ(I),DMPRAT(I)
 WRITE(13,*)FREQ(I),EPHA(I)
C
500 CONTINUE
C
C--Plot to the screen
C
 CALL INITT (960)
 CALL BINITT
 CALL NPTS (INUM)
 CALL CHECK (FREQ,C)
 CALL DLIMX ( 5.0, 30.0 )
 CALL DLIMY ( 0.0,1000.0 )
 CALL DSPLAY (FREQ,C)
 CALL HLABEL (400,50,1.0,'FREQUENCY (HERTZ)')
 CALL HLABEL (400,675,1.0,'DYNAMIC DAMPING 0.0kV/mm')
 CALL VLABEL (50,500,1.0,'DAMPING')
 CALL HLABEL (40,150,1.0,'N*S/M')
 CALL NPTS (2)
 CALL LINE (1)
 CALL CPLOT (XWN,YWN)
```

```
 CALL ANMODE
 CALL HOME
C
C--Next plot (stop for viewing of previous plot)
C Plot stiffness
C
 WRITE (6,*) ' '
 WRITE (6,*) ' <RETURN> for next plot '
 READ (5,*)
C
 YWN(2) = 0.15E6
 CALL INITT (960)
 CALL BINITT
 CALL NPTS (INUM)
 CALL CHECK (FREQ,K)
 CALL DLIMX ( 5.0, 30.0 )
 CALL DLIMY ( 0.0, 2.5E5 )
 CALL DSPLAY (FREQ,K)
 CALL HLABEL (400,50,1.0,'FREQUENCY (HERTZ)')
 CALL HLABEL (400,675,1.0,'DYNAMIC STIFFNESS 0.0kV/mm')
 CALL VLABEL (50,500,1.0,'STIFFNESS')
 CALL HLABEL (40,200,1.0,'N/M')
 CALL NPTS (2)
 CALL LINE (1)
 CALL CPLOT (XWN,YWN)
 CALL ANMODE
 CALL HOME
C
C--Next plot (stop for viewing of previous plot)
C Plot stiffness
C
 WRITE (6,*) ' '
 WRITE (6,*) ' <RETURN> for next plot '
 READ (5,*)
C
 YWN(2) = 10.0
 CALL INITT (960)
 CALL BINITT
 CALL NPTS (INUM)
 CALL CHECK (FREQ,DMPRAT)
 CALL DLIMX ( 5.0, 30.0 )
 CALL DLIMY (.0, 0.50 )
 CALL DSPLAY (FREQ,DMPRAT)
 CALL HLABEL (400,50,1.0,'FREQUENCY (HERTZ)')
 CALL HLABEL (400,675,1.0,'DAMPING RATIO 0.0kV/mm')
 CALL VLABEL (50,500,1.0,'RATIO')
 CALL NPTS (2)
 CALL LINE (1)
 CALL CPLOT (XWN,YWN)
 CALL ANMODE
 CALL HOME
C
C--Next plot (stop for viewing of previous plot)
C Plot of phase angle
```

```
C
 WRITE (6,*) ' '
 WRITE (6,*) ' <RETURN> for next plot '
 READ (5,*)
C
C--Rebuild the model to insure it matches the data
C
 DO 600 I = 1, INUM, 1
 W = FREQ(I) * 2.0 * 3.141592
 CTEMP2 = CMPLX ( (K(I)-M*(W**2)), W*C(I) ) /
 1 CMPLX ( K(I),C(I)*W )
 CTEMP1 = (1.0,0.0)/CTEMP2
 MMAG(I) = SQRT ( (REAL(CTEMP1))**2 + (IMAG(CTEMP1))**2 )
 MPHA(I) = ATAN2 ( IMAG(CTEMP1), REAL(CTEMP1) )
 MPHA(I) = ( 180.0 / 3.141592 ) * MPHA(I)
600 CONTINUE
C
 CALL INITT (960)
 CALL BINITT
 CALL RECOVR
 CALL NPTS (INUM)
 CALL DLIMX ( 0.0, 30.0 )
 CALL DLIMY ( 0.0, 5.0 )
 CALL DSPLAY (FREQ,EMAG)
 CALL LINE (-1)
 CALL SYMBL (4,5)
 CALL CPLOT (FREQ,MMAG)
 CALL ANMODE
 CALL HOME
C
C--Next plot (stop for viewing of previous plot)
C Plot of phase angle
C
 WRITE (6,*) ' '
 WRITE (6,*) ' <RETURN> for next plot '
 READ (5,*)
CALL INITT (960)
 CALL BINITT
 CALL RECOVR
 CALL NPTS (INUM)
 CALL DLIMX ( 0.0, 30.0 )
 CALL DLIMY ( -180.0, 180.0 )
 CALL DSPLAY (FREQ,EPHA)
 CALL LINE (-1)
 CALL SYMBL (3,5)
 CALL CPLOT (FREQ,MPHA)
 CALL ANMODE
 CALL HOME
     CLOSE(11)
     CLOSE(12)
END
```

Appendix B

The representation of the Jacobian zeta function and the elliptic integrals are made using the following identities. The Jacobian zeta function is evaluated using the definition found in Milne-Thomson (1932) and Moretti (1964):

$$\Im(u) = \int_0^u dn(t)^2 dt - u\frac{E}{K} \tag{B-42}$$

where *dn(t)* is the difference-amplitude, E is the complete elliptic integral of the second kind, and K is the complete elliptic integral of the first kind. The complete elliptic integral of the second kind, E, can be evaluated by the following expression:

$$E = \int_0^{\frac{\pi}{2}} [1 - m(\sin\phi)^2]\, d\phi. \tag{B-43}$$

The complete elliptic integral of the first kind can be expressed as:

$$K = \int_0^{\frac{\pi}{2}} \frac{d\phi}{[1 - m(\sin\phi)^2]}. \tag{B-44}$$

The relationships used to express the elliptic integrals and the Jacobian zeta function produce results that are sixth place accurate compared to Milne-Thomson (1950). Equations (B-1), (B-2), and (B-3) are evaluated using a twelfth order Gaussian integration. The *FORTRAN* programs are found at the end of this appendix.

The representation of the sine-amplitude, *sn()*, cosine-amplitude, *cn()*, and the difference-amplitude, *dn()*, functions are made using the series approximations found in Abramowitz & Stegun (1970). The computer routines to evaluate these functions are included at the end of this appendix.

The differentiation of equation (3-4), on page 23, to produce the strength of the electric field is accomplished by using identities of the Elliptic functions. The differentiation of equation (3-4) is as follows:

$$\frac{dy}{dw} = \frac{2Kd}{\pi}\frac{d}{dw}(\Im(w + iK')) + \frac{d}{dw}(id) \tag{B-45}$$

The complex argument of the Jacobian zeta function can be expanded by the use of an identity found in Lawden (1989):

$$\Im(w+iK') = \Im(w) - \frac{i\pi}{m} + cs(w)\,dn(w) \tag{B-46}$$

where *cs(w)* is equal to the cosine-amplitude divided by the sine-amplitude. Applying the following identities:

$$\Im(w) = E(w) - w\frac{E}{K} \tag{B-47}$$

$$\frac{dE}{dw} = dn^2(w), \tag{B-48}$$

produces,

$$\frac{dy}{dw} = \frac{2Kd}{\pi}\left(dn^2(w) - \frac{E}{K} + \frac{d}{dw}\left[\frac{cn(w)\,dn(w)}{sn(w)}\right]\right). \tag{B-49}$$

Carrying out the differentiation with respect to w and using the identity,

$$dn^2(w) + m^2 sn^2(w) = 1 \tag{B-50}$$

to combine and simplify terms, the electric field strength equation given in Chapter 3 as equation (3-11) is produced.

The following programs evaluate the Elliptic functions, the complete elliptic integrals of the first and second kind, and the Jacobian zeta function:

The elliptic cosine-amplitude function, *cn()*.

```
 SUBROUTINE JACOBCN(CNU,U,M)
 REAL PI,C,CN,K1,K,E,E1,B,Q,M,MR,U,V,VV,N,N1,N2,CNU,CN1
    COMMON PI,K,K1,E,E1
C ***************** COMPUTES THE JACOBIAN CN(U) FUNCTION ******************
 C = 0.0
 CN = 0.0
 B = -1.0 * PI * (K1/K)
 Q = EXP(B)
 V = U * PI/2./K
```

```
MR = SQRT(M)
VV = 2.0 * PI/MR/K
DO N = 0.,100.
N1 = 2.0 * N + 1.0
N2 = N + .5
C = ((Q**N2)/(1.+Q**N1))*COS(N1*V)
CN1 = C + CN
CN = CN1
C = 0.0
CN1 = 0.0
END DO
CNU = VV*CN
RETURN
END
```

The elliptic sine-amplitude function, *sn()*.

```
    SUBROUTINE JACOBSN(SNU,U,M)
    REAL PI,S,SN,E,K,K1,B,Q,M,MR,U,V,VV,N,N1,N2,SNU,SN1,E1
    COMMON PI,K,K1,E,E1
C ***************** COMPUTES THE JACOBIAN SN(U) FUNCTION ******************
    S = 0.0
    SN = 0.0
    B = -1.0 * PI * (K1/K)
    Q = EXP(B)
    V = U * PI/2./K
    MR = SQRT(M)
    VV = 2.0 * PI/MR/K
    DO N = 0.,100.
        N1 = 2.0 * N + 1.0
        N2 = N + .5
        S = ((Q**N2)/(1.-Q**N1))*SIN(N1*V)
        SN1 = S + SN
        SN = SN1
        S = 0.0
        SN1 = 0.0
    END DO
    SNU = VV*SN
    RETURN
    END
```

The Elliptic difference-amplitude function, *dn()*.

```
 SUBROUTINE JACOBDN(DNU,U)
 REAL PI,D,DN,E,E1,K1,K,B,Q,U,V,VV,VG,N,N1,DNU,DN1
    COMMON PI,K,K1,E,E1
C ***************** COMPUTES THE JACOBIAN DN(U) FUNCTION ******************
 D = 0.0
 DN = 0.0
 B = -1.0 * PI * (K1/K)
 Q = EXP(B)
 V = U * PI/2./K
 VV = 2.0 * PI/K
    VG = PI/(2.0*K)
 DO N = 1.,100.
```

```
N1 = 2.0 * N
D = ((Q**N)/(1.+Q**N1))*COS(N1*V)
DN1 = D + DN
DN = DN1
D = 0.0
DN1 = 0.0
END DO
DNU = VG + VV*DN
    RETURN
END
```

The complete elliptic integral of the first kind, *K*.

```
    SUBROUTINE ELLIPK(TOT,HLM,M)
C ********** CALCULATES THE ELLIPTIC INTEGRAL OF THE FIRST KIND (K) *********
    REAL ARG,SARG,T(24),W(24),INT,HLM,LLM,XX,DX,TOT,M,PI
    COMMON PI,K,K1,E,E1
    INT = 0.0
C ***************************************************************************
C ***** GAUSSIAN INTEGRATION TWELFTH ORDER ********
C ***************************************************************************
C ***** ABSCISSAS & WEIGHT FACTORS ********
C ***** p.916 Abramowitz & Stegun, Handbook of Mathematical Functions ********
C ***** Dover Publications, Inc., New York, (1965). ********
C ***************************************************************************
    T(1) = 0.064056892862605
    T(2) = 0.191118867473616
    T(3) = 0.315042679696163
    T(4) = 0.433793507626045
    T(5) = 0.545421471388839
    T(6) = 0.648093651936975
T(7) = 0.740124191578554
T(8) = 0.820001985973902
T(9) = 0.886415527004401
T(10) = 0.938274552002732
T(11) = 0.974728555971309
T(12) = 0.995187219997021
T(13) = -0.064056892862605
T(14) = -0.191118867473616
T(15) = -0.315042679696163
T(16) = -0.433793507626045
T(17) = -0.545421471388839
T(18) = -0.648093651936975
T(19) = -0.740124191578554
T(20) = -0.820001985973902
T(21) = -0.886415527004401
T(22) = -0.938274552002732
T(23) = -0.974728555971309
T(24) = -0.995187219997021
    W(1) = 0.127938195346752
    W(2) = 0.125837456346828
    W(3) = 0.121670472927803
    W(4) = 0.115505668053725
    W(5) = 0.107444270115965
    W(6) = 0.097618652104113
```

```
      W(7) = 0.086190161531953
      W(8) = 0.073346481411080
      W(9) = 0.059298584915436
      W(10) = 0.044277438817419
      W(11) = 0.028531388628933
      W(12) = 0.012341229799987
      W(13) = 0.127938195346752
      W(14) = 0.125837456346828
      W(15) = 0.121670472927803
      W(16) = 0.115505668053725
      W(17) = 0.107444270115965
      W(18) = 0.097618652104113
      W(19) = 0.086190161531953
      W(20) = 0.073346481411080
      W(21) = 0.059298584915436
      W(22) = 0.044277438817419
      W(23) = 0.028531388628933
      W(24) = 0.012341229799987
C ********************************************************************************
      LLM = 0.0
      DX = (HLM - LLM)/2.
      DO I=1,24
         XX = ((HLM-LLM)*T(I) + HLM + LLM)/2.
ARG = 1.0 - M*((SIN(XX))**2.)
SARG = (ARG)**-0.5
         INT = W(I)*SARG + INT
      END DO
      TOT = DX*INT
      RETURN
      END
```

The complete elliptic integral of the second kind, *E*.

```
      SUBROUTINE ELLIPE(TOT,HLM,M)
C ********** CALCULATES THE ELLIPTIC INTEGRAL OF THE SECOND KIND (E) *********
      REAL ARG,SARG,T(24),W(24),INT,HLM,LLM,XX,DX,TOT,M,PI
      COMMON PI,K,K1,E,E1
      INT = 0.0
C ********************************************************************************
C ***** GAUSSIAN INTEGRATION TWELFTH ORDER ********
C ********************************************************************************
C ***** ABSCISSAS & WEIGHT FACTORS ********
C ***** p.916 Abramowitz & Stegun, Handbook of Mathematical Functions ********
C ***** Dover Publications, Inc., New York, (1965). ********
C ********************************************************************************
      T(1) = 0.064056892862605
      T(2) = 0.191118867473616
      T(3) = 0.315042679696163
      T(4) = 0.433793507626045
      T(5) = 0.545421471388839
      T(6) = 0.648093651936975
 T(7) = 0.740124191578554
 T(8) = 0.820001985973902
 T(9) = 0.886415527004401
```

```
T(10) = 0.938274552002732
T(11) = 0.974728555971309
T(12) = 0.995187219997021
T(13) = -0.064056892862605
T(14) = -0.191118867473616
T(15) = -0.315042679696163
T(16) = -0.433793507626045
T(17) = -0.545421471388839
T(18) = -0.648093651936975
T(19) = -0.740124191578554
T(20) = -0.820001985973902
T(21) = -0.886415527004401
T(22) = -0.938274552002732
T(23) = -0.974728555971309
T(24) = -0.995187219997021
    W(1) = 0.127938195346752
    W(2) = 0.125837456346828
    W(3) = 0.121670472927803
    W(4) = 0.115505668053725
    W(5) = 0.107444270115965
    W(6) = 0.097618652104113
W(7) = 0.086190161531953
W(8) = 0.073346481411080
W(9) = 0.059298584915436
W(10) = 0.044277438817419
W(11) = 0.028531388628933
W(12) = 0.012341229799987
W(13) = 0.127938195346752
W(14) = 0.125837456346828
W(15) = 0.121670472927803
W(16) = 0.115505668053725
W(17) = 0.107444270115965
W(18) = 0.097618652104113
W(19) = 0.086190161531953
W(20) = 0.073346481411080
W(21) = 0.059298584915436
W(22) = 0.044277438817419
W(23) = 0.028531388628933
W(24) = 0.012341229799987
C ********************************************************************************
    LLM = 0.0
    DX = (HLM - LLM)/2.
    DO I=1,24
        XX = ((HLM-LLM)*T(I) + HLM + LLM)/2.
ARG = 1.0 - M*((SIN(XX))**2.)
SARG = (ARG)**0.5
        INT = W(I)*SARG + INT
    END DO
    TOT = DX*INT
    RETURN
    END
```

The Jacobian zeta function, $\Im(w)$

```
    SUBROUTINE ZETA(Z,U)
```

```
C ***************************************************************************
C ********** COMPUTES THE JACOBIAN ZETA FUNCTION ACCURATE TO SIX PLACES *******
C ********** The Jacobian ZETA Function is defined as Z(U) = E(U) - UE/K *******
C ********** This definition is found in L. M. Milne-Thomson, Jacobian *******
C ********** Elliptic Function Tables, Dover (1950) pp. 31. *******
C ********** The function E(U) is evaluated using the identity found on *******
C ********** page 26 of Milne-Thomson. *******
C ***************************************************************************
      REAL Z,U,EU,E,K,K1,PI,UU,E1
      COMMON PI,K,K1,E,E1
      UU = U
      CALL GAUSS1(EU,U)
      Z = EU - U*E/K
      RETURN
      END
```

The electric field calculation program, *EFIELD*.

```
      PROGRAM EFIELD
      COMMON PI,K,K1,E,E1
C ***************************************************************************
C *********** This program calculates the electric field around two parallel ***
C *********** disk electrodes using the transformation solution in Moon & ***
C *********** Spencer's Field Theory Handbook page 76 & 85. ***
C ***************************************************************************
      REAL*8 PI,M,A,HLM,K,K1,A1,U,ZU,SNU,CNU,DNU,DNU2,V,V1,ZV1,SNV1,CNV1,DNV1
      REAL*8 NY1,SX1,SY1,X,Y,E,E1,SNV12,VV,D1,NX1,MAG,DNV,SNV,CNV,DNR,RX1,RX2
      REAL*8 RX,RXS,IY,IYS,MAGS1,MAGS2,MAGS,M2
      OPEN(UNIT=10,FILE="efield.dat",ACCESS='SEQUENTIAL')
      OPEN(UNIT=11,FILE="emag2.dat",ACCESS='SEQUENTIAL')
1     FORMAT(E12.6,2X,E12.6)
      PI = 3.141592654
      M = 0.5
      M2 = M**2.
      A = 2.50
      HLM = PI/2.
      CALL ELLIPK(K,HLM,M)
      CALL ELLIPE(E,HLM,M)
       IF(M.EQ.0.5) THEN
K1 = K
                E1 = E
ELSE
M1 = 1.0 - M
CALL ELLIPK(K1,HLM,M1)
                CALL ELLIPE(E1,HLM,M1)
END IF
      A1 = 2.*K*A/PI
           DO U=0.0,K,.1
           CALL ZETA(ZU,U)
           CALL JACOBSN(SNU,U,M)
           CALL JACOBCN(CNU,U,M)
           CALL JACOBDN(DNU,U)
           DNU2 = (DNU)**2.
                DO V=0.0,K,.1
```

```
            V1 = V + K1
            CALL ZETA(ZV1,V1)
            CALL JACOBSN(SNV1,V1,M)
            CALL JACOBCN(CNV1,V1,M)
            CALL JACOBDN(DNV1,V1,M)
            SNV12 = (SNV1)**2.
            VV = PI*V/2./K/K1
            D1 = 1.0 - DNU2*SNV12
            NX1 = M*SNU*CNU*DNU*SNV12
            NY1 = DNU2*SNV1*CNV1*DNV1
            SX1 = ZU + NX1/D1
            SY1 = ZV1 + VV - NY1/D1
            X = A1*SX1
            Y = A1*SY1
            WRITE(10,1)X,Y
            IF(X.GT.0.0.AND.X.LT.2.17) THEN
                SNV = 0.0
                CNV = 1.0
                DNV = 1.0
                DNR = (CNV*CNV+M*SNU*SNU*SNV*SNV)**2.
                RX1 = K*DNU*DNU*DNV*DNV*CNV*CNV
                RX2 = K*M2*SNU*SNU*SNV*SNV*CNU*CNU
                RX = RX1 + RX2 - E*DNR
                RXS = (RX)**2.
                IY = 2.*K*DNU*DNV*CNV*M*SNU*CNU*SNV
                IYS = (IY)**2.
                MAGS1 = (PI*DNR*RX/(2.*A*(RXS+IYS)))**2.
                MAGS2 = (P1*DNR*IY/(2.*A*(RXS+IYS)))**2.
                MAGS = MAGS1 - MAGS2
                MAG = SQRT(MAGS)
                WRITE(*,*)"THE VALUE OF X"
                WRITE(*,*)X
                WRITE(11,1)U,MAG
                END IF
            END DO
        END DO
    CLOSE(10)
    CLOSE(11)
    STOP
    END
```

The program to calculate the magnitude of the electric field strength, *EMAG*.

```
    PROGRAM EMAG
    REAL U,A,M,PI,K,E,DNU,DNU2,ZU,SNV,CNV,DNV,SNV2,SNU2
    REAL SNU,CNU,CNU2,DD,TT,EU,EV,K1,SNV12,SNV1
    REAL DNV2,CNV2,CNV4,CNV3,AR,AI,XR,YI,XR2,YI2,EU2,EV2
    REAL MAG,X,DK,PP,V1,SF,ZMAX,U1
    COMMON PI,K,K1,E,E1
    OPEN(UNIT=10,FILE="elect1.dat",ACCESS='SEQUENTIAL')
    K = 1.8540747
    K1 = K
    E = 1.3506439
    m = .5
```

```
A = 2.5
ZMAX = 0.146872
PI = 3.141592654
SF = 15.875/(2.*A*K*ZMAX/PI)
E3 = 2.*K*A/PI
DK = 2.*K
PP = -0.5
V = -.10*K1
    V1 = V + K
    CALL JACOBSN(SNV,V,M)
    CALL JACOBCN(CNV,V,M)
    CALL JACOBDN(DNV,V)
    CALL JACOBSN(SNV1,V1,M)
    SNV12 = SNV1**2.
    SNV2 = SNV**2.
    DNV2 = DNV**2.
    CNV2 = CNV**2.
    CNV4 = CNV**4.
    CNV3 = CNV**3.
DO U1=0.0,1.1,.1
    U = (1.-U1)*K
    CALL JACOBDN(DNU,U)
    CALL JACOBSN(SNU,U,M)
    CALL JACOBCN(CNU,U,M)
    CALL ZETA(ZU,U)
    DNU2 = (DNU)**2.
    SNU2 = SNU**2.
    CNU2 = CNU**2.
    DD = 1. - DNU2*SNV12
    TT = SNU*CNU*DNU
    AR = CNV4*CNU2 + SNU2*SNV2*DNU2*DNV2*CNV2
    AI = 2.*CNV3*CNU*SNU*SNV*DNU*DNV
    XR = CNV2*SNU2*DNV2 - SNV2*CNU2*DNU2*CNV4
    YI = 2.*CNV3*CNU*SNU*SNV*DNU*DNV
    XR2 = XR**2.
    YI2 = YI**2.
    EU = -E3*((XR*AR - AI*YI)/(XR2+YI2) + E/K)
    EU2 = EU**2.
    EV = -E3*(XR*AI+AR*YI)/(XR2+YI2)
    EV2 = EV**2.
    MAG = ((EU2 + EV2)**PP)*1000.
    X = E3*(ZU + (M*TT*SNV12/DD))*SF
    WRITE(10,*)X,MAG
END DO
CLOSE(10)
STOP
END
```

Appendix C

The numerical evaluation of the radial and axial velocity components is accomplished using the following FORTRAN program:

```
PROGRAM RVEL
COMPLEX*16 KE,EX,BETA,ARG1,ARG2,ALPHA,ALPHA2,E1,E2,E3,E4
COMPLEX*16 G,H,DU,DU2,G1(400,1),VW,EO,CMPRO,U(400,251)
COMPLEX*16 V(400,1),A1INV(400,400),A1(400,400),WORK(400,800)
COMPLEX*16 A,B,C,D1,D2,D3,D4,D5
REAL*8 DR,DR2,R,R2,DZ,DZ2,DZ3,Z,LEN
REAL*8 OMEGA(251),RHOF,MU,RA,RE,M,AF,AS,RHOS
REAL*8 PI,RHOC,VTEMP
REAL*4 OMEGA2(251),URE,UIM,UPLOT(40),Z1(40),R1(10)
REAL*4 VPLOT1(40),VPLOT2(40),VPLOT3(40),VPLOT4(40),VPLOT5(10)
INTEGER ZLEN,KMIN,KMAX,KMAX2,K1,K,I,J,L,INUM
INTEGER ZCOUNT,N,IFLAG
CHARACTER*11 FILE1
C
C ***********************************************************************
C ****************** PROBLEM PARAMETERS *************************
C ****************** 39 - delta z & 9 delt r ****************************
C ***********************************************************************
C
RHOF = 994.76
RA = 0.0375
RE = 0.015875
LEN = 1.257
DR = (RA-RE)/9.
DR2 = DR**2
DZ = LEN/39.
DZ2 = DZ**2
DZ3 = DZ**3
M = 16.3295
EX = CMPLX ( 6.6E7 , 0.0 ) * CMPLX ( 1.0 , 0.27)
EO = EX
RHOS = 1200.0
AF = 0.003626134
AS = 0.001449173
RHOC = (RHOS*AS+RHOF*AF)/(AS+AF)
CMPRO = CMPLX ( RHOC , 0.0 )
PI = 4.0*ATAN(1.0)
FILE1 = "filter0.dat"
DO K =1,40
A1(K,K) = CMPLX( 1.0, 0.0)
G1(K,1) = CMPLX(0.0,0.0)
END DO
KMAX = 40
A = CMPLX((1./(2.*DR2*DZ)),0.0)
C = CMPLX((1./(2.*DZ3)),0.0)
D1 = CMPLX((7./DZ3),0.0)
D2 = CMPLX((-12./DZ3),0.0)
```

```
 D3 = CMPLX((9./DZ3),0.0)
 D4 = CMPLX((-5./(2.*DZ3)),0.0)
 D5 = CMPLX((-3./(2.*DZ3)),0.0)
C
C ***************************************************************************
C ************** FREQUENCY VALUES ***************************************
C ***************************************************************************
C
 OPEN(UNIT=10,FILE=FILE1,STATUS='old')
100 CONTINUE
 READ(10,*,END=110) OMEGA(INUM),URE,UIM
 OMEGA2(INUM) = OMEGA(INUM)
 INUM = INUM +1
 GOTO 100
110 CLOSE(10)
 INUM = INUM - 1
C
L= 124
C DO L=1,INUM
C
C ***************************************************************************
C ************** MATRIX ASSEMBLY ****************************************
C ***************************************************************************
C
 KE = CMPLX(OMEGA(L),0.0) / (SQRT(EX/CMPRO))
 BETA = EX*KE*CMPLX(0.0, AS/(M*OMEGA(L)**2) )
 ARG1 = BETA + CMPLX(1.0 , 0.0)
 ARG2 = BETA - CMPLX(1.0 , 0.0)
 ALPHA = KE*CMPLX(0.0 , LEN)
C
 ZCOUNT = 0
 KMAX2 = KMAX
 DO I=2,9
 R = REAL(I-1)*DR + RE
 R2 = R**2
 B = CMPLX((1./(R2*DZ)),0.0)
 KMIN = KMAX2 + 1
 KMAX2 = I*KMAX
 ZLEN = 0
 DO K=KMIN,KMAX2
 ZLEN = ZLEN + 1
 Z = REAL(ZLEN - 1)*DZ
 ALPHA2 = KE*CMPLX(0.0 , Z)
 E1 = EXP(CMPLX(-1.0,0.0)*ALPHA)
 E2 = EXP(ALPHA2)
 E3 = EXP(CMPLX(-1.0,0.0)*ALPHA2)
 E4 = EXP(ALPHA)
 G = (ARG1*E1)/(ARG2*E4+ARG1*E1)
 H = (ARG2*E4)/(ARG2*E4+ARG1*E1)
 DU = KE*CMPLX(0.0,1.0)*(G*E2 - H*E3)
 DU2 = -1.*(KE**2)*(G*E2 + H*E3)
 IF(K.EQ.KMIN.OR.K.EQ.KMAX2)THEN
 A1(K,K) = CMPLX(1.0,0.0)
 G1(K,1) = CMPLX(0.0,0.0)
```

```
GOTO 10
END IF
IF(K.EQ.(KMIN+1))THEN
A1(K,K-41) = -A
A1(K,K-39) = A
A1(K,K-1) = CMPLX(2.0,0.0)*A + B
A1(K,K) = D4
A1(K,K+1) = D3 - CMPLX(2.0,0.0)*A - B
A1(K,K+2) = D2
A1(K,K+3) = D1
A1(K,K+4) = D5
A1(K,K+39) = -A
A1(K,K+41) = A
G1(K,1) = CMPLX( (1./R), 0.0 )*DU2
GOTO 10
END IF
IF(K.EQ.(KMAX2-1))THEN
A1(K,K-41) = -A
A1(K,K-39) = A
A1(K,K-4) = -D5
A1(K,K-3) = -D1
A1(K,K-2) = -D2
A1(K,K-1) = -D3 + CMPLX(2.0,0.0)*A + B
A1(K,K) = -D4
A1(K,K+1) = CMPLX(-2.0,0.0)*A - B
A1(K,K+39) = -A
A1(K,K+41) = A
G1(K,1) = CMPLX( (1./R), 0.0 )*DU2
GOTO 10
END IF
A1(K,K-41) = -A
A1(K,K-39) = A
A1(K,K-2) = -C
A1(K,K-1) = CMPLX(2.0,0.0)*C + CMPLX(2.0,0.0)*A + B
A1(K,K+1) = CMPLX(-2.0,0.0)*C - CMPLX(2.0,0.0)*A - B
A1(K,K+2) = C
A1(K,K+39) = -A
A1(K,K+41) = A
G1(K,1) = CMPLX( (1./R), 0.0 )*DU2
10 CONTINUE
END DO
END DO
C
C
C
C
ZLEN = 1
DO I=361,400
Z = REAL(ZLEN - 1)*DZ
Z1(ZLEN) = Z
A1(I,I) = CMPLX(1.0,0.0)
ALPHA2 = KE*CMPLX(0.0 , Z)
E1 = EXP(CMPLX(-1.0,0.0)*ALPHA)
E2 = EXP(ALPHA2)
```

```
E3 = EXP(CMPLX(-1.0,0.0)*ALPHA2)
E4 = EXP(ALPHA)
G = (ARG1*E1)/(ARG2*E4+ARG1*E1)
H = (ARG2*E4)/(ARG2*E4+ARG1*E1)
DU = KE*CMPLX(0.0,1.0)*(G*E2 - H*E3)
VW = CMPLX(RA,0.0)*DU
IF(I.EQ.361.OR.I.EQ.400)THEN
G1(I,1) = CMPLX(0.0,0.0)
ELSE
G1(I,1) = VW
END IF
ZLEN = ZLEN + 1
END DO
ZLEN = 1
DO I=1,40
Z = REAL(ZLEN - 1)*DZ
Z1(ZLEN) = Z
A1(I,I) = CMPLX(1.0,0.0)
ALPHA2 = KE*CMPLX(0.0 , Z)
E1 = EXP(CMPLX(-1.0,0.0)*ALPHA)
E2 = EXP(ALPHA2)
E3 = EXP(CMPLX(-1.0,0.0)*ALPHA2)
E4 = EXP(ALPHA)
G = (ARG1*E1)/(ARG2*E4+ARG1*E1)
H = (ARG2*E4)/(ARG2*E4+ARG1*E1)
U(ZLEN,L) = G*E2 + H*E3
ZLEN = ZLEN + 1
END DO

C
C
C END DO

DO K=1,400
DO J=1,400
IF (A1(K,J).NE.CMPLX(0.0,0.0))THEN
WRITE(20,*) " ROW=",K," COLUMN=",J," VALUE=",A1(K,J)
END IF
END DO
END DO
DO K=1,400
WRITE(21,*) " ROW=",K," VALUE=",G1(K,1)
END DO
N = 400
IFLAG = 0
CALL CMINV(A1,A1INV,WORK,N,IFLAG)
WRITE(*,*) "IFLAG=",IFLAG, "IF ZERO THEN NON SINGULAR MATRIX"
READ(*,*)
I = 400
J = 400
K = 1
CALL DCMMLT(V,A1INV,G1,I,J,K)
DO K=201,240
K1 = K - 200
```

```
VPLOT1(K1) = ABS(V(K,1))
IF(VPLOT1(K1).LE.1.E-10)THEN
VPLOT1(K1) = 0.0
END IF
END DO
DO K=1,40
VPLOT2(K) = ABS(V(K,1))
IF(VPLOT2(K).LE.1.E-10)THEN
VPLOT2(K) = 0.0
END IF
END DO
DO K=81,120
K1 = K - 80
VPLOT3(K1) = ABS(V(K,1))
IF(VPLOT3(K1).LE.1.E-10)THEN
VPLOT3(K1) = 0.0
END IF
END DO
DO K=361,400
K1 = K - 360
VPLOT4(K1) = ABS(V(K,1))
IF(VPLOT4(K1).LE.1.E-10)THEN
VPLOT4(K1) = 0.0
END IF
END DO
I = 1
DO K=3,363,40
VPLOT5(I) = ABS(V(K,1))
IF(VPLOT5(K).LE.1.E-10)THEN
VPLOT5(K) = 0.0
END IF
I = I + 1
END DO
DO I = 2,9
R1(I) = REAL(I-1)*DR + RE
END DO
R1(1) = RE
R1(10) = RA
C
DO J=1,40
UPLOT(J) = ABS(U(J,L))
END DO
C
DO K=1,400
VTEMP = ABS(V(K,1))
WRITE(15,*) VTEMP
END DO

C
C
C Plotting Routines Follow (PLOT 10)
C Plot of axial velocity functions at r=ra
C
C
```

```
 CALL INITT (960)
 CALL BINITT
 CALL NPTS (40)
 CALL CHECK (Z1,UPLOT)
 CALL DSPLAY (Z1,UPLOT)
 CALL HLABEL (400,50,1.0,'Axial Distance (m)')
 CALL HLABEL (250,675,1.0,'Axial Velocity at the Wall')
 CALL VLABEL (50,500,1.0,' Velocity (dimless)')
 CALL ANMODE
 CALL HOME
C
C
 READ(*,*)
C
 CALL INITT (960)
 CALL BINITT
 CALL NPTS (40)
 CALL CHECK (Z1,VPLOT2)
CALL DSPLAY (Z1,VPLOT2)
 CALL HLABEL (400,50,1.0,'Axial Distance (m)')
 CALL HLABEL (250,675,1.0,'Radial Velocity at the Electrodes')
 CALL VLABEL (50,500,1.0,' Velocity (dimless)')
 CALL ANMODE
 CALL HOME
C
 READ (*,*)
C
 CALL INITT (960)
 CALL BINITT
 CALL NPTS (40)
 CALL CHECK (Z1,VPLOT1)
CALL DLIMY (0.0,0.05)
 CALL DSPLAY (Z1,VPLOT1)
 CALL HLABEL (400,50,1.0,'Axial Distance (m)')
 CALL HLABEL (250,675,1.0,'Radial Velocity at r=2.8cm')
 CALL VLABEL (50,500,1.0,' Velocity (dimless)')
 CALL ANMODE
 CALL HOME
C
 READ(*,*)
C
 CALL INITT (960)
 CALL BINITT
 CALL NPTS (40)
 CALL CHECK (Z1,VPLOT3)
CALL DSPLAY (Z1,VPLOT3)
 CALL HLABEL (400,50,1.0,'Axial Distance (m)')
 CALL HLABEL (250,675,1.0,'Radial Velocity at r=2.07cm')
 CALL VLABEL (50,500,1.0,' Velocity (dimless)')
 CALL ANMODE
 CALL HOME
C
 READ(*,*)
C
```

```
 CALL INITT (960)
 CALL BINITT
 CALL NPTS (40)
 CALL CHECK (Z1,VPLOT4)
CALL DLIMY (0.0,0.105)
 CALL DSPLAY (Z1,VPLOT4)
 CALL HLABEL (400,50,1.0,'Axial Distance (m)')
 CALL HLABEL (250,675,1.0,'Radial Velocity at the Wall')
 CALL VLABEL (50,500,1.0,' Velocity (dimless)')
 CALL ANMODE
 CALL HOME
C
 READ(*,*)
C
 CALL INITT (960)
 CALL BINITT
 CALL NPTS (10)
 CALL CHECK (R1,VPLOT5)
CALL DLIMY (0.0,0.105)
 CALL DSPLAY (R1,VPLOT5)
 CALL HLABEL (400,50,1.0,'Radial Distance (m)')
 CALL HLABEL (250,675,1.0,'Radial Velocity at 2-Delta z')
 CALL VLABEL (50,500,1.0,' Velocity (dimless)')
 CALL ANMODE
 CALL HOME
C
C
999 END
C
C

C CMINV--Complex Matrix INVersion
C
 SUBROUTINE CMINV (C,CINV,WORK,N,IFLAG)
C
C--Notes
C If IFLAG = 1, the matrix is singular
C Working precision (artificial zero) = 1E-6
C
C--External variables
 INTEGER N,IFLAG
 COMPLEX*16 C(N,N),CINV(N,N),WORK(N,2*N)
C
C--Internal variables
 INTEGER I,J,IP,IROW,JROW,JCOL,K
 COMPLEX*16 MAXPIV,S1,C1,SWITCH
 REAL*8 BMAG,T
C
 DO I = 1, N, 1
 DO J = 1, N, 1
 WORK(I,J) = C(I,J)
 END DO
 END DO
C
```

```
      DO 130 I = 1, N, 1
      DO 120 J = 1, N, 1
      WORK(I,J+N) = ( 0.0, 0.0 )
      IF (I.EQ.J) WORK(I,J+N) = ( 1.0, 0.0 )
  120 CONTINUE
  130 CONTINUE
C
      J = 1
      I = 1
  140 IP = I
      MAXPIV = WORK(I,J)
C
      DO 150 IROW = I+1, N, 1
      S1 = WORK(IROW,J)
      IF (ABS(S1) .LT. ABS(MAXPIV)) GOTO 150
      IP = IROW
      MAXPIV = WORK(IROW,J)
  150 CONTINUE
C
      IF (IP.EQ.1) GOTO 170
      DO 160 JROW = 1, 2*N, 1
      SWITCH = WORK(IP,JROW)
      WORK(IP,JROW) = WORK(I,JROW)
      WORK(I,JROW) = SWITCH
  160 CONTINUE
C
  170 BMAG = ABS(MAXPIV)
C
      IF (BMAG .LT. 1E-6) GOTO 900
      DO 190 IROW = I+1, N, 1
      DO 180 JROW = J+1, 2*N, 1
      C1 = WORK(IROW,J)*WORK(I,JROW)/WORK(I,J)
      WORK(IROW,JROW) = WORK(IROW,JROW)-C1
  180 CONTINUE
      WORK(IROW,J) = ( 0., 0. )
  190 CONTINUE
      I = I+1
      J = J+1
C
      IF ((I.LT.N) .AND. (J.LT.N)) GOTO 140
C
      DO 210 I = 1, N, 1
      C1 = WORK(I,I)
      DO 200 J = I, 2*N, 1
      WORK(I,J) = WORK(I,J)/C1
  200 CONTINUE
  210 CONTINUE
C
      DO 240 I = N, 2, -1
      DO 230 J = I-1, 1, -1
      C1 = WORK(J,I)
      DO 220 JCOL = J+1, 2*N, 1
      WORK(J,JCOL) = WORK(J,JCOL)-C1*WORK(I,JCOL)
  220 CONTINUE
```

```
230 CONTINUE
240 CONTINUE
C
 DO 260 I = 1, N, 1
 DO 250 J = 1, N, 1
 CINV(I,J) = WORK(I,J+N)
250 CONTINUE
260 CONTINUE
 IFLAG = 0
C
 T = 0.
 K = 0
CC--The norm of the matrix inversion is T
CC DO 190 I = 1, N, 1
CC DO 190 J = 1, N, 1
CC C1 = ( 0., 0. )
CC DO 180 K = 1, N, 1
CC C1 = C1+C(I,K)*WORK(K,J)
CC180 CONTINUE
CC S1 = ( -1., 0. )*C1
CC IF (I.EQ.J) S1 = S1 + ( 1., 0. )
CC T = T + (REAL(S1)**2) + (IMAG(S1)**2)
CC190 CONTINUE
CC T = SQRT(T)
C
 WRITE(*,*) "IFLAG FROM SUB=",IFLAG
 RETURN
C
900 IFLAG = 1
 RETURN
 END
C
C
C DCMMLT--Double precision, Complex Matrix MuLTiplication
C
C--Matrix multiplication (A=BC)
C
 SUBROUTINE DCMMLT (A,B,C,I,J,K)
C
C--Externl Variables
 INTEGER I,J,K
 COMPLEX*16 A(I,K),B(I,J),C(J,K)
C--Internal variables
 INTEGER L,M,N
DO 30 L = 1, I, 1
 DO 20 M = 1, K, 1
 A(L,M) = ( 0.0 , 0.0)
 DO 10 N = 1, J, 1
 A(L,M) = A(L,M) + B(L,N)*C(N,M)
 10 CONTINUE
 20 CONTINUE
 30 CONTINUE
RETURN
 END
```

Appendix D

The numerical evaluation of the damping contribution of the ER fluid is accomplished using the following FORTRAN program:

```
PROGRAM DAMP
COMPLEX*16 KE,BETA,ARG1,ARG2,EX,CMPRO,G1
COMPLEX*16 EO,ALPHA,ALPHA2,E1,E2,E3,E4,G,H
COMPLEX*16 PON1,PON2,TT1,TT2,TT3,TT4
REAL*8 V(10,40),DVDR(10,40),DVDZ(10,40),EV,MSE
REAL*8 DUDZ(40),LEN,VT(400),NU,T(40),T1,TSUM
REAL*8 DVDR2,DVDZ2,DUDZ2,GAMA,GAMA2,M,AS,SUSZ2
REAL*8 PHI(10,40),MU,YIELDS,OMEGA(1),PI,COEF
REAL*8 AF,RHOS,RHOF,RHOC,RA,RE,DR,DZ,ADA,SUSZ(40)
REAL*8 FDVDZ(8),BDVDZ(8),FDVDR(38),R(10)
REAL*8 FDVDZ1,BDVDZ1,DVDR1,TH,T2
INTEGER I,J,INUM,ICOUNT
CHARACTER*13 FILE1,FILE2
FILE1 = 'new04.txt'
C
C ***********************************************************************
C ****************** PROBLEM PARAMETERS *************************
C ****************** VELOCITIES FROM PROB5.F *********************
C ****************** 39 - delta z & 9 delt r *****************************
C ***********************************************************************
C
PI = 4.0*ATAN(1.0)
RHOF = 994.76
MU = 931.0
YIELDS = -505.
OMEGA(1) = 68.9554
AS = 0.001449173
AF = 0.003626134
RHOS = 1200.
RHOC = (RHOS*AS+RHOF*AF)/(AS+AF)
CMPRO = CMPLX ( RHOC , 0.0 )
M = 16.3295
EX = CMPLX ( 6.6E7 , 0.0 ) * CMPLX ( 1.0 , 0.27)
EO = EX
NU = 0.39
G1 = EX/CMPLX( 2.*(1.+NU) , 0.0 )
RA = 0.0375
RE = 0.015875
LEN = 1.257
DR = (RA-RE)/9.
DZ = LEN/39.
R(1) = RE
R(10) = RA
TH = 5.715E-3
T2 = TH**2
C
C ***********************************************************************
```

```
C ************** READ IN RADIAL VELOCITY VALUES *********************
C ******************************************************************
 INUM = 1
 OPEN(UNIT=10,FILE=FILE1,STATUS='OLD')
100 CONTINUE
 READ(10,*,END=110) VT(INUM)
 INUM = INUM +1
 GOTO 100
110 CLOSE(10)
 INUM = INUM - 1
C
C ******************************************************************
C ******* CONVERT INDICIES TO VELOCITY GRID LABELS ***************
C ******************************************************************
C
 ICOUNT = 1
 DO I=1,10
 DO J=1,40
 V(I,J) = VT(ICOUNT)
 IF(V(I,J).LT.1.D-12) THEN
 V(I,J) = 0.0
 END IF
 ICOUNT = ICOUNT + 1
 END DO
 END DO
C
C ******************************************************************
C ************ CALCULATE THE AXIAL VELOCITY AND DUDZ ***************
C ******************************************************************
C
 KE = CMPLX(OMEGA(1),0.0) / (SQRT(EX/CMPRO))
 BETA = EX*KE*CMPLX(0.0, AS/(M*OMEGA(1)**2) )
 ARG1 = BETA + CMPLX(1.0 , 0.0)
 ARG2 = BETA - CMPLX(1.0 , 0.0)
 ALPHA = KE*CMPLX(0.0 , LEN)
 DO I=1,40
 Z = REAL(I - 1)*DZ
 ALPHA2 = KE*CMPLX(0.0 , Z)
 E1 = EXP(CMPLX(-1.0,0.0)*ALPHA)
 E2 = EXP(ALPHA2)
 E3 = EXP(CMPLX(-1.0,0.0)*ALPHA2)
 E4 = EXP(ALPHA)
 G = (ARG1*E1)/(ARG2*E4+ARG1*E1)
 H = (ARG2*E4)/(ARG2*E4+ARG1*E1)
 DUDZ(I) = ABS(KE*CMPLX(0.0,1.0)*(G*E2 - H*E3))
 SUSZ(I) = ABS(KE**2*CMPLX(-1.,0.0)*(G*E2 + H*E3))
 END DO
C
C ******************************************************************
C ******************** CALCULATE DVDR AND DVDZ *********************
C ******************************************************************
C
 DO I=2,9
 DO J=2,39
```

```
DVDR(I,J) = (V(I+1,J) - V(I-1,J))/(2.*DR)
DVDZ(I,J) = (V(I,J+1) - V(I,J-1))/(2.*DZ)
FDVDR(J) = (4.*V(2,J) - V(3,J))/(2.*DR)
FDVDZ(I) = (4.*V(I,2) - V(I,3))/(2.*DZ)
BDVDZ(I) = (-4.*V(I,39) + V(I,38))/(2.*DZ)
END DO
END DO
C
C ***************************************************************************
C ********** CALCULATE THE DISSIPATION FUNCTION *********************
C ***************************************************************************
C
DO I=2,9
R(I) = REAL(I-1)*DR + RE
DO J=2,39
DUDZ2 = (DUDZ(J))**2
DVDR2 = (DVDR(I,J))**2
DVDZ2 = (DVDZ(I,J))**2
VOR2 = (V(I,J)/R(I))**2
GAMA2 = 2.*DVDR2 + 2.*VOR2 + 2.*DUDZ2 + DVDZ2
GAMA = SQRT(GAMA2)
PHI(I,J) = YIELDS*GAMA - MU*GAMA2
END DO
END DO
C
C ******************** ALONG THE WALL
C
DO J=2,39
DVDR1 = (1./(2.*DR))*(3.*V(10,J)-4.*V(9,J)+V(8,J))
DVDR2 = (DVDR1)**2
VOR2 = (V(10,J)/R(10))**2
DUDZ2 = (DUDZ(J))**2
SUSZ2 = (SUSZ(J))**2
GAMA2 = 2.*DVDR2 + 2.*VOR2 + 2.*DUDZ2 + SUSZ2
GAMA = SQRT(GAMA2)
PHI(10,J) = YIELDS*GAMA - MU*GAMA2
END DO
C
C ******************** AT THE ENDS
C
PHI(1,1) = YIELDS*SQRT(2.)*DUDZ(1) - 2.*MU*(DUDZ(1))**2
PHI(1,40) = YIELDS*SQRT(2.)*DUDZ(40) - 2.*MU*(DUDZ(40))**2
FDVDZ1 = (4.*V(10,2) - V(10,3))/(2.*DZ)
GAMA2 = 2.*(DUDZ(1))**2 + FDVDZ1**2
GAMA = SQRT(GAMA2)
PHI(10,1) = YIELDS*GAMA - MU*GAMA2
BDVDZ1 = (-4.*V(10,39) + V(10,38))/(2.*DZ)
GAMA2 = 2.*(DUDZ(40))**2 + BDVDZ1**2
GAMA = SQRT(GAMA2)
PHI(10,40) = YIELDS*GAMA - MU*GAMA2
C
C ******************** AT ELECTRODES
C
DO J=2,39
```

```
 DVDR2 = (FDVDR(J))**2
 DUDZ2 = (DUDZ(J))**2
 GAMA2 = 2.*DVDR2 + 2.*DUDZ2
 GAMA = SQRT(GAMA2)
 PHI(1,J) = YIELDS*GAMA - MU*GAMA2
 END DO
C
C ****************** AT FORWARD SIDE
C
 DO I=2,9
 DVDZ2 = (FDVDZ(I))**2
 DUDZ2 = (DUDZ(1))**2
 GAMA2 = 2.*DVDZ2 + 2.*DUDZ2
 GAMA = SQRT(GAMA2)
 PHI(I,1) = YIELDS*GAMA - MU*GAMA2
 END DO
C
C ****************** AT AFT SIDE
C
 DO I=2,9
 DVDZ2 = (BDVDZ(I))**2
 DUDZ2 = (DUDZ(40))**2
 GAMA2 = 2.*DVDZ2 + 2.*DUDZ2
 GAMA = SQRT(GAMA2)
 PHI(I,40) = YIELDS*GAMA - MU*GAMA2
 END DO
C
C ***************************************************************************
C ***************** PRINT DISSIPATION FUNCTION ********************
C ***************************************************************************
C
 DO I=1,10
 DO J=1,40
 WRITE(3,*) I,J,PHI(I,J)
 END DO
 END DO
C
C ***************************************************************************
C ***************** CALCULATE MAXIMUM STRAIN ENERGY IN HOSE ***************
C ***************************************************************************
C
 KE = CMPLX(OMEGA(1),0.0) / (SQRT(EX/CMPRO))
 BETA = EX*KE*CMPLX(0.0, AS/(M*OMEGA(1)**2) )
 ARG1 = BETA + CMPLX(1.0 , 0.0)
 ARG2 = BETA - CMPLX(1.0 , 0.0)
 ALPHA = KE*CMPLX(0.0 , LEN)
 PON1 = CMPLX(0.0,2.*LEN)*KE
 PON2 = CMPLX(0.0,-2.0*LEN)*KE
 E1 = EXP(CMPLX(-1.0,0.0)*ALPHA)
 E4 = EXP(ALPHA)
 G = (ARG1*E1)/(ARG2*E4+ARG1*E1)
 H = (ARG2*E4)/(ARG2*E4+ARG1*E1)
 TT1 = CMPLX(T2*(1.+NU),0.0)*EX
 TT2 =(KE*G**2)/(CMPLX(0.,2.))*(CMPLX(1.,0.0)-EXP(PON1))+
```

```
! (KE*H**2)/(CMPLX(0.,2.))*(EXP(PON2)-CMPLX(1.,0.0))+
! CMPLX(2.*LEN,0.0)*G*H*KE**2
TT3 = CMPLX(T2*RAD**2/2.,0.0)*G1
TT4 =(KE**3*G**2/CMPLX(0.0,2.))*(EXP(PON1)-CMPLX(1.0,0.0))+
! (KE**3*H**2/CMPLX(0.0,2.))*(CMPLX(1.0,0.0)-EXP(PON2))+
! CMPLX(2.*LEN,0.0)*G*H*KE**4
MSE = ABS(TT1*(TT2)+TT3*(TT4))
C
C ***************************************************************************
C ************** INTEGRATE THE DISSIPATION FUNCTION WRT R *****************
C ************** USING TRAPEZOIDAL RULE *****************
C ***************************************************************************
C
 DO J=1,40
 T(J) = (DR/2.)*(PHI(1,J)*R(1) + 2.*PHI(2,J)*R(2)
 ! + 2.*PHI(3,J)*R(3) + 2.*PHI(4,J)*R(4) +
 ! 2.*PHI(5,J)*R(5) + 2.*PHI(6,J)*R(6) +
 ! 2.*PHI(7,J)*R(7) + 2.*PHI(8,J)*R(8) +
 ! 2.*PHI(9,J)*R(9) + PHI(10,J)*R(10))
 END DO
C
C ***************************************************************************
C ************** INTEGRATE THE INTEGRAL OF PHI WRT R WRT Z *****************
C ************** USING THE TRAPEZOIDAL RULE ****************
C ***************************************************************************
C
 TSUM = 0.0
 DO J=2,39
 T1 = 2.0*T(J)
 TSUM = TSUM + T1
 END DO
 EV = (DZ/2.)*(T(1) + TSUM + T(40))
C
C ***************************************************************************
C ***************** CALCULATE THE LOSS TANGENT *************************
C ***************************************************************************
C
 COEF = -4.0*PI*OMEGA(1)
 ADA = COEF*(EV/MSE)/(4.*PI)
 WRITE (4,*) ADA,OMEGA(1),EV,MSE
C ***************************************************************************
C ***************** END IT ALL ***********************************
C ***************************************************************************
C
 END
```

Appendix E

The following are transfer functions from the attenuation experiments listed as frequency, real component, and imaginary component:

Zero volt data set:

5.00936484935587, -1.10337, 0.0648265
5.04520795952135, -1.10601, 0.0645547
5.08130753504421, -1.10865, 0.0642812
5.11766541099064, -1.1113, 0.0640061
5.15428343555713, -1.11396, 0.0637293
5.19116347016442, -1.11662, 0.0634508
5.22830738955214, -1.11929, 0.0631708
5.26571708187407, -1.12108, 0.0632235
5.30339444879418, -1.12287, 0.0632762
5.34134140558323, -1.12466, 0.0633289
5.37955988121621, -1.12645, 0.0633816
5.41805181847029, -1.12825, 0.0634343
5.4568191740237, -1.13006, 0.063487
5.49586391855509, -1.13186, 0.0635398
5.53518803684378, -1.13367, 0.0635922
5.57479352787061, -1.13964, 0.0663836
5.61468240491955, -1.14565, 0.0692031
5.65485669568011, -1.15167, 0.0720507
5.69531844235031, -1.15773, 0.0749267
5.7360697017406, -1.16381, 0.0778313
5.77711254537831, -1.16992, 0.0807647
5.81844905961304, -1.17605, 0.0837271
5.86008134572268, -1.18221, 0.0867188
5.90201152002021, -1.18536, 0.0865969
5.94424171396131, -1.18852, 0.0864737
5.98677407425269, -1.19169, 0.0863493
6.02961076296122, -1.19486, 0.0862236
6.07275395762383, -1.19804, 0.0860967
6.11620585135821, -1.20123, 0.0859685
6.15996865297431, -1.20443, 0.085839
6.20404458708656, -1.20764, 0.0857084
6.24843589422705, -1.21365, 0.088573
6.29314483095932, -1.21968, 0.0914642
6.33817366999316, -1.22573, 0.0943823
6.38352470030007, -1.23181, 0.0973276
6.42920022722967, -1.23791, 0.1003
6.47520257262684, -1.24405, 0.1033
6.5215340749498, -1.2502, 0.106328
6.56819708938893, -1.25638, 0.109383
6.61519398798653, -1.2639, 0.111838
6.66252715975738, -1.27145, 0.114317
6.7101990108102, -1.27905, 0.116823
6.75821196446992, -1.2867, 0.119355

6.80656846140093, -1.29438, 0.121913
6.85527095973108, -1.30211, 0.124498
6.9043219351767, -1.30988, 0.12711
6.95372388116837, -1.3177, 0.129748
7.00347930897777, -1.32647, 0.134464
7.05359074784524, -1.3353, 0.139237
7.10406074510842, -1.34417, 0.14407
7.15489186633169, -1.35309, 0.148962
7.20608669543662, -1.36205, 0.153913
7.25764783483332, -1.37107, 0.158925
7.30957790555269, -1.38013, 0.163998
7.36187954737972, -1.38924, 0.169133
7.41455541898761, -1.39916, 0.174167
7.46760819807296, -1.40913, 0.179267
7.52104058149191, -1.41917, 0.184431
7.57485528539717, -1.42926, 0.189661
7.62905504537612, -1.43942, 0.194958
7.68364261658988, -1.44964, 0.200321
7.73862077391336, -1.45992, 0.205753
7.79399231207632, -1.47026, 0.211252
7.84976004580539, -1.4874, 0.223861
7.90592680996723, -1.50467, 0.236744
7.96249545971259, -1.52208, 0.249907
8.01946887062142, -1.53962, 0.263355
8.07684993884912, -1.55728, 0.27709
8.1346415812737, -1.57508, 0.291119
8.19284673564408, -1.59301, 0.305445
8.25146836072941, -1.61106, 0.320073
8.31050943646951, -1.6322, 0.351255
8.36997296412631, -1.65318, 0.383287
8.42986196643642, -1.67398, 0.416179
8.49017948776483, -1.69459, 0.449943
8.55092859425959, -1.715, 0.484591
8.61211237400776, -1.73518, 0.520132
8.67373393719232, -1.75511, 0.556579
8.73579641625028, -1.77479, 0.593942
8.79830296603197, -1.78975, 0.621358
8.86125676396132, -1.80459, 0.649279
8.92466101019748, -1.81929, 0.67771
8.98851892779739, -1.83385, 0.706655
9.05283376287973, -1.84826, 0.736121
9.11760878478982, -1.86251, 0.76611
9.18284728626591, -1.8766, 0.796628
9.2485525836065, -1.89051, 0.827679
9.31472801683894, -1.91431, 0.874014
9.3813769498892, -1.93785, 0.921634
9.4485027707529, -1.96108, 0.970562
9.51610889166751, -1.98398, 1.02082
9.58419874928581, -2.00654, 1.07242
9.65277580485059, -2.02871, 1.1254
9.72184354437059, -2.05047, 1.17976
9.79140547879772, -2.0718, 1.23554
9.86146514420551, -2.08356, 1.48898
9.9320261019689, -2.07378, 1.75815

10.0030919389452, -2.0398, 2.04207
10.0746662676566, -1.97895, 2.33949
10.1467527264736, -1.88847, 2.64881
10.2193549797999, -1.76561, 2.96814
10.292476718259, -1.6076, 3.29521
10.3661216588817, -1.41173, 3.62739
10.4402935452948, -1.2304, 3.6703
10.5149961479116, -1.04824, 3.70432
10.5902332641236, -0.865664, 3.72949
10.6660087184934, -0.68311, 3.74583
10.7423263629493, -0.50099, 3.7534
10.8191900769809, -0.319717, 3.75229
10.8966037678364, -0.139697, 3.7426
10.9745713707213, 0.0386734, 3.72444
11.0530968489983, 0.165588, 3.66589
11.1321841943889, 0.288549, 3.6039
11.2118374271761, 0.407499, 3.53866
11.2920605964091, 0.522387, 3.47034
11.3728577801088, 0.633171, 3.39914
11.4542330854754, 0.739816, 3.32524
11.5361906490968, 0.842292, 3.24883
11.6187346371592, 0.940579, 3.17008
11.7018692456589, 1.01659, 3.08223
11.7855987006152, 1.08856, 2.99378
11.8699272582859, 1.15656, 2.90489
11.9548592053829, 1.22063, 2.81566
12.0403988592906, 1.28085, 2.72623
12.1265505682853, 1.33728, 2.63671
12.213318711756, 1.39, 2.54721
12.3007077004275, 1.43907, 2.45785
12.388721976584, 1.45701, 2.37815
12.4773660142954, 1.47302, 2.29977
12.5666443196444, 1.48715, 2.22272
12.6565614309559, 1.49948, 2.147
12.7471219190274, 1.51008, 2.07264
12.8383303873615, 1.51899, 1.99962
12.9301914723999, 1.52629, 1.92797
13.022709843759, 1.53203, 1.85767
13.1158902044674, 1.52187, 1.79827
13.2097372912049, 1.51119, 1.74028
13.3042558745432, 1.50002, 1.68369
13.3994507591885, 1.48839, 1.62846
13.495326784226, 1.47633, 1.57458
13.5918888233652, 1.46386, 1.52202
13.6891417851884, 1.451, 1.47076
13.7870906133997, 1.43779, 1.42077
13.8857402870766, 1.42908, 1.38503
13.985095820923, 1.42017, 1.34992
14.085162265524, 1.41106, 1.31545
14.1859447076028, 1.40176, 1.2816
14.2874482702793, 1.39229, 1.24836
14.3896781133304, 1.38264, 1.21573
14.4926394334523, 1.37283, 1.18369
14.5963374645247, 1.36287, 1.15224

14.7007774778771, 1.34796, 1.11843
14.8059647825561, 1.33301, 1.08539
14.9119047255962, 1.31805, 1.05309
15.0186026922906, 1.30307, 1.02154
15.1260641064658, 1.28808, 0.990703
15.2342944307569, 1.27309, 0.960578
15.3432991668853, 1.25811, 0.93115
15.4530838559385, 1.24314, 0.902406
15.5636540786517, 1.22565, 0.877228
15.6750154556914, 1.20832, 0.85264
15.7871736479413, 1.19115, 0.828629
15.9001343567899, 1.17415, 0.805184
16.0139033244205, 1.15731, 0.782292
16.128486334103, 1.14065, 0.759942
16.2438892104876, 1.12415, 0.738123
16.3601178199015, 1.10781, 0.716824
16.4771780706465, 1.09367, 0.698965
16.5950759132998, 1.07966, 0.681476
16.7138173410163, 1.06579, 0.664351
16.8334083898329, 1.05204, 0.647583
16.9538551389762, 1.03843, 0.631165
17.0751637111705, 1.02495, 0.615091
17.19734027295, 1.0116, 0.599354
17.3203910349714, 0.99838, 0.583949
17.4443222523303, 0.987492, 0.568335
17.5691402248788, 0.97666, 0.553029
17.6948512975459, 0.965885, 0.538027
17.8214618606598, 0.955166, 0.523323
17.9489783502729, 0.944507, 0.508913
18.0774072484893, 0.933907, 0.494792
18.2067550837937, 0.923368, 0.480955
18.3370284313835, 0.912892, 0.467398
18.4682339135033, 0.901829, 0.455514
18.6003781997812, 0.890866, 0.443866
18.7334680075679, 0.880004, 0.432451
18.8675101022784, 0.869241, 0.421265
19.0025112977356, 0.858578, 0.410303
19.1384784565168, 0.848015, 0.399562
19.2754184903027, 0.837551, 0.389037
19.4133383602284, 0.827187, 0.378727
19.5522450772377, 0.818453, 0.368185
19.6921457024389, 0.809769, 0.357843
19.8330473474644, 0.801135, 0.347698
19.9749571748318, 0.792551, 0.337747
20.117882398308, 0.784019, 0.327987
20.2618302832762, 0.775539, 0.318415
20.4068081471048, 0.767111, 0.309028
20.5528233595198, 0.758736, 0.299824
20.6998833429789, 0.749574, 0.290475
20.8479955730494, 0.740486, 0.281323
20.9971675787879, 0.731471, 0.272365
21.1474069431229, 0.72253, 0.263597
21.2987213032407, 0.713663, 0.255015
21.451118350973, 0.704869, 0.246618

21.6046058331886, 0.69615, 0.238401
21.7591915521865, 0.687505, 0.230361
21.9148833660933, 0.679203, 0.223979
22.0716891892618, 0.670984, 0.217723
22.2296169926739, 0.662848, 0.211591
22.3886748043459, 0.654794, 0.205582
22.5488707097359, 0.646822, 0.199692
22.7102128521554, 0.638931, 0.19392
22.8727094331832, 0.631121, 0.188264
23.0363687130822, 0.62339, 0.182722
23.201199011219, 0.615438, 0.176317
23.3672087064876, 0.607563, 0.170052
23.5344062377343, 0.599765, 0.163926
23.7028001041876, 0.592043, 0.157935
23.8723988658897, 0.584397, 0.152078
24.0432111441318, 0.576827, 0.146353
24.2152456218924, 0.569332, 0.140756
24.3885110442784, 0.561912, 0.135284
24.5630162189703, 0.554718, 0.130574
24.7387700166691, 0.547602, 0.125966
24.9157813715477, 0.540562, 0.121458
25.0940592817052, 0.533598, 0.117049
25.2736128096238, 0.526709, 0.112736
25.4544510826299, 0.519896, 0.108518
25.636583293358, 0.513157, 0.104393
25.8200187002177, 0.506491, 0.10036
26.0047666278648, 0.499596, 0.0975242
26.1908364676749, 0.49279, 0.0947482
26.3782376782212, 0.486073, 0.0920305
26.5669797857547, 0.479443, 0.0893701
26.7570723846891, 0.4729, 0.0867658
26.9485251380883, 0.466442, 0.0842167
27.1413477781573, 0.460069, 0.0817217
27.3355501067374, 0.453779, 0.07928
27.5311419958041, 0.449221, 0.0757675
27.7281333879691, 0.444692, 0.0723204
27.9265342969857, 0.440194, 0.0689376
28.1263548082579, 0.435726, 0.0656185
28.3276050793527, 0.431287, 0.0623619
28.5302953405171, 0.426879, 0.0591672
28.7344358951974, 0.422501, 0.0560334
28.9400371205638, 0.418154, 0.0529597
29.1471094680369, 0.414111, 0.0492884
29.3556634638199, 0.410083, 0.045686
29.5657097094332, 0.406072, 0.0421519
29.7772588822534, 0.402077, 0.0386851
29.9903217360561, 0.398098, 0.0352847

1.6kV/mm data set:

5.00936484935587, -1.12156, 0.145606
5.04520795952135, -1.12377, 0.145392

5.08130753504421, -1.12597, 0.145176
5.11766541099064, -1.12819, 0.14496
5.15428343555713, -1.1304, 0.144741
5.19116347016442, -1.13262, 0.144522
5.22830738955214, -1.13484, 0.144301
5.26571708187407, -1.1412, 0.14538
5.30339444879418, -1.1476, 0.146467
5.34134140558323, -1.15403, 0.147562
5.37955988121621, -1.1605, 0.148664
5.41805181847029, -1.167, 0.149773
5.4568191740237, -1.17354, 0.150891
5.49586391855509, -1.18012, 0.152016
5.53518803684378, -1.18673, 0.15315
5.57479352787061, -1.18822, 0.157185
5.61468240491955, -1.18971, 0.161231
5.65485669568011, -1.19118, 0.165289
5.69531844235031, -1.19264, 0.169358
5.7360697017406, -1.19409, 0.173439
5.77711254537831, -1.19553, 0.177531
5.81844905961304, -1.19696, 0.181634
5.86008134572268, -1.19837, 0.185748
5.90201152002021, -1.20449, 0.188217
5.94424171396131, -1.21063, 0.190707
5.98677407425269, -1.21681, 0.193217
6.02961076296122, -1.22301, 0.195748
6.07275395762383, -1.22925, 0.198301
6.11620585135821, -1.23551, 0.200874
6.15996865297431, -1.2418, 0.203469
6.20404458708656, -1.24813, 0.206086
6.24843589422705, -1.25409, 0.212327
6.29314483095932, -1.26007, 0.218627
6.33817366999316, -1.26605, 0.224986
6.38352470030007, -1.27203, 0.231403
6.42920022722967, -1.27803, 0.237881
6.47520257262684, -1.28403, 0.244418
6.5215340749498, -1.29003, 0.251016
6.56819708938893, -1.29604, 0.257675
6.61519398798653, -1.30294, 0.26137
6.66252715975738, -1.30987, 0.265098
6.7101990108102, -1.31683, 0.268859
6.75821196446992, -1.32382, 0.272654
6.80656846140093, -1.33085, 0.276481
6.85527095973108, -1.33791, 0.280343
6.9043219351767, -1.345, 0.284239
6.95372388116837, -1.35213, 0.288169
7.00347930897777, -1.36227, 0.294675
7.05359074784524, -1.37247, 0.301266
7.10406074510842, -1.38274, 0.307942
7.15489186633169, -1.39307, 0.314704
7.20608669543662, -1.40346, 0.321553
7.25764783483332, -1.41392, 0.328489
7.30957790555269, -1.42444, 0.335515
7.36187954737972, -1.43503, 0.34263
7.41455541898761, -1.44729, 0.357958

7.46760819807296, -1.45955, 0.373547
7.52104058149191, -1.47181, 0.3894
7.57485528539717, -1.48407, 0.405519
7.62905504537612, -1.49632, 0.421908
7.68364261658988, -1.50857, 0.438569
7.73862077391336, -1.52082, 0.455505
7.79399231207632, -1.53305, 0.472718
7.84976004580539, -1.55109, 0.495428
7.90592680996723, -1.56916, 0.518661
7.96249545971259, -1.58727, 0.542425
8.01946887062142, -1.6054, 0.566728
8.07684993884912, -1.62356, 0.591579
8.1346415812737, -1.64173, 0.616986
8.19284673564408, -1.65991, 0.642957
8.25146836072941, -1.6781, 0.669502
8.31050943646951, -1.69056, 0.723522
8.36997296412631, -1.70188, 0.7788
8.42986196643642, -1.712, 0.83533
8.49017948776483, -1.72087, 0.893104
8.55092859425959, -1.72844, 0.952111
8.61211237400776, -1.73465, 1.01234
8.67373393719232, -1.73946, 1.07378
8.73579641625028, -1.74279, 1.13642
8.79830296603197, -1.72345, 1.23235
8.86125676396132, -1.69957, 1.3291
8.92466101019748, -1.67106, 1.42649
8.98851892779739, -1.63779, 1.52433
9.05283376287973, -1.59966, 1.62242
9.11760878478982, -1.55659, 1.72055
9.18284728626591, -1.50848, 1.81851
9.2485525836065, -1.45525, 1.91606
9.31472801683894, -1.40242, 1.96552
9.3813769498892, -1.34794, 2.01355
9.4485027707529, -1.29186, 2.0601
9.51610889166751, -1.23422, 2.10512
9.58419874928581, -1.17505, 2.14855
9.65277580485059, -1.1144, 2.19034
9.72184354437059, -1.05231, 2.23045
9.79140547879772, -0.988827, 2.26883
9.86146514420551, -0.891035, 2.2847
9.9320261019689, -0.793596, 2.29662
10.0030919389452, -0.69666, 2.30464
10.0746662676566, -0.600374, 2.30883
10.1467527264736, -0.504879, 2.30924
10.2193549797999, -0.410315, 2.30594
10.292476718259, -0.316815, 2.29901
10.3661216588817, -0.224512, 2.28852
10.4402935452948, -0.187982, 2.25906
10.5149961479116, -0.152403, 2.22949
10.5902332641236, -0.117764, 2.19982
10.6660087184934, -0.0840522, 2.17008
10.7423263629493, -0.0512553, 2.14027
10.8191900769809, -0.0193615, 2.11041
10.8966037678364, 0.0116414, 2.08051

10.9745713707213, 0.0417658, 2.05059
11.0530968489983, 0.0730891, 2.04366
11.1321841943889, 0.10421, 2.03627
11.2118374271761, 0.135122, 2.02843
11.2920605964091, 0.165819, 2.02014
11.3728577801088, 0.196295, 2.0114
11.4542330854754, 0.226543, 2.00222
11.5361906490968, 0.256558, 1.9926
11.6187346371592, 0.286333, 1.98256
11.7018692456589, 0.329404, 1.96497
11.7855987006152, 0.371837, 1.94652
11.8699272582859, 0.413615, 1.92721
11.9548592053829, 0.454724, 1.90706
12.0403988592906, 0.495148, 1.88611
12.1265505682853, 0.534873, 1.86436
12.213318711756, 0.573884, 1.84184
12.3007077004275, 0.612169, 1.81856
12.388721976584, 0.636575, 1.77931
12.4773660142954, 0.659878, 1.74021
12.5666443196444, 0.682097, 1.70127
12.6565614309559, 0.703252, 1.66252
12.7471219190274, 0.723363, 1.62397
12.8383303873615, 0.742449, 1.58564
12.9301914723999, 0.76053, 1.54754
13.022709843759, 0.777626, 1.50968
13.1158902044674, 0.784808, 1.47336
13.2097372912049, 0.791375, 1.43757
13.3042558745432, 0.797345, 1.40229
13.3994507591885, 0.802734, 1.36754
13.495326784226, 0.807561, 1.33331
13.5918888233652, 0.811841, 1.29959
13.6891417851884, 0.815592, 1.2664
13.7870906133997, 0.818827, 1.23372
13.8857402870766, 0.819807, 1.20533
13.985095820923, 0.820455, 1.17738
14.085162265524, 0.820781, 1.14986
14.1859447076028, 0.820796, 1.12276
14.2874482702793, 0.820507, 1.09609
14.3896781133304, 0.819926, 1.06983
14.4926394334523, 0.819061, 1.04399
14.5963374645247, 0.817921, 1.01857
14.7007774778771, 0.816017, 0.995458
14.8059647825561, 0.813911, 0.972708
14.9119047255962, 0.81161, 0.950315
15.0186026922906, 0.80912, 0.928272
15.1260641064658, 0.806448, 0.906579
15.2342944307569, 0.803599, 0.885232
15.3432991668853, 0.80058, 0.864227
15.4530838559385, 0.797397, 0.843561
15.5636540786517, 0.791747, 0.822189
15.6750154556914, 0.785996, 0.801227
15.7871736479413, 0.780151, 0.780667
15.9001343567899, 0.774215, 0.760504
16.0139033244205, 0.768196, 0.740732

16.128486334103, 0.762097, 0.721346
16.2438892104876, 0.755924, 0.70234
16.3601178199015, 0.749681, 0.683708
16.4771780706465, 0.741407, 0.668098
16.5950759132998, 0.733177, 0.652792
16.7138173410163, 0.724992, 0.637786
16.8334083898329, 0.716853, 0.623074
16.9538551389762, 0.708761, 0.60865
17.0751637111705, 0.700717, 0.594511
17.19734027295, 0.692722, 0.58065
17.3203910349714, 0.684777, 0.567065
17.4443222523303, 0.679091, 0.553622
17.5691402248788, 0.673386, 0.540417
17.6948512975459, 0.667665, 0.527449
17.8214618606598, 0.661928, 0.514712
17.9489783502729, 0.656179, 0.502204
18.0774072484893, 0.650419, 0.489923
18.2067550837937, 0.644649, 0.477863
18.3370284313835, 0.638874, 0.466024
18.4682339135033, 0.631346, 0.454746
18.6003781997812, 0.623873, 0.443694
18.7334680075679, 0.616455, 0.432864
18.8675101022784, 0.609092, 0.422252
19.0025112977356, 0.601785, 0.411855
19.1384784565168, 0.594534, 0.401668
19.2754184903027, 0.58734, 0.391689
19.4133383602284, 0.580202, 0.381912
19.5522450772377, 0.574609, 0.374684
19.6921457024389, 0.569056, 0.36757
19.8330473474644, 0.563541, 0.360568
19.9749571748318, 0.558065, 0.353677
20.117882398308, 0.552627, 0.346895
20.2618302832762, 0.547229, 0.340221
20.4068081471048, 0.541869, 0.333653
20.5528233595198, 0.536547, 0.327189
20.6998833429789, 0.530681, 0.320716
20.8479955730494, 0.524869, 0.314353
20.9971675787879, 0.519108, 0.308098
21.1474069431229, 0.5134, 0.301949
21.2987213032407, 0.507743, 0.295904
21.451118350973, 0.502139, 0.289962
21.6046058331886, 0.496585, 0.284121
21.7591915521865, 0.491083, 0.27838
21.9148833660933, 0.487254, 0.270971
22.0716891892618, 0.483414, 0.263685
22.2296169926739, 0.479562, 0.25652
22.3886748043459, 0.475699, 0.249474
22.5488707097359, 0.471828, 0.242548
22.7102128521554, 0.467949, 0.235738
22.8727094331832, 0.464063, 0.229043
23.0363687130822, 0.460169, 0.222463
23.201199011219, 0.455076, 0.216616
23.3672087064876, 0.45002, 0.210881
23.5344062377343, 0.444999, 0.205256

23.7028001041876, 0.440015, 0.19974
23.8723988658897, 0.435068, 0.19433
24.0432111441318, 0.430158, 0.189025
24.2152456218924, 0.425284, 0.183824
24.3885110442784, 0.420447, 0.178724
24.5630162189703, 0.415179, 0.174142
24.7387700166691, 0.409965, 0.169652
24.9157813715477, 0.404806, 0.165252
25.0940592817052, 0.399701, 0.160941
25.2736128096238, 0.39465, 0.156716
25.4544510826299, 0.389653, 0.152576
25.636583293358, 0.384708, 0.14852
25.8200187002177, 0.379817, 0.144546
26.0047666278648, 0.374856, 0.140424
26.1908364676749, 0.369948, 0.136389
26.3782376782212, 0.365094, 0.13244
26.5669797857547, 0.360292, 0.128575
26.7570723846891, 0.355542, 0.124793
26.9485251380883, 0.350844, 0.121093
27.1413477781573, 0.346198, 0.117471
27.3355501067374, 0.341603, 0.113929
27.5311419958041, 0.336053, 0.110949
27.7281333879691, 0.330589, 0.108036
27.9265342969857, 0.325211, 0.105191
28.1263548082579, 0.319918, 0.10241
28.3276050793527, 0.314707, 0.0996929
28.5302953405171, 0.309579, 0.0970383
28.7344358951974, 0.30453, 0.0944446
28.9400371205638, 0.299561, 0.0919106
29.1471094680369, 0.294683, 0.0892497
29.3556634638199, 0.28988, 0.0866523
29.5657097094332, 0.285151, 0.0841171
29.7772588822534, 0.280496, 0.0816427
29.9903217360561, 0.275912, 0.0792279

Appendix F

The application of the ER test module to isolate a vibration sensitive device from an excitation source is illustrated in this example. The attenuation of the longitudinal vibration utilizing the ER test module of Chapter 2 is shown in Figure F.1. In this figure, the device to be isolated is accomplished by the addition of the ER damper. The specification of the ER damper response is defined in the Attenuation Experiments in Chapter 2. The attenuation factor, defined as the attenuation (in decibels) per length of the damper, can be evaluated from the transmissibility experiments of Chapter 2. In the case of the ER test module at 1.6 kV/mm, the attenuation produced with respect to the zero voltage case (Figure 2.13, page 22) was 4 dB. This value is obtained from the difference between the magnitudes of the amplitude ratio. The resulting attenuation factor of the energized state of 1.6 kV/mm becomes 3.2 dB/m.

The attenuation factor can be used as a design parameter to specify the required length of an ER damper to provide the desired attenuation to the vibration sensitive equipment in Figure F.1. The damper length is obtained by dividing the desired attenuation level (in decibels) by the attenuation factor. This first order specification of the damping capacity of the device is limited to a linear structure and harmonic excitation. The practical application of the ER damper as a "black box" device could be optimized by designing the resonant frequency of the damper to match the frequency of the maximum excitation. This technique is referred to as tuning the damper.

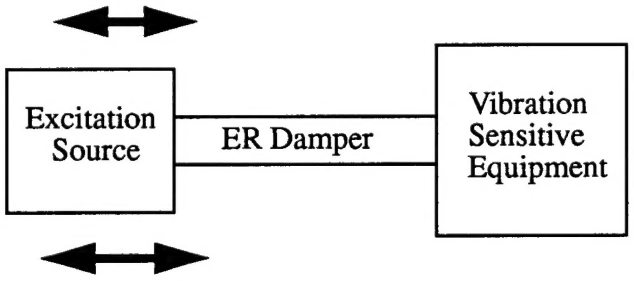

Figure F.1. Illustration of ER Damper Application

INITIAL DISTRIBUTION LIST

Addressee	No. of Copies
Defense Technical Information Center	12
University of Hartford (Professor F. Lahey)	1